The Henryk Niewodniczański Institute of Nuclear Physics
Polish Academy of Sciences

The role of mechanical interactions in prostate cancer therapy and cell resistance to anti-cancer drugs

Andrzej Kubiak

Thesis submitted for Degree of Doctor of Philosophy in Physics
Prepared under the supervision of
Prof. dr hab. Małgorzata Lekka (thesis supervisor)
Prof. dr hab. n. med. Piotr Laidler (thesis supervisor)

Kraków 2021

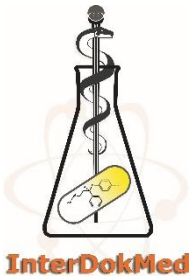

Rozprawa doktorska powstała w trakcie realizacji
Środowiskowych Studiów Doktoranckich
w ramach Projektu nr POWR.03.02.00-00-I013/16,
"Interdyscyplinarność dla medycyny innowacyjnej" InterDokMed,
realizowanych w ramach Programu Operacyjnego Wiedza Edukacja Rozwój 2014-2020,
współfinansowanego ze środków Europejskiego Funduszu Społecznego

The greatest teacher failure is.

Master Yoda

ACKNOWLEDGMENTS

Doing a Ph.D. costs a lot of effort – it will be impossible without the help, assistance, and presence of many people in my personal and professional life.

First of all, I want to thank my wife **Natalka** very much for her love, patience, wisdom, and motivation. Without her assistance, it will be hardly impossible to finish this work. She was always motivating me to do science and do not give up on multiple challenges and failures. Apart from being my wife, Natalka is also a brilliant and talented scientist – I appreciated her help in confocal imaging.

I want to express my gratitude to my **Parents** and auntie **Aga** for their support and for giving me the strength to complete my Ph.D. Your presence was very important for me in those years. You gave me a lot of love and support!

Special appreciation comes to my scientific supervisors – first of all, **Prof. Małgorzata Lekka**. After four years, I need to say that I was lucky to join her group. Thanks to her supervision, I was able to do a lot of good science and learn from my mistakes. Apart from her vast knowledge and experience, she always believed in me and allowed me to develop my scientific career. I know that many of my friends could envy me having such a supervisor. Another piece of luck in my scientific career was my second supervisor – **Prof. Piotr Laidler**. He is an amazing person with outstanding knowledge, achievements and remarkable modesty. He always had time for me, and I know I can rely on him. It was a pleasure to have such supervisors!

This work could not be done without my scientific internship in **Prof. Alessandro Podesta'** team at Università degli Studi di Milano Statale in Milano, Italy. I want to thank **Alessandro**, **Matteo Chighizola,** and **Carsten Schulte** for our work on multilayer analysis of DU145 cell mechanics. We did a great job, and I believe we will do a lot more in the future.

I would like to express my gratitude to all my colleagues from the Department of Biophysical Microstructures (located at the Institute of Nuclear Physics, Polish Academy of Sciences). My very interesting and fruitful time of Ph.D. will not be so happy without my colleagues – **both Asia's, Basia, Kanji, Marcin, Renata, Tomek, Bartek** and our guest from Japan **Masaya**. Together we did a lot of exciting experiments, about which I will not write here. I believe that our friendship will continue.

I would like to thank all co-authors of our paper published in *Nanoscale*, namely **Dr Damian Ryszawy (R.I.P.)** and **Maciek Pudeł**ek from Faculty of Biochemistry, Biophysics, and Biotechnology, Jagiellonian University in Kraków, for assistance in image stream technique, **Dr Małgorzata Lasota** from Chair of Medical Biochemistry Jagiellonian University Medical College assistance in flow cytometry experiments, **Julita Wesołowska, Prof. Agnieszka Basta-Kaim** from The May Insitute of Pharmacology for assistance in confocal imaging. Special thanks in this place come for **Damian**. He helped me a lot during the first steps of my scientific career. It was harder to work without his advice and a good sense of humour.

I want to acknowledge **Dr Sebastian Glatt,** Max Plan Research Group Leader at MBC in Kraków, who told me how to do high IF science. He also said that I would be frustrated multiple times while doing my Ph.D. I was, but I was better prepared for it thanks to him.

Finally, I want to thank my **Family** and **Friends.** Your support and time together mean a lot to me!

LIST OF PUBLICATIONS

Publications included in thesis:

1. **A.Kubiak**, M.Chighizola, C.Schulte, N.Bryniarska, J.Wesołowska, M.Pudełek, M.Lasota, D.Ryszawy, A.Basta-Kaim, P.Laidler, A.Podesta, M.Lekka. "*Stiffening of Prostate Cancer Cells Driven by Actin Filaments – Microtubules Crosstalk Confers Resistance to Microtubule-Targeting Drugs*." – ***Nanoscale,* 13 (2021) 6212**.
2. **A.Kubiak**#[1], T.Zieliński#, J.Pabijan, M.Lekka, "*Nanomechanics in Monitoring the Effectiveness of Drugs Targeting the Cancer Cell Cytoskeleton.*" – ***Int. J. Mol. Sci.* 21 (2020) 8786**.
3. **A.Kubiak** et al. *"Link between nuclear organization and cellular mechanics revealed by glutamine starvation of prostate cancer cells"* – **in preparation**
4. T.Zieliński**#**, **A. Kubiak#**, K.Gnanachandran, M.Lekka, *"Elasticity maps allow determining mechanical properties of various cellular components"* – **in preparation**

Other publications:

1. N.Bryniarska#, **A.Kubiak#**, M.Lekka, A.Basta-Kaim, "*The emerging role of mechanical factors in the treatment of nervous system disorders – dark and light sides of the force*" – submitted to ***Pharmacological Reports***
2. J.Raczkowska, B.Orzechowska, S.Patryas, K.Awsiuk, **A.Kubiak**, M.Kinoshita, M.Okamoto, J.Bobrowska, T.Stachura, J.Soja, K.Sładek, M.Lekka, *Effect of substrate stiffness on physicochemical properties of normal and fibrotic lung fibroblasts*" – ***Materials, 13 (2020) 4495.***
3. J.Zemła, J.Bobrowska, **A.Kubiak**, T.Zieliński, J.Pabijan, K.Pogoda, P.Bobrowski, M.Lekka, *"Indenting Soft Samples (Hydrogels and Cells) with Cantilevers Possessing Various Shapes of Probing Tip."* – ***Eur. Biophys. J. 49 (2020) 485.***
4. A.Łabędź-Masłowska#, N.Bryniarska#, **A. Kubiak#**, T.Kaczmarzyk, M.Sekula-Stryjewska, S.Noga, D.Boruczkowski, Z.Madeja, E.Zuba-Surma,*"Multilineage Differentiation Potential of Human Dental Pulp Stem Cells—Impact of 3d and Hypoxic Environment on Osteogenesis in Vitro."* – ***Int. J. Mol. Sci. 21 (2020) 6172.***
5. N.Bryniarska#, **A.Kubiak#**, A.Łabędź-Masłowska, E.Zuba-Surma, *"Impact of Developmental Origin, Niche Mechanics and Oxygen Availability on Osteogenic Differentiation Capacity of Mesenchymal Stem/Stromal Cells."* – ***Acta Biochim. Pol. 66 (2019) 491.***
6. N.Bryniarska#, **A.Kubiak#**, M.Lekka. A.Basta-Kaim, „The emerging role of mechanical and topographical factors in the development and treatment of nervous system disorders – dark and light sides of the force" – **submitted**.

[1] # – these authors contributed equally.

Abstract

Cancer is the second leading cause of death in the world. Hence, extensive research has been conducted for many years to create effective anti-cancer therapies. These studies, often very advanced and based on reliable biological knowledge, still encounter many difficulties. It is because cancer cells are characterized by their ability to develop drug resistance. In practice, this means that even a tiny group of cells that survive aggressive chemotherapy can lead to tumour rebirth. Moreover, there is then a greater risk that the daughter cells resulting from divisions of drug-resistant cells will also be more resistant to chemotherapy. Research at the biological and biochemical levels has identified multiple mechanisms of drug resistance. Among them is the action of transmembrane pumps - made of protein channels. Such pumps can pump drugs out of cells, thus protecting them against their effects. This knowledge became the basis for clinical trials targeting transmembrane pumps. The results, however, have turned out to be disappointing so far. Hence, it becomes necessary to find alternative methods to accurately assess both the resistance of cancer cells and the effectiveness of the drugs themselves. Atomic force microscopy (AFM) is a technique that allows you to study the mechanical properties of living cells. Previous studies have shown that cancer cells are more deformable than the corresponding healthy cells.

This dissertation aims to find an answer to whether the chemotherapeutic agents affect the mechanics of cancer cells and whether such changes can be regarded as markers of drug resistance in prostate cancer cells. As anti-cancer drugs affect the cytoskeleton and cell nuclei, cell elasticity maps were recorded for different cell compartments and sampling depths. This allowed for the determination of mechanical properties within the cell nuclei and lamellipodia. Conducting such advanced experiments using atomic force microscopy required a separate validation of these methods on a model system of bladder cells that have already been measured many times. In addition, these studies were complemented by experiments describing the biological response of cells to drugs. Thanks to such an approach, it was possible to understand the importance of the physical response of the cell at a given stage of the biological drug activity. In the last step, the results obtained in standard experiments were supplemented with studies on cells grown in conditions simulating the starvation of the tumour environment.

The obtained results show that prostate cancer cells show a mechanical response to the action of anti-cancer drugs. This response is not directly related to how the drugs work but to

the drug effects (including the ability to kill cancer cells). For the three drugs studied here, namely, docetaxel, vinflunine, and colchicine, cells stiffen in response to their action. Notably, by conducting these studies as a function of time, it was possible to show the time-dependent changes in the mechanical properties of cells and identify for which drug causing the least damage in cells the mechanical response to appears the latest. A significant increase in cell stiffness was also observed in the case of starved cells. These cells were also less susceptible to the effects of docetaxel, an anti-cancer drug used to treat prostate cancer. Hence, the obtained results confirm that changes in the mechanical properties of cells enable a quantitative assessment of the anticancer drug effect.

Streszczenie

Choroby nowotworowe stanowią drugą najczęstsza przyczynę zgonów na świecie. Stąd też od wielu lat prowadzi się szeroko zakrojone badania mające na celu stworzenie skutecznych terapii przeciwnowotworowych. Badania te, często bardzo zaawansowane i oparte na rzetelnej wiedzy biologicznej, wciąż napotykają na szereg trudności. Dzieje się tak dlatego, iż komórki nowotoworowe charakteryzuje zdolność do wykształcania lekooporności. W praktyce oznacza to, że nawet bardzo mała grupa komórek, które przeżyją agresywną chemoterapię, może doprowadzić do odrodzenia się guza. Co więcej istnieje wtedy większe ryzyko, iż komórki potomne powstające w wyniku podziałów komórek lekoopornych, będą również bardziej oporne na zastosowaną chemoterapię. Badania na poziomie biologicznym i biochemicznym pozwoliły na zidentyfikowanie szeregu mechanizmów lekooporności. Wśród nich jest działanie transbłonowych pomp – stworzonych z kanałów białkowych. Pompy takie są w stanie wypompowywać leki z komórek, chroniąc je w ten sposób przed ich działaniem. Ta wiedza stała się podstawą to prób klinicznych celujących właśnie w transbłonowe pompy. Wyniki jednak, jak dotąd okazują się być rozczarowujące. Stąd też konieczne staje się znalezienie alternatwynych metod pozwalających na dokonanie trafnej oceny zarówno lekkooporności komórek rakowych jak i skuteczności działania samych leków. Mikroskopia sił atomowych jest techniką pozwalającą na badanie właściwości mechanicznych żywych komórek. W dotychczasowych badaniach pozwoliła no wykazanie, iż komórki rakowe są bardziej odkształcalne niż odpowiadające im komórki zdrowe.

Celem niniejszej rozprawy doktorskiej było znalezienie odpowiedzi na pytanie, czy działanie chemioterapeutyków wpływa na własności mechaniczne komórek rakowych i czy takie zmiany można traktować jako markery lekooporności komórek raka prostaty. Z uwagi na fakt, że leki przeciwnowtworowe oddziałują na cytoskielet oraz jądra komórkowe – w niniejszej pracy rejestrowano mapy elastyczności komórek dla różnych obszarów na komórce i głębokości próbkowania. Pozwoliło to na wyznaczenie właściwości mechanicznych w obrębie jąder komórkowych oraz lamelipodiów. Przeprowadzenie tak zaawansowanych eksperymentów z zastosowaniem mikroskopii sił atomowych wymagało ich osobnej weryfikacji prowadzonej na wielokrotnie już mierzonym modelowym układzie komórek raka pęcherza moczowego. Dodatkowo badania te zostały uzupełnione eksperymentami opisującymi biologiczną odpowiedź komórek na działanie leków. Dzięki takiemu podejściu było możliwe zrozumienie znaczenia mechanicznej odpowiedzi komórek na określonym etapie biologicznego działania leku. W ostatnim etapie, wyniki uzyskane

podczas standardowych eksperymentów uzupełniono o badania nad komórkami hodowanymi w warunkach imitujących środowisko guza tj. w przypadku braku składników odżywczych.

Wyniki uzyskane w ramach tej pracy doktorskiej wykazują, iż komórki raka prostaty wykazują mechaniczną odpowiedź na działanie leków przeciwnowotworowych. Odpowiedź ta nie jest bezpośrednio związana z mechanizmem działania leków ale ze skutkami działania leków (w tym zdolnością do zabijania komórek rakowych). W przypadku trzech badanych leków, a mianowicie, docetakselu, winfluniny i kolchicyny, komórki sztywnieją w odpowiedzi na ich działanie. Warto zauważyć, że przeprowadzając te badania w funkcji czasu, można było wykazać zależne od czasu zmiany właściwości mechanicznych komórek oraz zidentyfikować, dla którego leku powodującego najmniejsze uszkodzenia w komórkach reakcja mechaniczna pojawia się najpóźniej. Istotny wzrost sztywności komórek zaobserwowano również w przypadku komórek głodzonych. Komórki te były również mniej podatne na działanie docetaxelu – leku przeciwnowtworowego stosowanego w terapii raka prostaty. Uzyskane wyniki potwierdzają zatem, że zmiany właściwości mechanicznych komórek pozwalają na ilościową ocenę działania leków przeciwnowotworowych.

LIST OF ABBREVIATIONS

3D – three-dimensional
AFM – atomic force microscopy
BAY 11-7082 – an inhibitor of κB kinase
CAFs – cancer-associated fibroblasts
COL – colchicine
CTR cells – control cells
cytoD – cytochalasin D
DMEM – Dulbecco's Modified Eagle's Medium
DPBS – Dulbecco's Phosphate Buffered Saline
DTX – docetaxel
DU145 – adherent cells of epithelial morphology, derived from 69 years old male patient suffering from carcinoma
FBS – Fetal Bovine Serum
HCV29 – cell line derived from a margin region of cancer derived from a male adult patient suffering from bladder carcinoma (another name non-malignant cell cancer of ureter).
L-GLN – L-glutamine
MDA-MB-231 – human breast adenocarcinoma cell line
MK-2206 – an allosteric inhibitor of a serine/threonine-specific protein kinase B
MTDs – microtubules targeting drugs
MTS – CellTiter 96® AQueous One Solution Cell Proliferation Assay
NTC – non-treated cells
PI – propidium iodine
TCA – tricarboxylic acid cycle
T24 – cell line derived from 81 years old female patient suffering transitional cell carcinoma.
VFL – vinflunine

TABLE OF CONTENTS

1. Introduction

Atomic force microscopy (AFM) was initially invented for imaging objects on a nanometer-scale with broad applications in physics and nanotechnology. While its working principle is based on the measurement of forces interacting between tip and sample, AFM was applied for studying the mechanical properties of the variety of samples. Here contact mechanics model proposed by Hertz and extended by Sneddon is utilized to deliver mechanical properties of samples while knowing mechanical properties of AFM cantilevers and geometrical parameters of tip situated at the end of AFM cantilever. Various samples, including nanostructures and soft samples, were studied using AFM to obtain information about their mechanical properties. Among the latter, biological samples are considered to fascinating targets for AFM-based nanomechanical characterization. During the progression of various diseases, not only biological features of cells and tissues change, but alterations in cell or tissue mechanics also accompany them.

Experiments with AFM use allowed observing differences in mechanical properties of cancer cells and their healthy counterparts for multiple types of cancer. For solid tumours, cancer cells were showed to be significantly softer. Such observation allows researchers to think about using the mechanical properties of cells as a helpful marker during a cancer diagnosis. On the other hand, it must be underlined that multiple types of cancers are still incurable despite very great efforts. One of the reasons for such a situation is that cancerous cells can develop drug resistance against drugs used in anticancer therapies. Efficient recognition and neutralization of drug resistance in cancer are now key challenges in designing various therapeutical approaches. One of the great examples of drug resistance against chemotherapy is the ability of cells to pump away drugs with the use of transmembrane protein channels. This biological knowledge leads to clinical trials aiming to target particular proteins creating channels. Unfortunately, the results of those clinical trials are, at this point, disappointing despite that biological cues leading to their design were very promising. Thus, a very urgent need arises to find methods allowing for better characterization of drug resistance and the general impact of drugs on cancerous cells. In the present work, AFM is proposed as a tool that allows to determination and describe biophysical markers of drug action.

The presented thesis aims to answer whether chemotherapeutic agents action affects prostate cancer cell mechanics and whether such changes might be treated as markers of drug resistance of prostate cancer cells. *Chapter 2* introduces biophysical approaches to measure mechanical properties of living biological samples and, consequently, the significance of mechanical factors in cancer progression. This chapter ends with the presentation of the aims of the thesis. In *Chapter 3*, materials used during the realization of the presented work are described. They were used to handle and prepare living samples to experiment. The techniques applied to characterize the properties of cancer cells are described in detail in *Chapter 4*. Three distinct AFM instruments were employed here to address the aims of the thesis. Thus, the chapter provides a step by step explanation of the basis applied in the measurements of mechanical properties with the use of AFM. It includes cantilever spring constant determination, photodetector sensitivity determination, and finally, self-manufacturing and characterization of spherical probes. Since the presented thesis aims to depict changes in mechanical properties of cells that result from the action of drugs affecting cytoskeleton, it was crucial to optimize the way of data analysis for various approaches of the AFM-based elasticity measurements used here. Thus, the last parts of *Chapter 4* describe the indentation depth analysis of cell mechanical properties, finite thickness correction in AFM measurements of thin samples, separating nuclear and peripheral contributions, and finally, statistical analysis to determine Young's modulus. Data analysis was validated using bladder cancer cell lines because these cell lines were measured multiple times in the Department of Biophysical Microstructures. The validation result is described in *Chapter 5*. *Chapter 6* presents the biological effects of microtubules targeting drugs (MTDs) on prostate DU145 cancer cells. The understanding of proliferation, cytotoxicity and potential drug resistance is crucial for understanding how particular drugs affect cancer cells. Finally, the experiments described in this chapter allow for proper concentrations of drugs for AFM measurements. Thanks to validation of sophisticated methodology achieved in *Chapter 5*, it was possible to perform time-dependent biological effects of MTDs action on prostate cancer cells (DU145). These results are presented in *Chapter 7*. Three MTDs are used, microtubules destabilizers (vinflunine – VFL, colchicine – COL) and stabilizer (docetaxel – DTX). AFM measurements were performed at 24, 48, and 72 hours of MTD treatment. Such an approach allows us to observe patterns of dynamic changes in the mechanical properties of prostate cancer cells. Because it is well established that cytoskeleton and nucleus reorganization are key factors responsible for the mechanical properties of living cells, fluorescent images of cancer cells were collected. In *Chapter 8*, a detailed analysis of the main cellular components undergoing

MTDs treatment is presented. This analysis helped to understand which of the structural elements of cells are responsible for time-dependant changes in prostate cancer cell mechanical properties after drug treatment. This chapter presents the AFM measurements of cells treated with actin depolymerizer used to demonstrate actin filaments contribution to VFL-induced stiffening. Because fluorescent imaging described in *Chapter 8* shows particular changes induced by drug action, it was crucial to determine changes in mechanical properties of specific cellular compartments. Results of those experiments are described in *Chapter 9*, with methodology precisely described in *Chapter 4*. Here data analysis allows for the determination of elastic moduli from different compartments of cells localized on the different depths of indentation (i.e. cell nucleus, cellular lamellipodia). Ultimately changes in mechanical properties of the nuclear region are crucial because they might directly affect gene expression and, in turn, drug resistance of cells. Thus, to better mimic natural conditions inside the tumour, prostate cancer cells undergo glutamine starvation. Such conditions are characteristic for tumour core, where resistant cancer cells reside. This procedure is described in *Chapter 10* with a particular impact on investigating how starvation affects the mechanical properties of cells.

Results presented in the thesis were obtained thanks to the close collaboration between the Department of Biophysical Microstructures at Institute of Nuclear Physics Polish Academy of Sciences in Kraków, Poland, Chair of Medical Biochemistry at Jagiellonian University Medical College in Kraków, Poland, and Department of Physics at Università degli Studi di Milano Statale in Milano, Italy.

2. Fundamentals and state of arts

2.1. Description of mechanical properties of soft samples

Forces loaded on each body cause their deformation. Description of the relationship between deformation and forces acting on the sample is related in a general way to modulus depicting mechanical properties of the body:

$$stress = elastic\ modulus\ \times strain \tag{2.1}$$

The particular definition of those three elements depends on the nature of force acting on a sample. In the case of force acting parallel to the long axis of the body (stretching or compression), the equation (2.1) takes the form:

$$\frac{F}{S} = E \times \frac{\Delta L}{L} \tag{2.2}$$

where stress is reflected by force (*F*) acting on a cross-sectional area (*S*) perpendicular to the action of this force and strain is a change of sample length (*ΔL*) related to the initial length (*L*) of the sample. The proportion between stress and strain is Young's modulus of the sample (*E*). Young's modulus is characteristic for a particular material, thus it can be applied to compare different samples (including biological ones) in terms of their mechanical properties.

In the case of sample deformation, which is perpendicular to sample long axis eq. 2.1 takes the form:

$$\frac{F}{S} = G \times \frac{\Delta x}{L} \tag{2.3}$$

Here, strain denotes also a force acting on the surface area of the sample (*S*), while stress is defined as the deformation of the sample in the perpendicular direction to the long axis (*Δx*) divided by its length (*L*). The proportion between stress and strain is reflected by Kirhoff modulus (*G*), which is characteristic for a given material as Young's modulus.

The action of hydrostatic pressure might deform the sample. In this case, eq. 2.1 takes the form:

$$p = K \times \frac{\Delta V}{V} \tag{2.4.}$$

where stress is reflected by hydrostatic pressure acting on the sample, while changes in volume denote the strain. The modulus describing the proportion between stress and strain is referred to as bulk modulus (*K*). In the case of the three aforementioned elastic moduli, strain is always a dimensionless parameter. Thus, elastic moduli are expressed in pascal (Pa).

2.2. Mechanical cues in cancer progression

Cancer development and progression have been one of the most investigated research topics. Multiples studies conducted so far have allowed us to establish that cancerous cells are characterized by the ability to evade apoptosis, sustain angiogenesis, invade tissue, and metastasize. They are characterized by self-sufficiency in growth signals, insensitivity to anti-growth signals and finally, limitless replicative potential. Those characteristic makes them ultimately hard target for therapy and create an urgent need for subsequent investigations (1). Up to date, multiple biochemical and genetic approaches have been applied to characterize cancerous cells and assess the efficacy of their treatment. Nevertheless, despite several years of studies in those topics, cancer is still the second cause of death in the European Union (2). Therefore more attention has to be paid to the role of physical cues in the mentioned above hallmarks of cancer. Precisely physical interaction has been shown to play a key role in processing biological signals inside cells that are then introducing cellular features promoting disease progression and resistance against therapy. For example, changes in matrix stiffness have been connected with sustained angiogenesis and mechanosensitive activity of proteins. For example, focal adhesion kinase (FAK) has been shown to inhibit the activity of proteins responsible for inducing apoptosis (p53 and Src) but also growth inhibitors (p15 and p21) (3). That physical alteration results from affected mechanical properties of both tissues and cells what is characteristic of cancer progression. Most studies show that cancerous cells are softer than their healthy counterparts, while cancerous tissue is reported to be stiffer than healthy tissue from the same organ (4–9). Such significant variation in mechanical properties of cancer cells directs researchers to ask the question of their reason and, in particular, possible meaning in cancer progression. First of all, stiffening of tumour stroma is a result of its fibrosis. Fibrosis is the process of nonphysiological accumulation of extracellular matrix proteins within the tumour stroma. Fibrosis is based on the secretion of dense collagen fibrils by cancer-associated fibroblasts (CAFs, (10)). One of the reported effects of CAFs on cancer progression is promoting metastasis. Originally it was believed that their activity relay on

secretory activity. Recently more pieces of evidence are indicating that also physical interaction mediated by those cells is capable of promoting metastasis. In this case, the interplay between tensile forces generated by the solid mass of cancer cells and CAFs facilitates the invasion of aggregates of cancerous cells deeper inside tissues (11). Thus, changes in physical properties are treated more seriously as significant factors of cancer progression (12). The processes of invasion and metastasis are directly connected with the interaction of cancerous cells with endothelial cells forming blood vessels. In this context, stiffening of the microenvironment has been shown to affect endothelial cells robustly. An increase in Young's modulus (within the range of 400 – 2700 – 22000 Pa) of substrate for endothelial cell culture has been associated with their increased proliferation and expression of CCN1 (CCN family member 1) protein. Its elevated expression on tumour-associated endothelial cells is associated with multiple cancer-promoting processes (including elevated expression of N-cadherin, which is the cadherin promoting interactions of cancer cells with endothelial cells that, as a consequence, lead to metastasis) (13). Ultimately stiffness of the microenvironment surrounding cancer cells has been shown to induce drug resistance in case of multiple cancers, including breast (14,15) and prostate cancers (16). It has been reported that increased stiffness of the microenvironment increases drug resistance of hepatocellular carcinoma cells treated with cisplatin (17), paclitaxel, 5-FU (18), oxaliplatin (18) and sorafenib (18), breast cancer cells treated with doxorubicin (14), rapamycin (19), melanoma cells treated with vemurafenib (20), pancreatic cancer cells treated with paclitaxel (21), and finally glioblastoma cells treated with temozolomide (22). On the other hand, a decrease in stiffness of the tumour microenvironment has been associated with the increased cancer resistance, also in the case of hepatocellular carcinoma (17) as well as myeloid leukemias treated with a variety of chemotherapeutic agents (23) or laryngeal squamous cancer treated with cisplatin or 5-FU (23). Nevertheless in most of aforementioned cases of solid tumors stiffening of tissue and ECM is tumor hallmark directly associated with increasing drug resistance. An opposite trend is reported for cancer cells, which are in general considered to be softer than their healthy counterparts. Such an increase in cellular deformability is usually connected with giving them advantage during invasion in complex and multibranched ECM as well as during squeezing between endothelial cells while cancer cells are invading blood vessels (8,9,24). Anyway, recent development in this field are providing surprising information about this mechanical hallmark of cancer cells. In case of treatment of ovarian cancer (OVACA433) cells its decreased stiffness measured with use of filtration methods have been associated with higher resistance against cisplatin (25). Another study about

ovarian cancer cells (OVCAR5 and SKOV3) showed opposite results. Here increased resistance of cells induced by activation of Rho (Rho family of GTPases) was associated with stiffening of cells. Inhibition of Rho was leading to decrease in both resistance against cisplatin as well as mean Young's modulus of ovarian cancer cells (26). Similarly as for DU145 prostate cancer, cells measured with use of magnetic twisting cytometry were stiffer in the case of paclitaxel resistant subpopulation (27). What is more, recently treatment of prostate cancer cell lines (PC-3, 22Rv1 and PNT1A) with docetaxel and cisplatin have been shown to significantly increase their Young's modulus (28). In light of the above reports, it turns out that physical methods for the characterization of biological samples might provide important information about action of particular drugs in context of the response to their use for treatment. Such possibilities seemed to be especially promising while thinking about drugs which affects cellular cytoskeleton architecture which is in turn a key factor responsible for establishment of physical properties of cells.

2.3. Microtubules interacting agents in the treatment of cancerous cells

Up to date, multiple approaches have been utilized to treat cancerous cells, in principle, based on targeting particular cancer hallmarks (1,29). Since cancer cells are characterized by rapid divisions, one of the most commonly used approaches is to deplete their proliferation. Thus the general idea of chemotherapy is to target mechanisms allowing cells to divide. Such chemotherapeutic agents could be alkylating agents, antimetabolites, hormones and antagonists, antitumor antibiotics, tyrosine-kinase inhibitors, cyclin-dependent kinase inhibitors, PI3K/Akt/mTOR inhibitors, Raf/MEK/ERK inhibitors, and finally, drugs that target microtubular network (30). The application of the latter ones is based on the principal rule of mitosis. The genetic material of cells stored in chromosomes is segregated into daughter cells using a mitotic spindle during cellular divisions. The mitotic spindle is a structure built up from microtubules anchored to chromosomes at one end, while at the other, they are connected to the centrosome. During mitosis, microtubular spindles pull chromosomes into the direction of centrosomes, resulting in the separation of sister chromosomes organized in the metaphase plate. Such pulling process requires physiological functionality of microtubules, which is based on their dynamics (31). In general, properly functioning microtubules are characterized by incessant dynamics, consisting of two types of instability: polymerization and depolymerization. During the first one, tubulin dimers bind to

guanosine-5'-triphosphate (GTP-tubulin dimers) added at the plus end of growing microtubules. GTP binding provides a conformation of tubulin dimer, which favours a stable structure of a whole microtubule. Such plus end is the target for the microtubules associated proteins like EB1 (microtubule-associated protein RP/EB family member 1) proteins participating in stabilising the growth of microtubules. GTP hydrolysis to guanosine diphosphate (GDP) in multiple tubulin dimers within the microtubule changes their conformation. This change results in a loss of a stable microtubule structure and results in its rapid depolymerization in so-called the catastrophe process. Notably, the existence of the GTP-rich part at the microtubule, which is localized downstream to the initial point of catastrophe, might result in a stoppage of depolymerization and return to polymerization in a process referred to as rescue. The ability of microtubules to dynamically change between a state of growth and shrinkage is responsible for their proper action during mitotic divisions because shrinkage of the mitotic spindle is responsible for pulling chromosomes away from the metaphase plate (32). Therapeutic approaches disrupt the proper functioning of microtubules by either depolymerizing them (and preventing rescues) or stabilizing them, making depolymerization and microtubules shrinkage impossible (31). In principle, microtubules and interacting agents are divided into three groups based on their binding mechanism with tubulin dimers (Fig. 2.1).

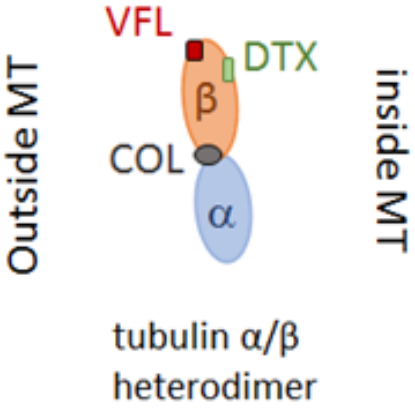

Fig. 2.1. Principle of MTDs action. Schematic presentation of binding sites for MTDs at tubulin dimer. Domains for three distinct families of drugs are presented: vinca alkaloids (as an example VFL), taxanes (as an example DTX) and colchicine binding time (as an example COL). Adopted and modified from Kubiak et al., Int. J. Mol. Sci., 21 (2020) 8786, under CC (47).

The first group consists of *vinca* alkaloids binding on the interface between alfa and beta subunits of tubulin dimers leading to depolymerization of microtubules. The second group makes drugs binding to the colchicine binding site localised on beta-tubulin and at the interdimeric interface. In the case of those drugs, the effect is similar to *vinca* alkaloids, i.e., the use of colchicine leads to tubulin depolymerization. Finally, the last family are taxanes that bind to β-tubulin inside microtubules lumen, leading to the straightening of tubulin filaments, even if the conformation of tubulin dimers is changed for catastrophe favouring by hydrolysis of GTP. Thus, as a result of the use of taxanes, microtubules became stabilized. Thus, all of the agents above, no matter whether they are polymerizing or depolymerizing microtubules, lead to failure in mitotic progression. As a result, cells that cannot divide become apoptotic and finally undergo cellular death (33). An excellent example are leukemic CCL B-cells that have exhibited dose-dependent apoptosis markers after treatment with nocodazole (a compound binding to the colchicine domain) (34). Nocodazole is genotoxic for murine bone marrow cells, which shows that ultimate caution must be considered while optimizing therapeutic approaches because genotoxicity might cause chromosome aberration dangerous in the case of hematogenic cells (35). In this field, finding new markers of drug action and drug resistance seem to be one of the emerging challenges in modern research. In the case of U2OS cells, colchicine and vinblastine have been shown to similarly affect the microtubular network of cells after 25 and 48 hours. Treatment of those cells with paclitaxel has been reported to exhibit a distinct effect on microtubules and cellular nuclei, leading to aggregation of tubulin in the nuclear region and the formation of polynucleated cells. In those cases, IC_{50} and IC_{80} drug doses[2] have been applied (36). Observation described in those subsections lets to ask the question of whether and if yes, how cytoskeleton treatment might contribute to the alteration of mechanical properties of cells, which might be used as a marker of drug action and could be considered to be connected with drug resistance.

2.4. Atomic force microscopy in studying of cellular biomechanics

Atomic force microscopy (AFM), initially developed to study object morphology in nanoscale, has been recently widely applied in biological studies (37). In principle, AFM serves as a routine technique for determining the mechanical properties of cells and tissues

[2] IC_N – is a value which is informing about a dose of particular compound which is able to kill *n%* of cells or cause *n%* decrease their proliferation. For example: IC_{50} denotes concentration of drug sufficient to kill 50% of cells.

(9). Physical principles standing behind that method are described in details in section 4. Up to date, AFM has been used to investigate a variety of cells, including stem cells (38,39), fibroblasts (40,41), endothelial, cardiac muscle and skeletal muscle cells (42), neurons (43) and ultimately cancerous cells (44). In the latter case, multiple studies have already shown that cancerous cells are softer than their healthy counterparts (8,9,45). The disturbance of cytoskeleton organization usually explained those changes. In that case, usually, the actin cytoskeleton has been considered. Importantly such changes are closely related to cell migration and invasion due to the crucial role of actin in those processes (46). On the other hand, it has to be underlined here that the cellular cytoskeleton consists of actin and microtubules, intermediate filaments, and adhesion molecules. Consequently, alterations in their expression and functioning are also supposed to affect cellular elasticity. As recently reviewed by Kubiak et al., multiple drugs have been already shown to affect cell mechanical properties (47). Effects of drugs on elastic moduli of cancerous cells obtained in a variety of studies are summarized in Table 2.1.

Table 2.1. The effect of various drugs on the mechanical properties of different cancer cells (adopted from Kubiak et al. (47)).

Drug	Cell type	Dose Time	Δ*E*	Reference
chitosan	non-malignant cell cancer of ureter (HCV29)	0.05% 40 min	no effect	Lekka et al. (48)
chitosan	transitional cell carcinoma (T24)	0.05% 40 min	↑	Lekka et al. (48)
human neutrophil peptide-1	prostate cancer (PC-3)	5 μM 4 h	↓	Gaspar et al. (49)
Disulfiram	prostate cancer (PC-3)	1 & 2 μM 24 h	↑	Ren et al. 2015 (50)
Tomatine	prostate cancer (PC-3)	1 & 3 μM 24 h	↑	Ren et al. 2015 (50)
BAY-11	prostate cancer (PC-3)	2 & 5 μM 24 h	↑	Ren et al. 2015 (50)
vaproic acid	prostate cancer (PC-3)	2 & 10 μM 24 h	↑	Ren et al. 2015 (50)
12-O-tetradecanoyl-phorbol-13-acetate	prostate cancer (PC-3)	2 & 20 μM 24 h	↑	Ren et al. 2015 (50)
Celebrex	prostate cancer (PC-3)	2 & 10 μM 24 h	↑	Ren et al. 2015 (50)
MK-2206	prostate cancer (PC-3)	2 & 10 μM 24 h	↑	Ren et al. 2015 (50)
NMDA	neuroblastoma (SH-SY5Y)	5 μM 1 h	↑	Fang et al. (51)
NMDA	neuroblastoma (SH-SY5Y)	200 μM 1 h	↑	Fang et al. (51)
Cetuximab	lung cancer (A549)	20 nM 12 h	↑	Zhang et al. (52)
Resveratrol	breast cancer (MCF-7)	50 μM 3 h	↓	Iturri et al. (53)
Resveratrol	breast cancer (MCF-7)	50 μM 6 h	no change	Iturri et al. (53)
Resveratrol	breast cancer (MCF-7)	50 μM 24 h	↑	Iturri et al. (53)
Resveratrol	breast cancer (MCF-7)	50 μM 48 h	↑	Iturri et al. (53)
Cisplatin	prostate cancer (22Rv)	24 μM 24 h	↑	Raudenska et al. (28)
Cisplatin	prostate cancer (PC-3)	93 μM 24 h	↑	Raudenska et al. (28)
Disulfiram-Cu	nasopharyngeal carcinoma cells (CNE-2Z)	200 & 400 nM 6 h	↑	Yang et al. (54)
Curcumin	liver carcinoma (HepG2)	0.78 & 1.56 μg/mL 24h	↑	Olugbami et al. (55)
K.senegalensis hydroethanolic extract	liver carcinoma (HepG2)	25 & 50 μg/mL 24h	↑	Olugbami et al. (55)
Dexamethasone	acute lymphoblastic leukemia (ALL)	1 μM –	↑	Lam et al. (56)
Daunorubicin	acute lymphoblastic leukemia (ALL)	1 μM –	↑	Lam et al. (56)

2.5. Aim of the thesis

Cancer therapy is still one of the biggest challenges in modern research. Despite the great effort and significant discoveries in biology, cancer is still the second leading cause of death worldwide after cardiovascular diseases. One of the fundamental reasons for finding a widely effective therapy is that cancer cells are characterized by developing drug resistance against antitumor agents. Moreover, novel, more precise therapeutic approaches based on recent clinical trials are significantly more expensive for treating many cancer patients. Thus, a better understanding of cellular response to chemotherapy seems crucial for achieving more efficient therapies available for many patients. Standard biomedical studies are still not efficient enough to provide good prognostic markers describing cancer cells' response against treatment with chemotherapeutic agents. On the other hand, recent developments in applied physics show that using physical parameters, i.e. elastic modulus of biological samples, allows discriminating between cancerous cells/tissues and their healthy counterparts. Highly redundant data, obtained by various research groups, make investigators and physicians start thinking about mechanical markers as diagnostic ones in neoplastic and other diseases (57–59). In the field of those developments, the question arises whether dynamic changes of mechanical properties of cancerous cells might be used as a prognostic marker of anticancer drug action. Thus, this thesis aims to answer whether chemotherapeutic agents action affects prostate cancer cells mechanics and whether such changes might be treated as markers of drug resistance of prostate cancer cells. The following specific objectives were defined:

- Validation of elasticity maps and multilayer approach for the determination of mechanical properties of cells.
- Characterization of biological effects of microtubules targeting drugs (MTDs) on prostate cancer cells.
- Characterization of time-dependent changes in mechanical properties of DU145 cells treated with three types of MTDs (colchicine and vinflunine, which destabilize microtubules and docetaxel, which stabilize microtubules).
- Evaluation of changes in the organization of the cytoskeleton being the cellular structure responsible for maintenance of physical properties of cells.
- Validation of the AFM-based elasticity approach towards separating mechanical response originating from nucleus regions or cell periphery.
- The determination of whether distinct mechanical properties can characterize prostate cancer cells pre-treated to exhibit drug-resistant functionality.

3. Materials

3.1 Antitumor drugs

Vinflunine Ditartrate (TRC Canada; V314500), characterized by the molecular weight of 1117,1 g/mol, was purchased in the form of powder. It was dissolved in distilled water to obtain its 1 mM stock concentration. For further experiments, the stock was diluted to obtain a desired final concentration in a cell culture medium.

Docetaxel (Sigma-Aldrich; 01885), characterized by the molecular weight of 807,9 g/mol, was purchased in the form of powder. It was dissolved in 99,8% ethanol (Sigma-Aldrich; V001229) to obtain a final concentration of 1000 nM. For further experiments, the stock was diluted to obtain a desired final concentration in a cell culture medium.

Colchicine (Sigma-Aldrich; C9754), characterized by a molecular weight of 399,4 g/mol, was purchased in the form of powder. It was dissolved in 99,8% ethanol (Sigma-Aldrich; V001229) to obtain a final concentration of 1000 nM again as above. For further experiments, the stock was diluted to obtain a desired final concentration in a cell culture medium.

Cytochalasin D is characterized by the molecular weight of 507.6 g/mol, and it was purchased as a powder. It was dissolved in DMSO. For further experiments, the stock was diluted to obtain a desired final concentration in a cell culture medium.

3.2. Cell cultures

The central core of the presented study described in the thesis was conducted on the DU145 cell line. These cells represent prostate cancer. They are adherent cells of epithelial morphology, derived from 69 years old male patient suffering from carcinoma. DU145 cells have been derived from brain metastasis.

For continuous cell culture, DU145 cells were cultured in a cell culture flask with the bottom surface of 25 cm^2 (TPP; 90026) in Dulbecco's Modified Eagle's Medium with high glucose (DMEM, Sigma-Aldrich; D5796) supplemented with 10% of heat-inactivated Fetal Bovine Serum (FBS, Sigma-Aldrich). Cells were passaged every 3-4 days using a 1x trypsin-EDTA solution (Sigma-Aldrich;59418C). To provide low-glucose conditions, cells were transferred to cell culture dishes and cultured in DMEM (Sigma-Aldrich; D5921) without phenol red, with low glucose supplemented with 2 mM L-glutamine and 10% FBS. In

experiments regarding starvation of cells, DMEM without phenol red, with low glucose, was supplemented only with FBS but not with L-glutamine.

Additionally, experiments included in the thesis were performed using two bladder cell lines:

- HCV29 cells: adherent non-malignant epithelial cells derived from a male adult patient suffering from bladder carcinoma. Cells were derived from the ureter (60).
- T24 cells: adherent cells of epithelial morphology, derived from 81 years old female patient suffering transitional cell carcinoma. Cells were derived from the bladder (60).

3.3 Drugs cytotoxicity and proliferation of prostate cancer cells

To determine the cytotoxicity of microtubules targeting drugs, CellTiter 96® AQueous One Solution Cell Proliferation Assay (MTS) (Promega; G3582) was used. As such, 3000 cells were seeded per well on a 96-well plate. After one day of incubation, the cell culture medium was replaced with the fresh one, and drugs were added to obtain the following concentrations:

- vinflunine: 0, 50, 100, 350, 500, 750 1000, 2000 [nM]
- colchicine: 0, 0.01, 0.05, 0.1, 0.25, 0.5, 1, 2 [nM]
- docetaxel: 0, 0.1, 0.5, 1, 2.5, 5, 10, 20 [nM].

Cells were then incubated with drugs for 72 hours. After this time, colourimetric measurements with a spectrophotometer (ELISA SPECTROstar Nano, BMG LABTECH) were performed. The absorbance was determined at 490 nm. Then obtained data were normalized to control and fitted to obtain IC_{50} dose for each drug.

The proliferation of cells was determined by counting trypsinized cells with the use o hematocytometer. Cells were seeded on multiwell plates in concentration 3000 cells/cm^2 and were counted after 24, 48, and 72 hours of incubation with drugs. For proliferation assessment following drug doses were chosen:

- vinflunine: 100 nM and 750 nM
- colchicine: 0.1 nM and 0.5 nM
- docetaxel: 1 nM and 5 nM.

The impact of drugs actin in low doses (100 nM VFL, 1 nM DTX and 0.1 nM COL) on cell death was investigated using flow cytometry. Cytometer (BD FACSCantoTM, Becton

Dickinson, New York, USA) (was accessible at the Chair of Pharmacology CMUJ). Cells were seeded in density 50 000 cells/per well in 6-well plates, and then after one night of culture, the cell culture medium was replaced with the fresh one, and drugs were added. After 48 and 72 hours of culture, the cell culture medium was collected for each of the investigated samples and then cells were trypsinized. Here it should be underlined that pooling together culture media with trypsinized cells allows determining the actual number of necrotic cells, which are detached from the substrate during the process of cellular death. The suspension obtained during this procedure was stained with 100 µl of binding buffer containing 5 µl of Annexin V-FITC and 5 µl of propidium iodine (PI) for 15 minutes. After this time, cells were analyzed using a flow cytometer.

3.4. Staining of cells for fluorescent imaging

To visualize cell structure, a fluorescent microscope (Olympus IX81, available in Department of Biophysical Microstructures at IFJ PAN) equipped with a fluorescence camera XC10 (1.4 mln pixels) and a Leica TCS SP8 X confocal laser-scanning microscope (Leica Microsystems CMS GmbH, Germany, available in the Laboratory of *in vivo* and *in vitro* Imaging at the Maj Institute of Pharmacology, Polish Academy of Sciences) were applied.

Cells were prepared as follows. After 72 hours of cell culture, cells were washed 2 times with Dulbecco's Phosphate Buffered Saline (DPBS, Sigma-Aldrich) and fixed with 3.7% paraformaldehyde for 30 minutes. After fixation, cells were washed 3 times with DPBS, and their membrane was permeabilized by 5 minutes of treatment by cold 0.2% Triton X-100 solution. After this step, cells were washed 3 times with DPBS and incubated overnight with anti-β-tubulin antibody conjugated with fluorescent dye Cy3 (1:200) (Sigma-Aldrich). After this period, cells were washed 3 times with DPBS and incubated for 60 minutes with phalloidin conjugated with Alexa Fluor 488 dye. Consequently, after this period, cells were washed 3 times with DPBS and incubated for 15 minutes with Hoechst 33342 (0.2 µg/mL). The last step was followed with 3 times wash of cells with DPBS and proper preparation for the following imaging. For epifluorescent imaging, cells were kept in DPBS, while for confocal microscopy, cells were immersed in a mounting medium (Mountant, Cambio).

Recorded fluorescent images were then analyzed using dedicated software: Leica Application Suite X software (3D Movie Editor, Leica Microsystems CMS GmbH,

Germany), CellSens Dimensions (Olympus) and ImageJ 1.51n (Wayne Rasband, National Institute of Health, USA).

3.5 Sample preparation for AFM measurements

Prostate cancer DU145 cells were seeded at the density of 5000 cells/cm^2 in DMEM without phenol red, with low glucose supplemented with 2 mM L-glutamine and 10% FBS. After one day of culture, drugs were added in desired concentrations, and cells were incubated with drugs for 24, 48 or 72 hours. For the measurements, cells were kept alive in a standard cell culture medium without phenol red. One sample with living cells was measured for about 1-1.5 hours.

Bladder cancer cells (HCV29 and T24) were seeded in density ~500 cells/cm^2 to obtain single cells after 24 hours of cell culture. After 24 hours, living cells were measured in a cell culture medium for the maximal time of 2 hours, which is a safe time for measurements of living cells.

In the experiments on starving cells, prostate DU145 cancer cells were seeded in the density of 5000 cells/cm^2 in DMEM without phenol red, with low glucose supplemented with 2 mM L-glutamine and 10% of heat-inactivated Fetal Bovine Serum. After one day of culture, the cell culture medium was replaced with a standard cell culture medium (control cells) or standard cell culture medium without 2 mM of L-glutamine (L-GLN depleted). For elasticity measurements, cells were washed 2 times with DPBS, and fixed with 3.7% paraformaldehyde for 30 minutes. After fixation, cells were washed 3 times with DPBS. Cell cluster maps were acquired in DPBS. At this step, fixation was applied to avoid DU145 cells movement during the acquisition of maps and obtain the highest probing accuracy.

3.6 Wound-healing assay of cancer cell migration

50 000 of DU145 cells were seeded per one Culture-Insert 2 Well in (ibid) and cultured overnight. After this time, inserts were removed, and the cell culture medium was replaced with a standard cell culture medium (control cells) or standard cell culture medium without 2 mM of L-glutamine (L-GLN depleted). Bright-field microscopy images of the wound between cell culture areas were acquired (time = 0 h). After 8 hours, bright-field

microscopy images of the wound were acquired (time = 8 h). Area of healed wound (*A*) was calculated from the following formula:

$$A = \frac{A_{0h}}{A_{8h}}$$

where A_{0h} is the area of wound intimately after the start of the experiment and A_{8h} is the area of wound after 8 hours of wound healing duration. The application of Culture-Insert 2 Well in (ibid) allowed for the highest accuracy of measurements, while standard scratch wound-healing assay done by pipet destruction of cells monolayer results in higher errors and data variability.

4. Experimental methods

4.1 Atomic force microscopy (AFM)

Atomic force microscopy (AFM) has been initially invented for imaging nanoscale objects with a lateral resolution of 30 Å and vertical resolution of 1 Å (61).

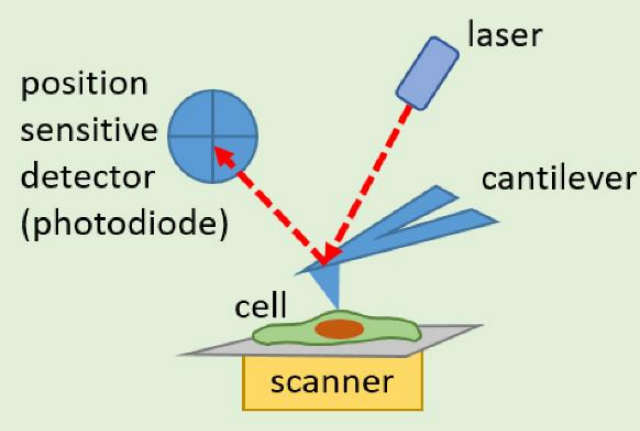

Fig. 4.1. *Schematic principle of AFM measurements of a cell. The cell is kept in a liquid chamber, providing living conditions for the cells. Deflection of cantilever resulting from its interaction with the cell surface is recorded by an optical system consisting of a laser and position-sensitive detector (photodiode). Adopted and modified from Kubiak et al., Int. J. Mol. Sci., 21 (2020) 8786, under CC* (47).

In the AFM, the force acting on the probing tip and the sample surface cause the deflection of the cantilever. The deflection is recorded with the use of an optical system. In a typical AFM, a laser beam is focused at the end of the cantilever. Cantilever deflection changes the position of the reflected laser beam. The position is measured by a position-sensitive detector, i.e. a photodiode (**Fig. 4.1**). In the optical system, the deflection of the cantilever is measured in volts; there is a need to properly calibrate the system to obtain precise information about cantilever deflection in the metric unit. AFM measurements aim to gain information about forces, thus, deflection of cantilever need to be calculated into force (F) of interaction following Hook's law which states:

$$F = k \times x \tag{4.1}$$

where *x* is the deflection of the cantilever and *k* is the spring constant of a cantilever. The deflection of the cantilever is measured in volts converted into force units using the following formula:

$$F[nN] = I\,[V] \times invA\left[\frac{nm}{V}\right] \times k\left[\frac{N}{m}\right] \tag{4.2}$$

where *I* is the signal recorded in the AFM in volts, *invA* is the photodetector sensitivity.

4.1.1 Cantilever spring contact determination

Cantilevers are most often manufactured from silicon nitride and are well characterized by the mean of their nominal physical and geometrical properties (i.e. thickness, length, geometrical descriptors of shape of the probe, spring constant and resonance frequency). Those parameters are then used to determine the actual spring constant of a cantilever, which is crucial for proper measurements of the physical properties of samples. The method used to determine the spring constant is based on the cantilever's thermal excitations, in which the resonant frequency of the cantilever free end is recorded. Boltzmann's equipartition theorem connects the resonant frequency of the thermally excited cantilever with the spring constant. The following equation reflects such relation:

$$\frac{1}{2}k\langle x^2\rangle = \frac{1}{2}k_B T \tag{4.3}$$

where *k* is cantilever spring constant, $\langle x^2\rangle$ is the time average of the amplitude vibration, k_B is Boltzmann constant, and *T* is the absolute temperature. The exemplary thermal spectrum of the cantilevers (ORC8, cantilever D, from Bruker) used in the thesis is presented in **Fig. 4.2**.

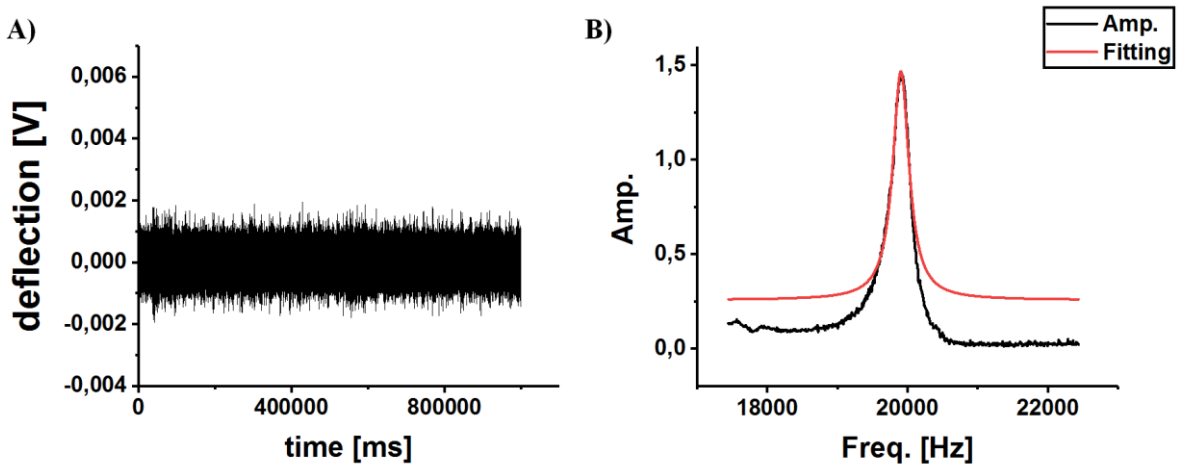

Fig. 4.2. (A) Deflection of the cantilever free end recorded as a function of time for the ORC8 cantilever type D used for the measurements. (B) A thermal spectrum obtained after applying the fast Fourier transform (FFT) to the data recorded in (B). The nominal resonant frequency (provided by the manufacturer) was 18 kHz. The actual resonant frequency was 19.9 kHz. The data were fitted with the Lorentzian function (the black line represents experimental data, while the red line is a fit).

Assuming that the mass of a particular cantilever is equal to nominal mass, the following rule was applied to determine the actual value of the force constant in relation to its nominal value:

$$k_{cant} = k_{nom} \times \left(\frac{f_{cant}}{f_{nom}}\right)^2 \tag{4.4}$$

where k_{can} is the actual cantilever spring constant, k_{nom} is the nominal cantilever spring constant provided by the manufacturer, f_{cant} is the measured resonant frequency, and f_{nom} is the nominal resonant frequency.

4.1.2 Photodetector sensitivity determination

Photodetector sensitivity is a factor linking the deflection recorded in volts with the corresponding deflection in nanometers. To obtain its value, the force curve is recorded on the stiff-undeformable substrate. In such a situation, the cantilever deflection reflects the position of the piezoelectric scanner.

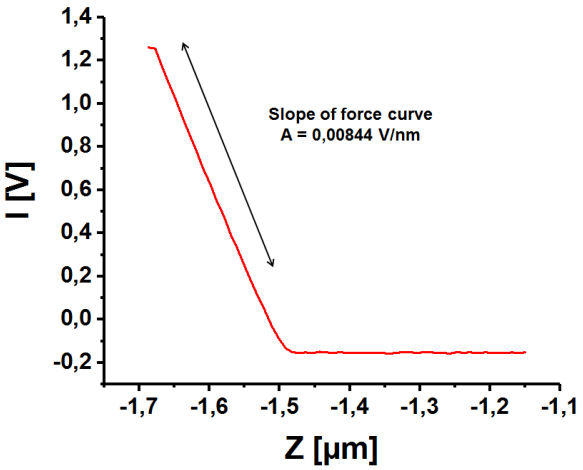

Fig. 4.3. *Representative calibration curve recorded on a glass coverslip surface with ORC8 cantilever type D. Red line presents experimental data, black line with arrows denotes fit range for slope determination.*

An exemplary force curve used for calibration of the photodetector sensitivity is presented in Fig. 4.3. The determined slope is the inverse of the photodetector sensitivity (*invA*), describing the relation between volts and nanometers. Its value for ORC8 cantilever type D is 0.00844 V/nm resulting in *invA* = 118.48 nm/V.

4.2 Self-manufacture and characterization of spherical probes

Spherical probes were manufactured as described previously by Indrieri et al.(62). The principle of this method of fabrication of spherical probes relies on the physical properties of substrates and glass microspheres used in this procedure. The protocol is based on roughness induced non-wetting phenomenon (63). The idea is to put glass microsphere at the material at which the formation of capillary forces will be ultimately lower than capillary forces between glass microsphere and free cantilever. Once such a situation is achieved, it is possible to catch the glass microsphere to cantilever relying on capillary forces and then fuse it with cantilever during baking in 780 ^{0}C. Capillary forces might be calculated as follow:

$$F_{cap} = 2\pi \mathrm{R}\gamma[\cos(\theta_1) + \cos(\theta_2)] \tag{4.5}$$

where R is the radius of the microsphere, γ is the surface tension of the liquid, and θ_1 and θ_2 are contact angles of surfaces between which capillary forces act. Thus in order to detach the glass sphere from the surface, it is crucial to obtain situation when:

$$F_{cantilever} > F_{surface} \quad (4.6)$$

where $F_{cantilever}$ is the capillary force between glass microsphere and cantilever and $F_{surface}$ is a capillary force of surface at which glass microspheres are prepared. The roughness-induced non-wetting phenomenon allows fulfilling this condition by properly functionalizing surface – in presented case slide microscopic glass.

Glass is well known to be characterized by ultimately low roughness with Root Mean Square – *RMS* ≈ 0.6 nm. It has been already shown that sputtering of glass slides with gold nanoparticles allows for increasing roughness of surface up to *RMS* ≈ 2.3 nm (62). Once the nano-roughness of material is increasing parallelly, its wetting angle is also increasing. In case of flat glass $\theta_1 = 0.08\pi$ while for gold-coated glass = 0.27π. Then, knowing the properties of the glass microsphere (radius $R = 5$ μm) and surface tension of the water ($\gamma = 0.07$ N/m) one can rewrite the equation for capillary force as follow:

$$F_{gold} = 2\pi * 5\mu m * 0.07\frac{N}{m}[\cos(0{,}08\pi) + \cos(0{,}08\pi)] = [\,2\pi * 5\mu m * 0.07\frac{N}{m}\,] \times 1.92 \quad (4.7)$$

$$F_{gold} = 2\pi * 5\mu m * 0.07\frac{N}{m}[\cos(0{,}08\pi) + \cos(0{,}27\pi)] = [2\pi * 5\mu m * 0.07\frac{N}{m}] \times 1.62 \quad (4.8)$$

Thus the relationship between those two forces is as follow:

$$\frac{F_{cantilever}}{F_{gold}} = \frac{1.82}{1.52} = 1.18 \quad (4.9)$$

This is significantly higher than for uncoated glass. The force of adhesion between cantilever and microsphere and microsphere and flat glass seems to be equal as so such an approach allows creating adhesion between glass microsphere and cantilever, which is sufficient for holding it in the oven to fuse microsphere with cantilever. Thus in the presented study, slide glass was put in plasma sputter coater in a vacuum with gold deposition parameters: $I = 20$ mA, $U = 1$ kV, and coating time $t = 30$ s (**Fig. 4.4**). Such time was sufficient to obtain a gold nano rough surface as described above.

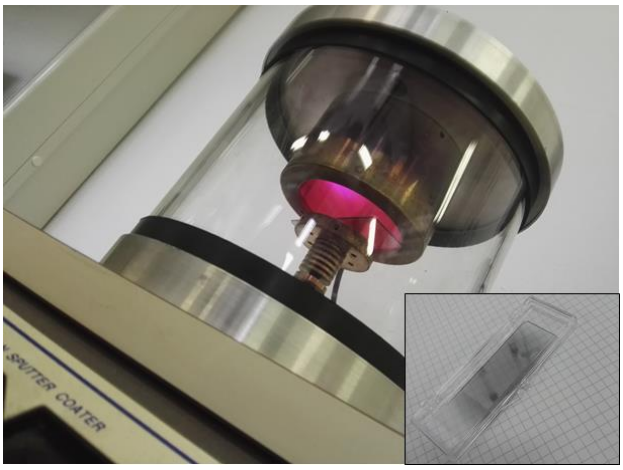

Fig. 4.4. *Gold sputter coater during plasma-induced coating of slide glass with a nanolayer of gold. Inset present representative gold-coated slide glass kept in a plastic box for isolation from interaction with a humid environment.*

In the next step, cantilevers with attached microspheres were very gently transported to the oven. Here, considerable caution was undertaken because rapid cantilever movement might lead to detachment of microsphere during transportation. The heating in the oven should be performed for 2 hours. At this time, the temperature inside the oven raised to desired 780 °C (**Fig. 4.5)**.

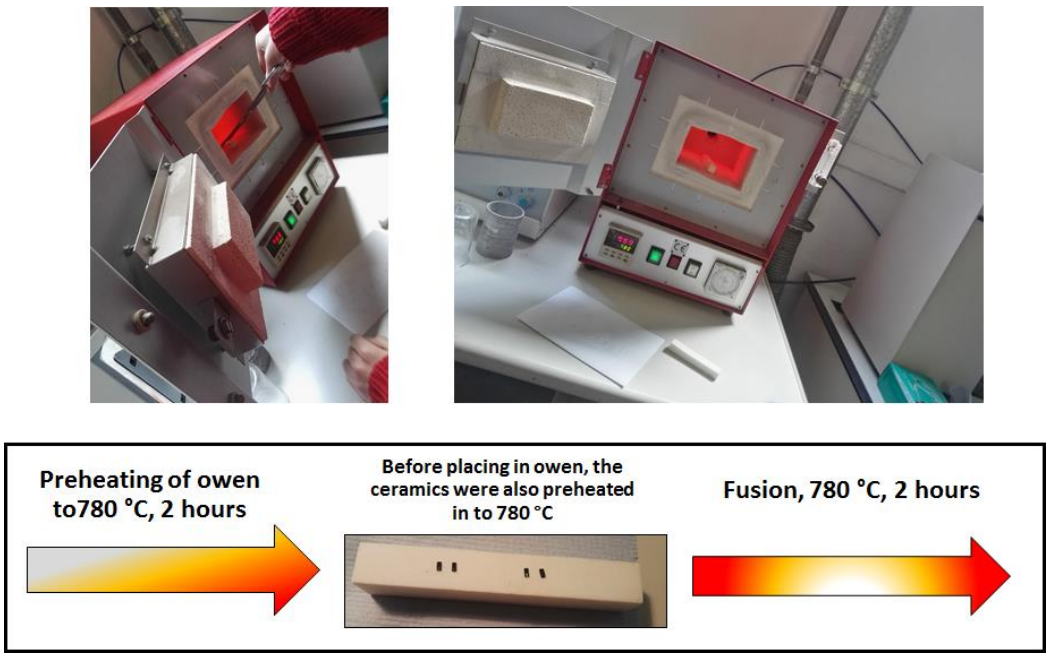

Fig. 4.5. *Scheme of the process of fusion of microsphere with the cantilever in the oven.*

It was essential to pre-heat ceramics used as an oven holder. Pre-heating preserve ceramics from the explosion might occur if ceramics is heated up to 780 °C. Such destruction results from microdamages present inside the ceramics. Once such protocol was applied, cantilevers were put on pre-heated ceramics inside the oven for 2 hours at 780 °C. After this time, the quality of fusion for each cantilever was verified under a light microscope. At this step, it was crucial to assess whether microspheres were attached to the central part of the edge of the cantilever (like in commercially available ones). Cantilevers that were not fulfilling this condition were excluded from the experiments.

In the final step, the characterization of each cantilever with an adequately attached microsphere was conducted. In the first step, a method of inverted imaging was applied with the use of TGT-1 diffraction grating (NT-MDT) with a nominal height of 0.3 – 0.7 µm, the tip curvature radius of $\leq$ 10 nm, effective area 2 x 2 mm, and tip angle 50° ± 10° (**Fig. 4.6.A**). For each of the fabricated cantilevers, at least 3 images on a grid of 20 x 20 µm were collected (**Fig. 4.6. B**). All images were then analyzed using basic geometrical principles to determine the probe radius used to create inverted images of a particular dimension using TGT-1 grating. Geometric descriptors of spherical cap obtained by inverted imaging might be described as follow (**Fig. 4.6. D**):

$$R = \frac{h^2+a^2}{2h} \tag{4.10}$$

$A = \pi a^2,$ and thus $A = \pi h(2R - h)$ and for volume:

$$V = \frac{\pi}{3}h^2(3R - h) \tag{4.11}$$

what finally gives an equation:

$$V = \frac{2\pi}{3}R^3\left(1 - \sqrt{1 - \frac{A}{\pi R^2}} - \frac{A}{2\pi R^2}\right)\left(2 + \sqrt{1 - \frac{A}{\pi R^2}}\right) \tag{4.12}$$

In such description, *h* and *a* might be directly measured from topographical images, while *V* and *A* might be calculated. Then the relationship between calculated parameters is done, and *R* is obtained as a fit parameter of the function describing this relationship. As a result of such a procedure, a unique *R* of each cantilever is obtained with high accuracy.

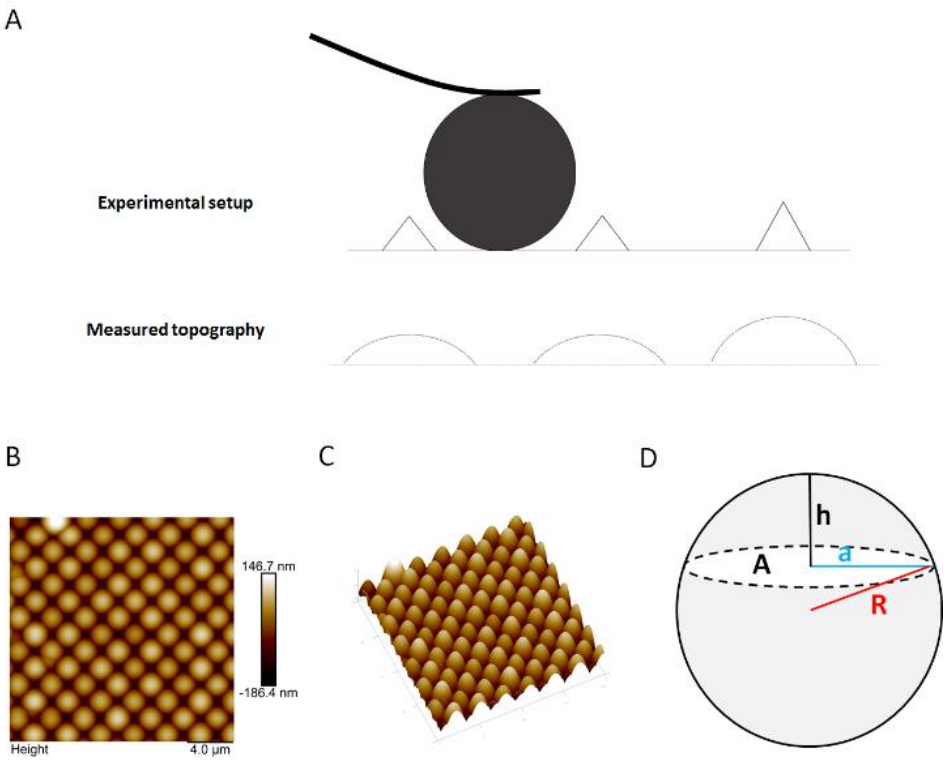

Fig. 4.6. *(A) Schematic principle of the method of inverted imaging with the use of AFM. (B) 2D topographical map of diffraction grating TGT-1. (C) 3D visualization of the topography of diffraction grating TGT-1. (D) Scheme of geometrical parameters used for determination of R from topographical maps.*

In the last step of characterization of spherical probes, their unique spring constant was determined using the thermal noise method (64). Spherical probes were prepared and characterized during an internship at the Department of Physics at Milano University.

4.3 Quantifying mechanical properties of soft objects using AFM data

4.3.1 Young's modulus determination

To obtain information on mechanical properties, the AFM measurements were realized as follows. Matrix of force curves was recorded over the nuclear region of the cell (**Fig. 4.7A**). In every single point of this matrix, the force curve reflects forces measured during both approach and retract of the cantilever (**Fig. 4.7A**). Then data were processed in order to determine Young's modulus of the sample measured in each of the points. Force versus

indentation curves were calculated by subtracting two force curves, i.e., the calibration curve was subtracted from the measured one (**Fig. 4.7B**).

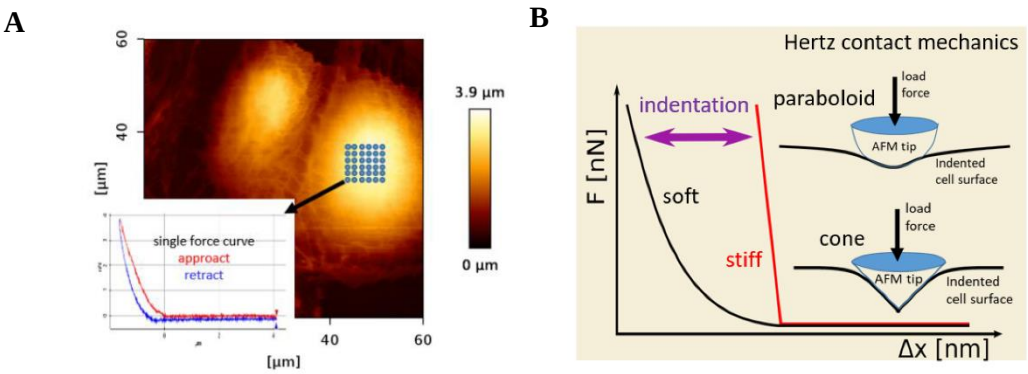

Fig. 4.7. *Principle of determination of mechanical properties of cells with the use of AFM. (a) Exemplary topography images recorded on DU145 cells on which a matrix of blue points was set over the nuclear region (inset – a representative force curve recorded in the single point of the matrix). (b) Principle of data analysis based on Hertz-Sneddon contact mechanics. Adapted and modified from Kubiak et al., Int. J. Mol. Sci., 21 (2020) 8786, under CC* (47).

Once the contact point was determined, the indentation depth was calculated as a difference of sample position (*Δx*, in **Fig. 4.7B**) taken for the same load force. The obtained relation between a force and indentation depth was analyzed using Hertz-Sneddon contact mechanics (65). Typically, AFM probes have a form of four-sided pyramids. Such a shape can be approximated either by a cone or a paraboloid. Thus, a relationship between force and indentation of the sample indented by a conical indenter is:

$$F(d) = \frac{2 \times \tan \alpha \times E'}{\pi} d^2 \tag{4.13}$$

while for paraboloidal approximation of indenter shape is as following:

$$F(d) = \frac{4 \times \sqrt{r} \times E'}{3} d^{3/2} \tag{4.14}$$

where F is the force, d is the indentation, α is the opening half-angle of probing tip, r is the radius of the tip, and E' is the reduced elastic modulus derived from the springs in the series connection modelling cantilever and cell mechanical properties:

$$\frac{1}{E'} = \frac{\left(1-\nu_{tip}^2\right)}{E_{tip}} + \frac{\left(1-\nu_{cell}^2\right)}{E_{cell}} \tag{4.15}$$

where *v* is the Poisson's ratio of the cantilever and cell, respectively. In the case of cells, its value is usually set to 0.5 because cells are often considered as an incompressible material.
The elastic modulus of the cantilever (typically, in GPa) is higher than that for living cells (typically, in kPa), thus:

$$E_{tip} \gg E_{cell} \tag{4.16}$$

As a result, the equation describing the reduced Young's modulus can be rewritten:

$$\frac{1}{E'} = \frac{(1-v_{cell}^2)}{E_{cell}} \tag{4.17}$$

Ultimately, the reduced elastic modulus of cells is:

$$E' = \frac{E_{cell}}{(1-v_{cell}^2)} \tag{4.18}$$

The elastic modulus of cells is derived by fitting the experimental data with the Hertz-Sneddon model depending on which approximation is the best in describing geometrical properties of the tip (**Fig. 4.8**).

A large database of data gathered the results of the AFM measurements of cell mechanical properties has already shown that in most cancers *(i)* cells are softer than their healthy counterparts (4,9,66,67), *(ii)* metastasis is associated with altered mechanical properties of cancer cells (68,69), *(iii)* disturbances in cell energetics might affect the mechanical stability of cancer cells (48), *(iv)* interactions between cells that occurs during wound healing affects their mechanical properties (41), and *(v)* mesenchymal stromal cells stiffen during prolonged culture, and those cells are characterized by low elastic modulus after transmigration (39). These findings demonstrate that AFM is a versatile technique used to characterise biomedical material with potential use in assessing processes associated with tumorigenesis and regeneration.

4.3.2 Indentation depth analysis of cell mechanical properties

The studies above rely on a standard approach in which a matrix of force curves is acquired, usually over the central part of cells corresponding to the nuclear region (**Fig. 4.7A**) (44). Thus, such a procedure is sufficient to perform comparative studies to discriminate between the overall mechanical properties of cells. Such defined mechanical properties are usually represented as a mean elastic modulus calculated considering all force curves

recorded within the central region of the cell. Analyzing different cellular compartments or mechanical properties characteristic for the particular depth of indentation are cases for which a specific data analysis approach has to be applied. The latter has been already proposed for AFM measurements of polymers and tissues by Kaushik et al. (70). It relies on the linearization of force curves and looking for different mechanical regimes. In principle, the first derivatives of linearized force curves show which part of the force curve is characterized by homogenous elastic modulus (within this range, the slope factor of the derivative remains constant). Thanks to such an approach, it is possible to choose particular indentation regimes which contribute to distinct cellular compartments characterized by the homogenous elastic modulus, which is ultimately different from surroundings (i.e. nucleus, actin cortex, cytoskeleton fibres). This method has a significant advantage over standard indentation-based approaches – it does not average moduli of different compartments within chosen indentation depts, but conversely, it separates between physically distinct organelles in the three-dimensional and highly heterogeneous sample. At the same time, the indentation-based analysis relies on an approach in which elastic modulus is obtained as a result of the fitting of the contact mechanics model to experimental data withing chosen range of indentation **(Fig. 4.8.).**

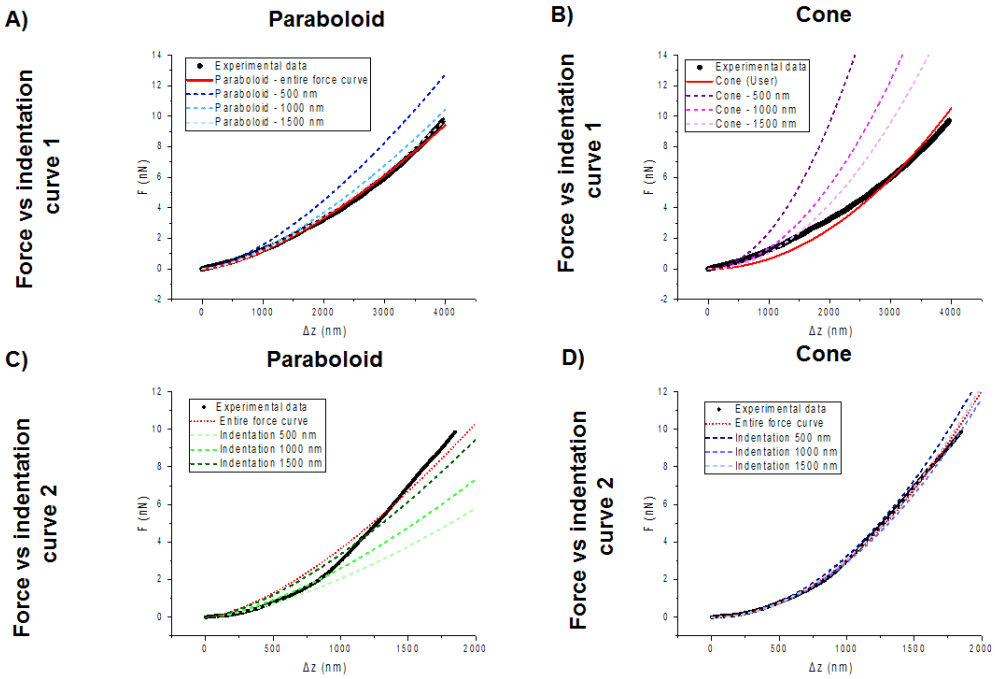

Fig. 4.8 Exemplary force versus indentation curves fitted with Hertz-Sneddon contact mechanics using two approximation of the AFM probe, i.e., cone (B,D) and paraboloid (A,C). Two force distinct force curves show that the fitting outcome depends on the chosen force curve and fitting range.

To interpret data obtained from AFM measurements, it is crucial to analyse AFM-derived data. As shown in **Fig. 4.8**, depending on a chosen force curve or fit range, different probing tip shape approximation might result in a proper fitting outcome. For force curve no 1, a paraboloidal approximation of indenter shape results in a better fitting outcome for all indentations (**Fig. 4.8A,B**). On the contrary, for force curve no 2, ultimately, a better fit is obtained for conical (**Fig. 4.8D**) approximation of indenter shape than for paraboloidal one (**Fig. 4.8C**). Such observation leads to the conclusion that fitting experimental data might introduce artefacts into final results. Importantly, in the case of force curves for which particular fit in entier range is the worst (**Fig. 4.8B,C**) fitting of experimental data within lower indentation (i.e. 500 nm) is resulting in the lowest deviation from experimental data. Thus in further experiments analysed with this approach, the indentation of 500 nm was chosen as it allows to fit experimental data with the lowest derivation from obtained model curves.

4.3.3 Finite thickness correction

While thinking about more precise determination of cell mechanical properties, it is desirable that nuclear region should be considered and cell body and lamellipodia (long cytoplasmic projections of cells usually filled with the cytoskeleton and used by cells to migrate). The height of lamellipodia is significantly lower than the nuclear region of a cell. As described above, AFM-derived data are analyzed using Hertz-Sneddon contact mechanics. The assumption is that the indented sample is an isotropic half-space with infinitive thickness. For low indentation depth and thick samples (i.e. the nuclear region of a cell), such assumption is treated to be fulfilled. However, for high indentation and thin samples (like cellular lamellipodia), the underlying stiff support affects the determination of Young's modulus. This leads to an overestimation of the elastic modulus. In past years, multiple approaches have been proposed to overcome that limitation in the AFM measurements of soft samples. In 2002 Dimitriadis et al. (71) proposed a method called *finite thickness correction* for paraboloidal indenter. In this approach, a cell is treated as a material semi-attached to a substrate resulting in the following equation allowing to correct force measured at such sample:

$$F = \frac{16}{9} E R^{1/2} \delta^{3/2} [1 + 1.009\mathrm{X} + 1.032\mathrm{X}^2 + 0.578\mathrm{X}^3 + 0.051\mathrm{X}^4] \qquad (4.19)$$

where the correction factor Δ is:

$$\Delta = [1 + 1.009X + 1.032X^2 + 0.578X^3 + 0.051X^4] \quad (4.20)$$

The equation (4.19) is an average of two equations, first derived using an imaging method for a bounded sample and second derived using the integral transform method, loosely placed at the substrate. The crucial part of this equation is parameter *X* which is calculated from the following equation:

$$X = \frac{\sqrt{R \times \delta}}{h} \quad (4.21)$$

where *F* is the corrected force, *E* is the elastic modulus of the sample, *R* is the radius of the spherical probe, δ is an indentation, and *h* is the sample height. As seen from those equations (4.19 and 4.21), sample height is the most crucial determinant of the correction value. A tip radius and indentation are raised to power ½, thus have lower significance in calculating finite thickness correction. Finite thickness correction is essential for elasticity maps presenting mechanical properties of the nuclear region and lamellipodia during the measurements performed by large spherical probes.

4.3.4 Separating nuclear and peripheral contributions

To separate information on mechanical properties of different mechanical components of DU145 cells treated with VFL, COL and DTX, AFM measurements were conducted using spherical probes (measurements were realized during the internship at the Department of Physics at Milano University). The AFM used was Bioscope Catalyst AFM (Bruker). Force applied during measurements was set 10 nN, pixel size was ~ 4 μm^2, while the total size of the map was dependent on the size of the measured cluster of cells. The applied protocol separating nuclear and peripheral contributions (72) is schematically shown in **Fig. 4.9**.

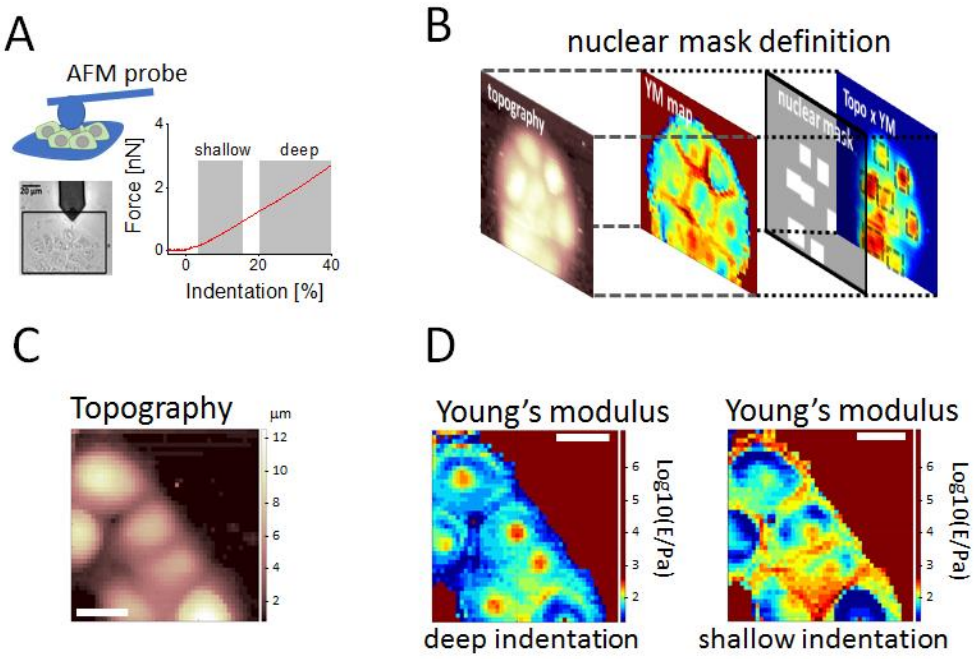

Fig. 4.9. *Principle of data analysis for advanced mechanical mapping of impact of microtubules-interacting drugs on DU145 mechanical properties. (A) Principle of force curve segmentation. (B) Principle of creation of mask for various cellular compartments. (C) Exemplary topography of DU145 cells growing in the cluster (D) Exemplary elasticity map of DU145 cellular cluster for deep and shallow indentation chosen by principle showed in (A). (reprinted with permission from Kubiak et al. Nanoscale 13 (2021) 6212 from The Royal Society of Chemistry)*

Briefly, each force curve was linearized by raising each of its points to the power of *2/3* in search of fragments showing a linear relationship between force and indentation. While the derivative of the linearized force curve is obtained, such linear fragments are characterized by the constant value of Young's modulus within one mechanical regime as a function of indentation. Applying this analysis to data obtained from DU145 cell clusters allowed to determine two regions (referred here as shallow and deep indentations) characterized by the distinct elastic modulus **(Fig. 4.9D).** In the next step, linearized force curves were fitted within the chosen mechanical regimes (in the range between δ_0 and δ by a simple linear fit where:

$$\delta - \delta_0 = \alpha F^* \tag{4.22}$$

The fitted parameter α is equalled to:

$$\alpha = \left(\frac{9}{16}\frac{1}{E\sqrt{R}}\right)^{\frac{2}{3}} \tag{4.23}$$

The F^* was defined as follows the $F^* = \left(\frac{F}{\Delta}\right)^{\frac{2}{3}}$. F^* denotes the linearized force after finite thickness correction, which was applied by dividing measured force F by correction factor Δ **(eq. 4.20).** In the last step of the analysis, so-called cell compartment masks were created to distinguish between different mechanical properties within the cell nuclear region and cell periphery. Such a mask can be obtained from a simple analysis of cellular topography where the highest parts of cells were considered to be localized directly above the cell nucleus (**Fig. 4.9C**). In the case of DU145 cells, this approach failed. Thus to overcome such a problem, a mask for analysis of particular cell compartments was prepared as point by point multiplication of matrixes representing both cell height and elastic modulus at each point. Such a mask was applied to determine regions of cell clusters corresponding to particular cell compartments.

4.3.5 Statistical analysis for the determination of Young's modulus

A lognormal distribution characterizes elastic moduli of cells measured by elasticity mapping. Thus to obtain a peak value of distribution, the semilog10 scale has been applied to presented data, and Gaussian has fitted such distribution. The median of elastic moduli for a particular cell cluster was then calculated for formula:

$$E_{median} = 10^{E_{peak}} \tag{4.24}$$

Followed by calculation of the standard deviation of the median (σ_{median}) as follow:

$$\sigma_{median} = \sqrt{\frac{\pi}{2}E_{median}}\frac{\sigma_g^{10}}{\sqrt{N}} \tag{4.25}$$

where σ_g^{10} is the geometric standard deviation, and N denotes the number of force curves considered. Overall error for one cellular cluster ($\sigma_{cluster}$) was then determined by summing quadrants of the standard deviation of median and instrumental error $\sigma_{instrumental}$.

$$\sigma_{cluster} = \sqrt{\sigma_{median}^2 + \sigma_{instrumental}^2} \tag{4.26}$$

Quantities depicted above were depicted to describe data distribution within one cell cluster (or data within the chosen cellular compartment of one cluster). To compare particular experimental groups mean elastic modulus of *n* clusters:

$$E_{mean} = \frac{\sum_i^n E_{median,i}}{n} \tag{4.27}$$

For mean elastic modulus determined from the equation (4.27), total error (σ_{total}) has been calculated as follow:

$$\sigma_{total} = \sqrt{\sigma_S^2 + \sigma_{mean}^2} \tag{4.28}$$

where σ_{total} is propagated error of the meanwhile σ_{mean} is the standard deviation of the mean, which are calculated from the following equations:

$$\sigma_S = \frac{1}{n}\sqrt{\sum_i \sigma_{median,i}^2} \tag{4.29}$$

and:

$$\sigma_{men} = \sqrt{\frac{\sum_i \left(E_{med,i} - E_{mean}\right)^2}{n}} \tag{4.30}$$

Calculations were obtained using custom-written software in the MATLAB environment available in the Department of Physics (Milano University).

5. Validation of the methodology used to analyze data

5.1 Introduction

In the presented thesis, two types of AFMs (Bioscope and Xe120 from Bruker and Park Systems, respectively) and, as a consequence, two types of probes (pyramidal and spherical) were applied to assess the effect of antitumor drugs on the mechanical properties of cells. The use of pyramidal probes carries the question of which approximation of the pyramidal shape (cone or paraboloidal) provides a better resolution. In contrast, spherical probes deliver data burdened by the effect of a stiff underlying substrate on the mechanical properties of cells. A comparison between the data analyzed with two approximations of the AFM tip is presented in the present chapter. A discussion relied on data obtained for bladder cancer cell lines (T24 and HCV29), chosen because they have already been characterized by the AFM elasticity measurements (66). It has already been shown that cancerous T24 cells are significantly softer than non-malignant HCV29 cells. Importantly the fold change in elastic moduli between those two cell lines was about a magnitude of 2 for indentation of 500 nm (66). Thus, those mechanically easy distinguishable cell lines are excellent model cell lines to verify which approximation is better. Such validation is needed as the studied DU145 cell line is not mechanically different from the accessible PC-3 or LNCaP cell lines as bladder cancer cells are (73). The effect of stiff substrate on the mechanical properties of prostate cancer cells treated with VFL is also described here.

5.2 Morphology of HCV29 and T24 bladder cancer cells

HCV29 cells (non-malignant cell cancer of ureter cells) are characterized by a fibroblast-like morphology with extensive cytoplasmic regions and lamellipodia. On top of the actin cortex, actin bundles forming stress fibres are visible in these cells (**Fig. 5.1A**).

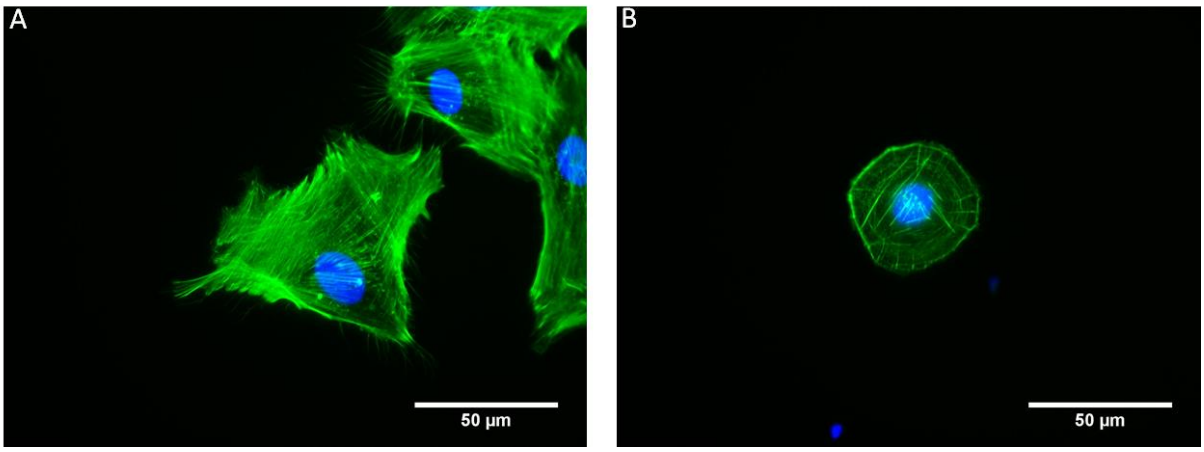

Fig. 5.1. *Fluorescent images of a) HCV29 and b) T24 cells showing the organization of actin filaments stained with phalloidin conjugated with Alexa-488 (green). Cell nuclei are labelled with Hoechst 33342, a dye-binding to DNA(blue).*

Cells derived from transitional cell carcinoma (T24 cells) are characterized by a round shape. The organization of actin filaments is similar to HCV29, i.e., actin cortex and stress fibres. Although their cancerous character, these cells still possess stress fibres. Their amount and thickness are smaller compared to those observed in HCV29 cells (**Fig. 5.1B**).

5.3 Elasticity properties of HCV29 and T24 cells

To determine the mechanical properties of bladder cancer cells, the elasticity maps were recorded over the whole individual cells **(Fig. 5.2)**. At each point in the map, a single force curve was recorded using the same cantilever type. This curve was further used to determine the elastic (Young's) modulus (according to the methodology described in Chapter 4.1). The data were fitted within the frame of Hertz contact mechanics using JPK software with two types of indenter shape approximations, namely, conical and paraboloidal. At this point, it should be noted that the shape of the ORC-8 cantilever is a four-sided pyramid, for which conical approximation is geometrically more accurate than the parabolic one. The obtained results are presented in **Fig. 5.2.**

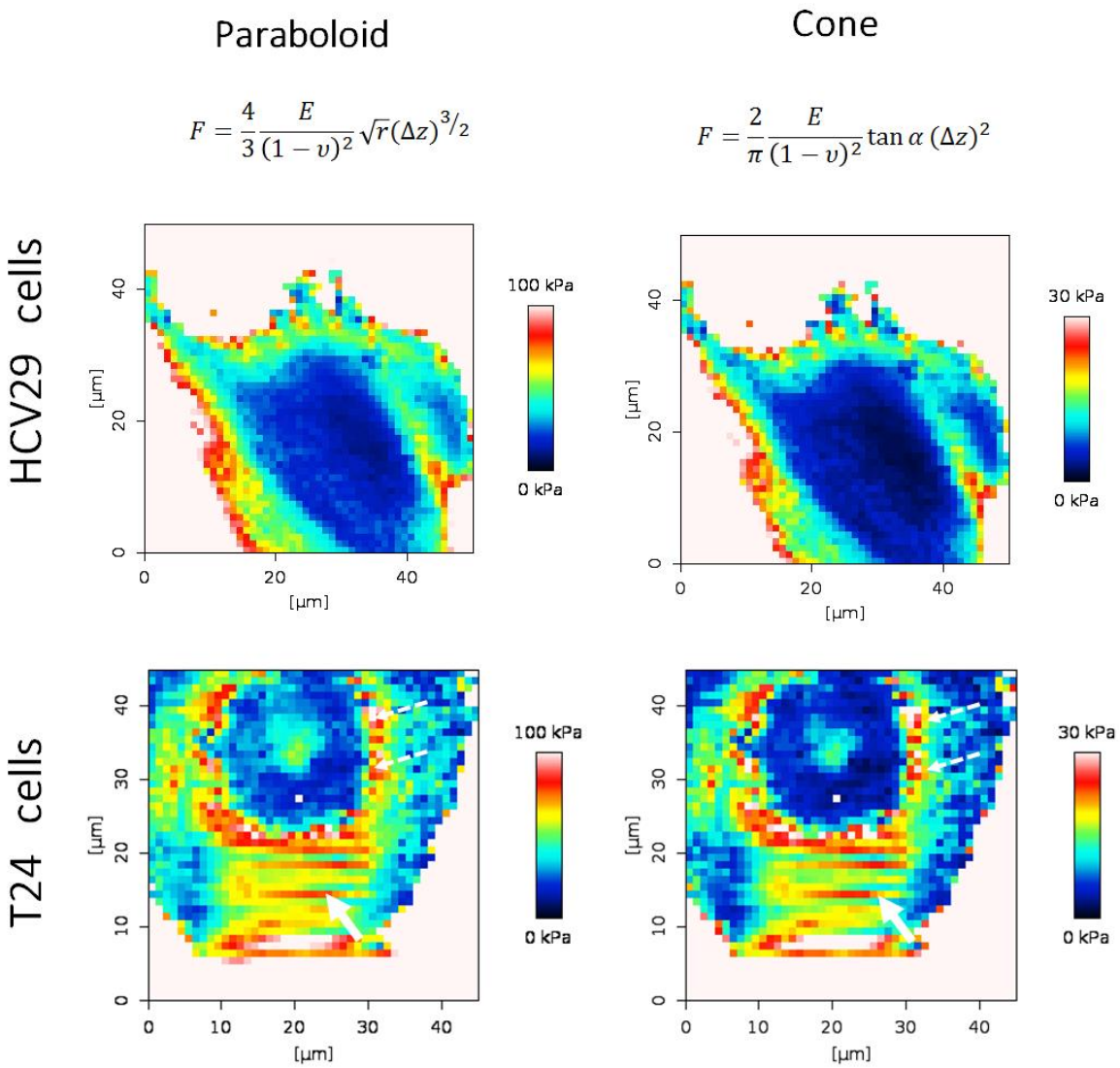

Fig. 5.2. *Representative elasticity maps of bladder cancer cells. The left panel represents the analysis result, assuming that the shape of the AFM tip can be approximated by a paraboloid, while the right panel – by a cone. Hertz-Sneddon contact mechanics was applied here to calculate Young's modulus.*

Elasticity maps, showing spatial Young's modulus distribution over a cell, reveal differences dependent on the cell type. For HCV29 cells, the stiffest part of the cell was located at the periphery. Then, the elastic modulus gradually decreased with the increasing height of the cell. The nuclear region was the softest part of HCV29 cells, regardless of the applied approximation of the AFM probe shape **(Fig. 5.2. top panel)**. Oppositely, in T24 cells, stiffer regions span from the border towards the cell centre. The nuclear region appears to be more deformable (i.e. smaller Young's modulus), except the very top part, in which elastic modulus increases. By comparing fluorescent and AFM images, one can conclude that the distribution

of mechanical properties is dependent on cellular morphology and cytoskeleton organization. Also, while comparing maps of mechanical properties to fluorescent images, the explanation might be again connected with the organization of the actin cytoskeleton. A weak actin cortex characterizes T24 cells. They possess a ring of stress fibres appearing around the cell nucleus (**Fig. 5.1b**). This observation is in line with the fact that soft gaps punctuate stiffer regions at the cell body of T24 – correlating in gaps between stress fibres observed in T24 cells fluorescent images (**Fig. 5.2**). In the case of HCV29 cells, a uniform increase in cell deformability seems to be associated with an increase in the height of the sample (**Fig. 5.2**). These cells are also characterized by a uniform distribution of dense actin cortex (**Fig. 5.1a**), thus, larger Young's modulus observed at the cell periphery might result from the substrate effects.

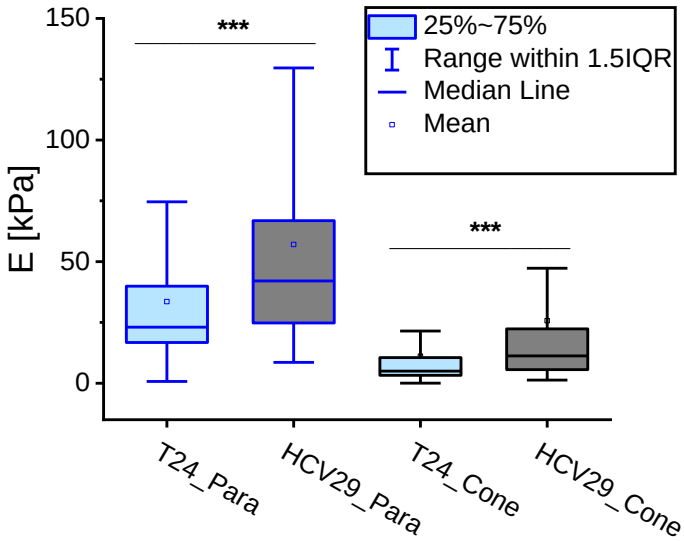

Fig. 5.3. *Box plot showing the variability of Young's modulus in cells. Data for both paraboloidal (PARA) and conical (CONE) approximations of indenter shape are presented. Data are presented in boxplots (25^{th} ~ 75th percentiles), with whiskers indicating a range within 1.5 interquartile range, horizontal line denotes mean, open square denotes mean, significance is calculated with t-test, *** - $p<0.001$.*

For the paraboloidal approximation of the indenter shape, the mean value of T24 cells elastic modulus is 33.6 ± 31.0 kPa (n = 5317, where n is the number of force curves taken into analysis and error is the standard derivation), while for HCV29 cells its value equals to 57.0 ± 50.2 kPa (n = 5660). When conical approximation of indenter shape is applied, the mean Young's for T24 cells is 11.1 ± 23.7 kPa (n = 5384), while for HCV29 cells, it is 25.7 ± 43.8

kPa (n = 5876). Independently of the applied approximations of the indenter shape, HCV29 cells are significantly stiffer than T24 cells. Such observation is in line with previously published data showing the same trend (66).

To evaluate the ability to detect the difference between the studied cells, the fold change (X^{model}) was calculated as follows:

$$X^{para} = \frac{E_{HCV29}^{para}}{E_{T24}^{para}} = 1.6993 \quad (5.1)$$

$$X^{cone} = \frac{E_{HCV29}^{cone}}{E_{T24}^{cone}} = 2.3183 \quad (5.2)$$

Smaller fold value denotes the worse capability to detect mechanics-related differences between two cell populations. In bladder cancer cells, the fold change is larger when a conical approximation of the AFM tip was applied, supporting the statements of larger sensitivity for conical probes. The fold change consideration help to decide which approximation of the tip shape should be used in pyramidal probes.

5.4. Finite thickness correction

To evaluate the effect of stiff substrate on mechanical properties of DU145 cells treated with vinflunine, the mechanical properties were analyzed with and without finite thickness corrections. As shown in **Fig. 5.4**, the mean height of DU145 cell clusters varies between ~4-6.5 µm. Thus one can state that the maximum mean indentation should be in the range of 400-650 nm. As shown in **Fig. 4.9**, such indentation is not sufficient to precisely visualize nuclear contribution. Thus, there is a need to use larger indentations. Consequently, the finite thickness correction has to be applied, particularly when spherical probes are applied. In this thesis, part of the measurements was conducted using spherical probes with 5 µm of diameter.

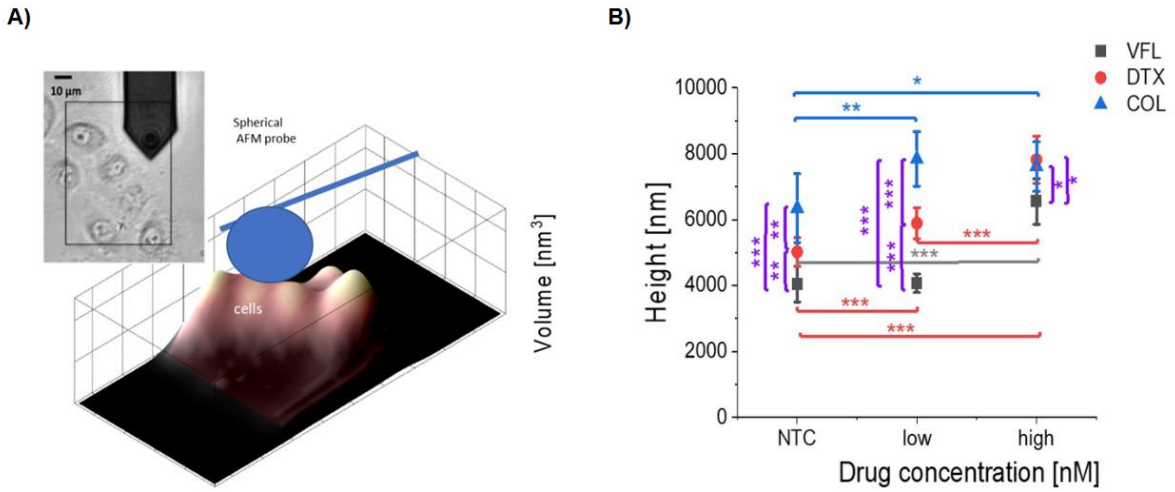

Fig. 5.4. Variation in mean height of DU145 cells measured with AFM. (A) example of 3D reconstruction of a height map of the cellular cluster. (B) The mean height of DU145 cell clusters in different conditions: NTC denotes the non-treated cells, VFL -treated for 72 h with vinflunine, DTX – treated for 72 h with docetaxel, COL – treated for 72 h with colchicine, low, high – denotes low, high MTDs concentrations, respectively. Data are presented as a mean ± σE; n = 8-12 clusters per condition. Statistical significance was estimated by unpaired t-Student test at the level of 0.05 (p < 0.05, ** p < 0.01, *** p < 0.001 (reprinted with permission from Kubiak et al. Nanoscale 13 (2021) 6212 from The Royal Society of Chemistry).*

To achieve maximum of the indentation of 2-3 microns, the load force was set to 10 nN what for multiple times exceed the threshold of 10% of sample height. Thus, the finite thickness correction is necessary to deliver Young's modulus accurately.

Although the finite thickness correction was applied to all data, the effect of stiff substrate on mechanical properties of DU145 cells is illustrated for cells treated with VFL (**Fig. 5.5**). Briefly, spherical probes with radius r = 5 µm were utilized to record the matrix of force curves over whole clusters of cells. Force curves were acquired both in the nuclear region and in thinner lamellipodia. Large probe together with small sample height introduced a need for finite thickness correction.

Data obtained from the measurements of cells acquired with the spherical probe were analyzed as described in subsections 4.3.3 and 4.3.4. When the analysis was performed without the application of finite-thickness correction, the elastic modulus was a function of cell height and did not depend on the intrinsic physical parameters of cells (**Fig. 5.5A**). In such a case, a lack of differences in sample elastic modulus was observed because elastic

modulus was a function of height (**Fig. 5.5C**). When the same experimental data were analyzed using finite-thickness correction, the dependence on the cluster height was compensated. Thus, the obtained modulus values can be linked with the intrinsic properties of the cells (**Fig. 5.5B**). In that case, dose-dependent stiffening was observed for DU145 cells growing in clusters (**5.5D**). Importantly, the trend of VFL dose-dependent stiffening was also visible in the case of cells measured using pyramidal probes (**Fig 5.5E**). Thus, such experimental results confirm that in AFM indentation experiments using spherical probes, finite thickness correction is obligatory. Without this correction, elastic modulus reflects sample height, leading to a lack of changes in determining the elastic modulus of cells known to differ in their mechanical properties (**Fig. 5.5A,C**).

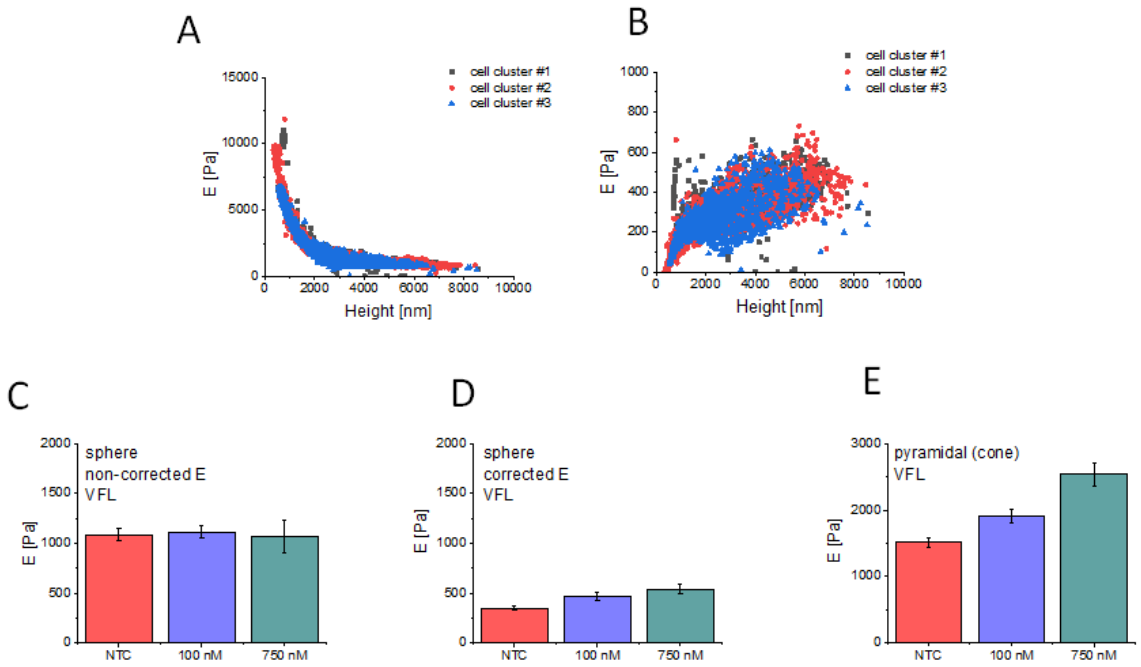

Fig. 5.5. Significance of finite-thickness correction. a) distribution of elastic modulus as a function of height when finite-thickness has been not applied for spherical indenters. b) distribution of elastic modulus as a function of height when finite-thickness has been applied for spherical indenters. c) Mean elastic moduli determined with the use of the spherical probe of DU145 cells cluster treated with VFL without finite-thickness correction d) mean elastic moduli determined with the use of the spherical probe of DU145 cells cluster treated with VFL with finite-thickness correction e) mean elastic moduli determined with the use of the pyramidal probe of DU145 cells cluster treated with VFL without finite-thickness correction (reprinted with permission from Kubiak et al. Nanoscale 13 (2021) 6212 from The Royal Society of Chemistry)

Measurements of DU145 cells performed with the pyramidal probe have been performed as follows. Briefly, a matrix of force curves has been recorded over the nuclear region of the cell with the use of a sharp tip characterized by a radius of curvature of 15 nm. Then, data were fitted with Hertz-Sneddon contact mechanics in the range of indentation of 500 nm to derive Young's modulus (**Fig. 4.9, 5.4B)**. For the nuclear region, this indentation was lower or equal to 10% of cell height; thus, the effect of the underlying substrate was not significant. Consequently, the obtained moduli changes revealed a dose-dependent stiffening analogous to cells measured with spherical AFM probes after finite thickness corrections (**Fig. 5.5E**).

5.5 Discussion

AFM has been so far utilized in studies concerning the mechanical properties of cells. Since multiple aspects of tumorigenesis are accompanied by changes in the physical properties of cells and tissues, studies in that field present a very promising approach that might be utilized both for a better understanding of cancer pathogenesis and attempts to design new therapies (3,9,74–77). Because AFM is a versatile method, recently, multiple efforts have been undertaken to improve the measurements towards obtaining more sophisticated information about the physical properties of cells. For example, modes of action allowing for simultaneous imaging and probing material stiffness have been developed (78). Such methods have been already successfully applied to probe cellular topography and nanomechanics (79). One of the drawbacks is that during mapping of cell with quantitative imaging, time for measuring each force curve is short, resulting in the shallow indentation and lower resolution of force versus indentation curve. Thus, obtaining more precise information about mechanical properties of cellular mechanics elasticity mapping with the recording of standard force curves over whole cells seems to be more precise and physically relevant. Such an approach have been already proposed by Puricelli et al. to investigate the mechanical properties of PC-12 rat pheochromocytoma cells and MDA-MB-231 human breast adenocarcinoma cells (72). In the present chapter, validation of such approaches was performed for cell lines that were already characterized by standard AFM elasticity measurements of bladder cell lines T24 and HCV29. In previous studies conducted by Ramos et al., T24 cells are about two times softer than HCV29 cells (66). A similar trend was obtained for bladder cancer cells studied here (Fig. 5.3). In Puricelli et al., authors use spherical probes characterized with radius in order of magnitude of cell height (72). Such

large probes during indentation of cells are affected by the presence of the stiff substrate leading to the overestimation of the elastic modulus. To minimize the impact of the stiff substrate, finite thickness correction for paraboloidal approximation of indenter shape was applied (71,72). Such correction was also proposed for the conical approximation of indenter shape by Gavara et al. (80) and then updated by Garcia P. & Garcia R. (81). In the present study, the use of the correction for measurements conducted using a pyramidal indenter was not necessary because cells were probed only within the nuclear region (which is the highest part of the cell), and the indentation depth chosen for data analysis was lower or equal to 10% of sample height (71).

The significance of stiff substrate is an important factor that might affect a proper interpretation of the AFM-based elasticity results obtained for cells growing on glass coverslips or plastic cell culture dishes (44,71,72,81–83). Rheinlaender et al. showed that soft substrate might also introduce an artefact during the estimation of elastic modulus of cells growing on such substrate (82). Observed softening of cells cultured on soft substrates results from changes in cells' mechanical properties but stems from the substrate’s properties. To avoid this effect, the authors proposed a correction of soft substrate contribution and showed that for microglia cells, substrate stiffness does not affect the elastic modulus of cells when the correction is appropriately applied (84). In conclusion, the elasticity maps are valuable for the nanomechanical characterization of living cells.

5.6. Summary

Analysis of data obtained during AFM measurements of cellular mechanical properties is crucial for delivering reliable conclusions. In order to ensure such an analysis method in this chapter, its evaluation was carefully performed. Two bladder cancer cell lines were utilized here (HCV29 and T24) for this purpose because their mechanical properties have already been characterized. Thus, those cells were the perfect model for the evaluation step. The following conclusions can be drawn out of the results obtained here:

- T24 cells significantly differ from HCV29 cells in the way how their cytoskeleton is organized. In HCV29 cells, actin is uniformly spread over the whole surface of the cells, while in T24 cells, actin stress fibres are visible in a ring around the cell nucleus.
- When elastic modulus means were compared, T24 cells were significantly softer than HCV29 cells.

- Maps of elastic modulus obtained for each point were strongly in line with the results of fluorescent imaging results. For HCV29 cells with the uniformly spread cytoskeleton, the elastic modulus increased with decreasing height, indicating the possible contribution of the underlying stiff substrate. Oppositely, for T24 cells, stiffer rings were detected in places corresponding to rings of actin stress fibres.
- The key element of elastic modulus determination is a fit of experimental data to the contact mechanics model. The detailed analysis of the elasticity maps shows the importance of choosing the model approximating the shape of the indenting AFM tip. For pyramidal tips, conical approximation allows for better visualization of differences between cells than a paraboloidal approximation.
- The impact of substrate stiffness might introduce artefacts, especially while AFM tips with large radius are utilized, and indentation exceeds 10% of sample height (i.e. lamellipodia). Application of finite thickness correction allowed to reduce artefacts arising from stiff substrate response. In detail, while DU145 cells were treated with VFL, it cased their dose-depended stiffening, when cells were measured with pyramidal probes and data were fitted with a conical approximation of indenter shape. In contrast, the measurements of cells with a spherical probe resulted in a lack of changes when data were analysed by a straightforward fit of the Hertz model. The same data measured with the spherical probe were analyzed by the Hertz model but using Dimitriadis finite-thickness correction. Consequently, DU145 cells treated with VFL exhibited dose-dependent stiffening – the same as in DU145 cells measured with pyramidal AFM tip.

To sum up, elastic maps showing a modulus of whole cells, including their different compartments, serve as a great method of investigating the mechanical properties of cells. However, a data analysis that considers AFM probe geometry and sample height must be applied to obtain reliable results.

6. Time-dependent biological effect of MTDs action on prostate cancer cells (DU145)

6.1 Objectives

The main objective of this part was to elaborate on the time-dependent impact of microtubule-targeting drugs (MTDs) on DU145 prostate cancer cells. Therefore, at the first steps of the studies, the biological effect of MTDs on prostate cancer DU145 cells was evaluated as a function of drug exposure (from 24h to 72h). MTDs cytotoxicity was determined using an MTS assay. Proliferation level was quantified by counting cell culture with and without the MTDs presence. The number of apoptotic cells was quantified using flow cytometry.

6.2 MTDs cytotoxicity assessed by MTS test

Important parameters needed to be assessed in evaluating potential anticancer drug are cytotoxicity, the best as selective as possible, and its impact on cell proliferation studied at first in vitro (cell culture model) and afterwards in vivo (animal model). In the present study, two methods were applied to assess the cytotoxicity of MTDs, namely, MTS assay (performed at IFJ PAN) and flow cytometry (performed with collaboration dr Malgorzata Lasota from Katedra Biochemii Lekarskiej, Collegium Mediucum UJ). Cell cytotoxicity was conducted for DU145 cells, treated with three types of MTDs: vinflunine (VFL), docetaxel (DTX), and colchicine (COL). Colourimetric MTS assay was performed after 72 h of drug treatment to determine IC_{50} value **(Fig. 6.1)**. In such a test, higher absorbance reflects higher cell viability. For each of investigated drugs, cells were treated with eight concentrations of the MTDs. The resulting relationship between drug concentration and cell viability was fitted with a drug-response function. The outcome of the fit is IC_{50} denoting the MTDs concentration at which 50% of cells died.

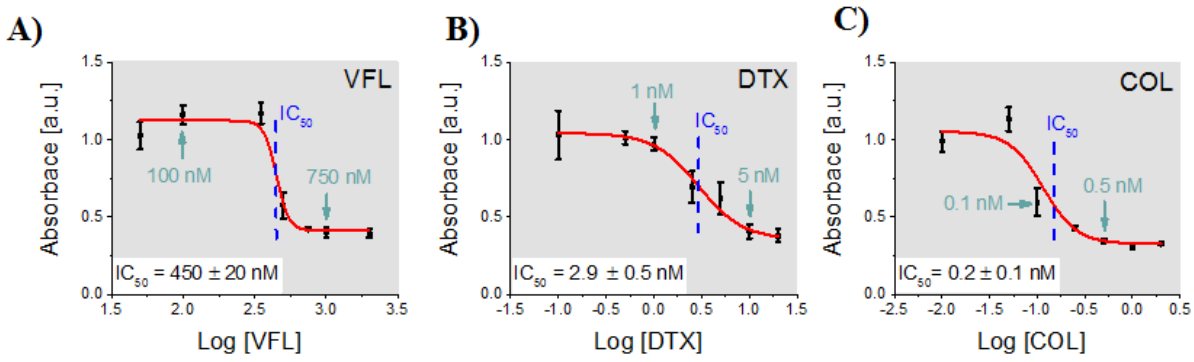

***Fig. 6.1**. MTS assay applied to determine the cytotoxicity level in DU145 cells treated with: A) vinflunine (VFL), B) docetaxel (DTX), C) colchicine (COL). Each point corresponds to mean absorbance ± standard derivation (for n = 3 repetitions). Data are fitted with a dose-response function that enables the determination of IC_{50} value for each applied drug (reprinted with permission from Kubiak et al. Nanoscale 13 (2021) 6212 from The Royal Society of Chemistry).*

The results are 450 ± 20 nM **(Fig. 6.1A)**, 2.9 ± 0.5 nM **(Fig. 6.1B)** and 0.2 ± 0.1 nM (**Fig. 6.1.C**) for VFL, DTX, and COL, respectively. Based on the obtained MTS results, two drug concentrations were chosen for each MTD for further experiments, i.e., low (below IC_{50}) and high (above IC_{50}). For VFL, the chosen concentrations were 100 nM and 750 nM, for DTX 1 nM and 5 nM, while for COL 0.1 nM and 0.5 nM.

In the next step, the amount of necrotic and apoptotic cells was quantified using flow cytometry. After 48 and 72 hours of the culture of DU145 in the presence of drugs in low doses, cells were incubated with propidium iodide (PI, which intercalates the DNA of cells with permeable membrane, i.e. necrotic cells) and annexin V, which is binding to phosphatidylserine (a plasma membrane phospholipid which is flipped to outer layer when cell start to undergo apoptosis). Such staining allows for the discrimination between four populations of cells: living (with a low signal from PI and annexin V), apoptotic (low signal from PI and strong from annexin V), and late apoptotic/necrotic (with a strong signal from PI and signal or its lack from annexin V). Obtained results are presented in **Fig. 6.2.**

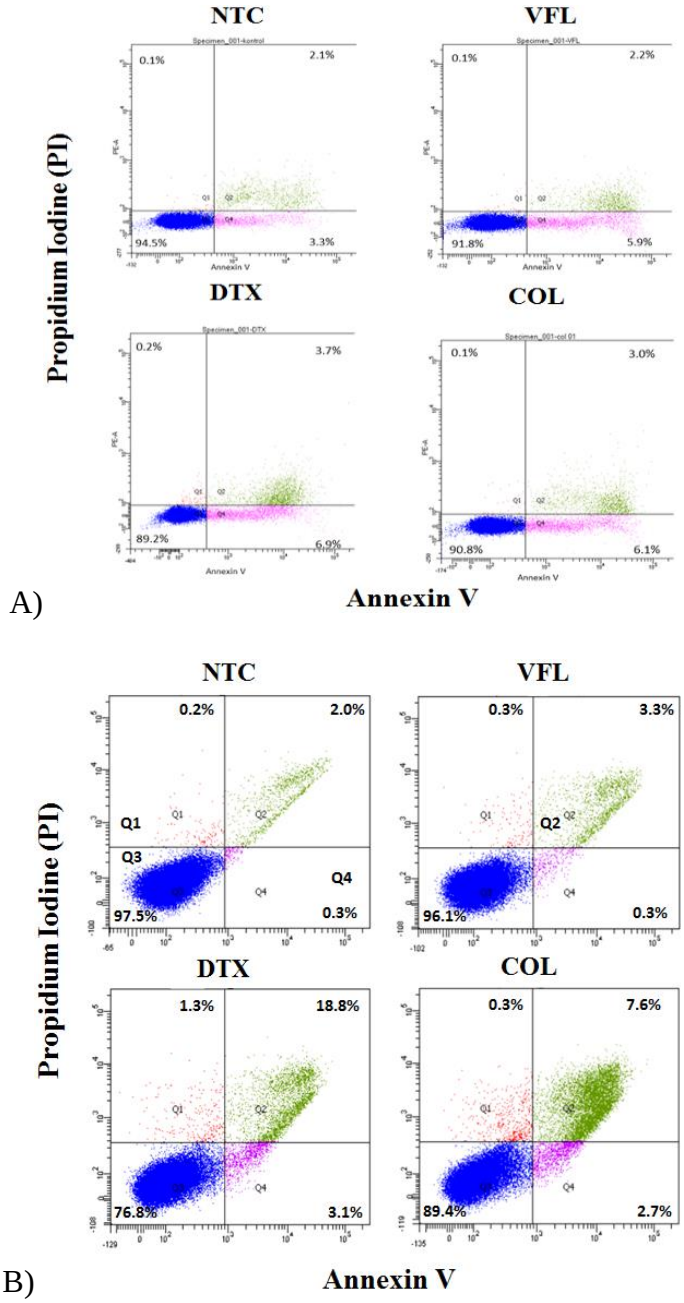

Fig. 6.2. *Flow cytometry was applied to quantify the number of necrotic and apoptotic cells treated with MTDs for A) 48h and B) 72h. Cross charts present the distribution of cells stained for markers of apoptosis (Annexin V) and necrosis (Propidium Iodine). Quadrant 3 denotes cells negative for both those markers – living cells, Q1 denotes cells positive for propidium iodide only – necrotic cells, Q2 denotes cells positive for both propidium iodide and Annexin V – late apoptotic cells, while Q4 denotes cells positive only for Annexin V – early apoptotic cells (reprinted with permission from Kubiak et al. Nanoscale 13 (2021) 6212 from The Royal Society of Chemistry).*

After 48 hours lack of significant changes in cellular viability between VFL-treated and COL and DTX-treaded cells was observed (viability in range of 89.2% to 91.8%, **Fig. 6.2A**). In fact, for all drugs, a slight decrease in viability was visible while comparing to NTC (**Fig. 6.2A**). While after 72 hours, in the case of the control cell, overall viability was very high, with 97.5% of living cells (**Fig. 6.2B**). 100 nM concentration of VFL hardly reduces the overall viability of DU145. The obtained level of living cells was 96.1 % (**Fig. 6.2b**). For cells treated with 0.1 nM of colchicine, viability decreased - 89.4% of living cells, while for docetaxel, mortality of cells was the highest with 76.8% of living cells (**Fig. 6.2B**). Those observations of the most substantial impact of DTX on DU145 cells viability were in line with the observation of proliferation analysis where the lower number of cells treated by low drug doses was characteristic for DTX treated cells (**Fig. 6.3B**). Notably, a significant drop in cellular viability between 48 and 72 hours was observed only for DTX treaded cells (from 89.2% to 76.8%, Fig. 6.3a,b), proving that this drug exerts the strongest effect on DU145 cells.

6.3. Proliferation level of DU145 cells upon MTDs action

The impact of MTDs on cell proliferation was determined in a time-dependent manner by counting control and drug-treated cells. **Figure 6.3**. presents changes in the number of DU145 cells treated with: 100 and 750 nM VFL (**Fig. 6.3A**), 1 and 5 nM DTX (**Fig. 6.3B**) and 0.1 and 0.5 nM COL (**Fig. 6.3C**). Control cells were continuously proliferating with the high increase in total cell number after 72 hours. In the case of all drugs used here in low concentrations (100 nM VFL, 1 nM DTX and 0.1 nM COL), lack of inhibition of proliferation was observed for cells treated for 24 and 48 hours (**Fig. 6.3A-C**). While it was shown that for all drugs in low doses (100 nM VFL, 1 nM DTX, and 0.1 nM COL), proliferation of DU145 cells decreased after 72 h of drug treatment (**Fig. 6.3**). After 72h of drug treatment, the highest decrease in proliferation rate was observed for docetaxel treated cells (**Fig. 6.3B**).

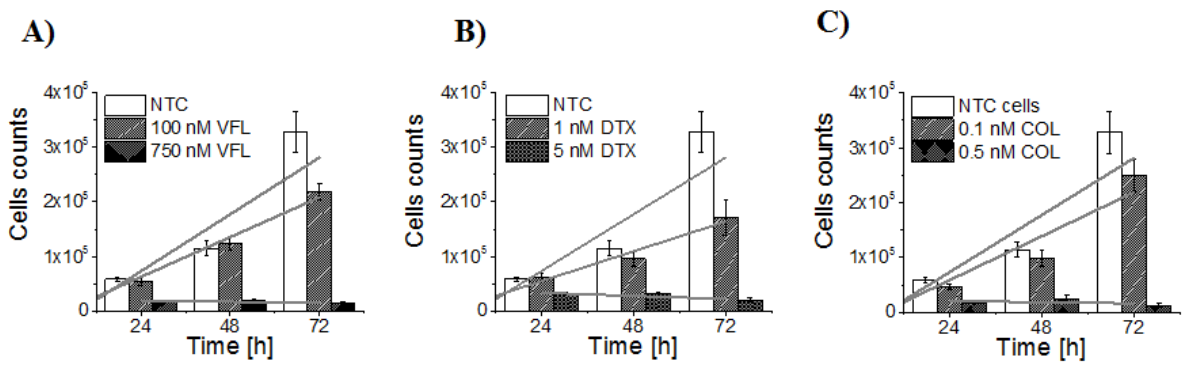

Fig. 6.3. *Proliferation assay for cells treated by A) vinflunine, B) colchicine, and C) docetaxel for 24, 48, and 72 hours. NTC – denotes non-treated control cells. Bars represent mean cell number at given experimental condition ± standard derivation (reprinted with permission from Kubiak et al. Nanoscale 13 (2021) 6212 from The Royal Society of Chemistry).*

High MTDs concentrations (750 nM VFL, 5 nM DTX and 0.5 nM COL) led to significant cellular mortality just after 24 h what was confirmed by a decrease in cell number in comparison to NTC and cells treated with low MTDs concentrations (**Fig. 6.3**). Cells treated with a high concentration of each drug did not proliferate what is confirmed by the lack of significant changes in their number between each time points (**Fig. 6.3**) Thus, the observation of such ultimately high cytotoxicity implies that a focus was made on low MTDs concentrations for further steps because they are more clinically applicable.

6.4 Potential resistance of DU145 cells

A calcein efflux assay was performed to probe whether cells treated with a particular drug in the low dose for 72 hours exhibit the potential of drug resistance. Such tests performed using flow cytometry allow determining how efficiently cells can pump out drugs. As observed, non-treated cells possess the highest potential to pump away calcein while comparing drug-treated cells (**Fig 6.4A,E**).

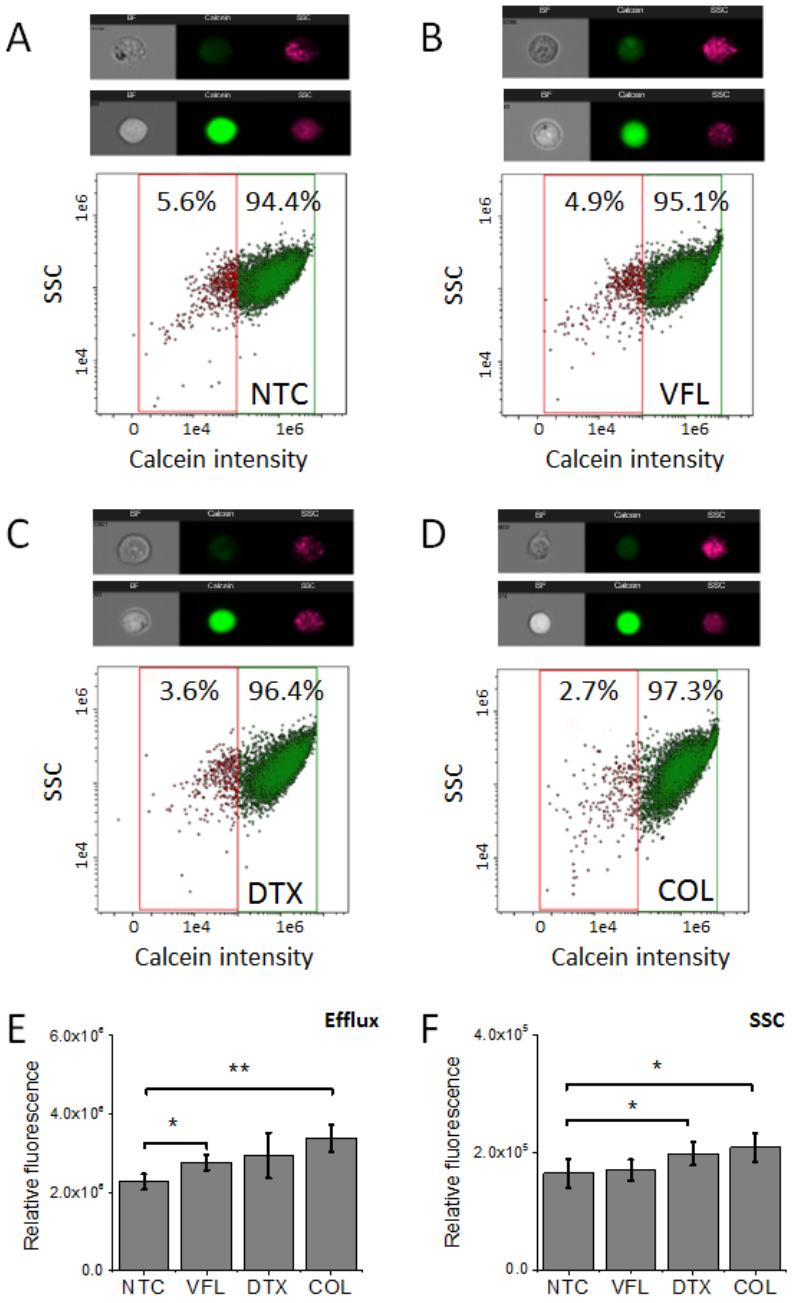

Fig. 6.4. *Impact of 72h of incubation with microtubules-interacting agents in low doses on the ability of DU145 cells to pump drug away from the cell body. Exemplary images of cells from ImageStream® imaging systems and charts showing the different populations of cells using their SSC and intensity of calcein fluorescence for A) NTC, B) 100 nM VFL, C) 1 nM DTX, and D) 0.1 nM COL, Relative fluorescence for E) efflux and F) side scatterSSC. (reprinted with permission from Kubiak et al. Nanoscale 13 (2021) 6212 from The Royal Society of Chemistry).*

Consequently, decreased percentage in cells that pumped away calcein as well as increased mean fluorescent intensity were observed for 1 nM DTX and 0.1 nM COL (**Fig. 6.4C-E)**,

while this significance was smaller for 100 nM VFL (**Fig. 6.4b,e)** in the case of 72 hours drug treatment. Such observation shows that cells treated by 1nM DTX and 0.1 nM COL are characterized by significantly impaired functioning of transmembrane pumps responsible for pumping drugs away from the cell body. In the case of 100 nM VFL, this impairment is significantly lower but still visible (**Fig. 6.4e**). Such findings imply whether finding direct, mechanical markers of anticancer drug resistance in cells is possible.

6.5 Discussion

MTDs have been already used in multiple therapeutic approaches as well as multiple preclinical studies are currently ongoing to increase the efficiency of their use in therapy (31). Vinflunine, *Vinca* alkaloids semisynthetic derivative, has been approved to treat bladder cancer in humans (85–87). In principle, it was shown to inhibit angiogenesis (88), migratory properties (89) as well as induce apoptosis in neuroblastoma cells even in low doses (90). In the latter case, IC_{50} was even lower (60 ± 12 nM) than showed for the studied here DU145 cells (450 ± 20 nM, **Fig.6.1A**) what is fully explainable by the difference between SK-N-SH neuroblastoma and DU145 prostate cancer cell lines, and in turns indicates than DU145 cells are ultimately more resistant against vinflunine than SK-N-SH cells. Also, L1210 murine leukemia cells are more susceptible to 48 h treatment with vinflunine than DU145 cells – the proliferation of L1210 cells treated with 100 nM of VFL was at a level of ~40% of control (91), while for DU145 cells 48 hours of treatment with such dose of VFL was not sufficient to affect proliferation (**Fig. 6.3A**). Finally, for murine leukemia P388-SS, P388-N.63, and P388-N2.5 cell lines, IC_{50} for vinflunine were in the range of 11.1 nM to 21.9 nM (92) what is again ultimately lower than in the case of DU145 cells (**Fig. 6.1A**). While in the case of bladder cancer, cell lines were characterized by high variability in their responsiveness against VFL treatment. HT1376, 5637, and SW780 cells have been characterized by higher IC_{50} dose (in the range of 1.73 – 4.67 μM) than in the case of DU145 (420 nM). UMUC3 (277 nM) and T24 (68 nM) cells were characterized by a lower IC_{50} dose (93) than showed for DU145 (**Fig. 5.1A**). Thus, based on the available literature, it could be stated that DU145 cells are relatively resistant against vinflunine while comparing with other cell lines.

Microtubules stabilizer – docetaxel has already been used in both therapies and preclinical studies of prostate cancer treatment. Because this drug is approved for clinical use against prostate cancer, multiple studies address drug resistance of prostate cancer cells against this

compound (94–96). Recently DU145 cells were shown to be sensitive for treatment with DTX in nanomolar concentration (0.6 – 5 nM). In principle, it was reported that treatment of DU145 cells with 1 nM DTX led to ~30% inhibition of cell growth which is in line with data obtained in the present study (**Figs. 6.2B, 6.3B**). It has already been shown that longer treatment of DU145 cells with DTX allows isolating a drug-resistant subpopulation of those cells. As a result subpopulation of such cells was even resistant against 50 nM DTX (97). Such observations provide strong evidence that there is an urgent need to find new methods to investigate better and diagnose drug resistance against DTX.

Finally, colchicine – a drug applied in gout treatment was used in the present study since its action leads to microtubules depolymerization on distinct from VFL mechanisms – and thus possibly drug resistance against it might result from its different way of action (31,98,99). While VFL is considered too toxic to treat cancer directly, promising results show that patients suffering from gout and treated with COL have a lower risk of cancer development (100). Parallelly *in vitro* studies have also confirmed that COL alone or COL-binding site drugs can potentially treat prostate cancer. COL has been reported to arrest cells in the G2/M phase, decrease mitochondrial potential and promote apoptosis in PC-3 prostate cancer cells (100). In principle, multiple drugs with a high affinity to the COL-binding site at tubulin are currently investigated in clinical trials for different cancers, including prostate cancer (101). Such observations ultimately show that resistance against colchicine should be well investigated and understood with the aim to increase therapy efficiency with those new, less toxic compounds.

6.5 Conclusions

The MTDs acting on DU145 prostate cancer cells induce distinct biological effects in a time- and dose-dependent manner. Results show that:

- high MTDs concentrations (above IC50) induce significant changes in cell viability after 72 hours of cells exposed to MTDs.
- the number of alive cells after 72h of their exposure to MTDs varied between 76.8% and 97.5% for DTX-treated and non-treated cells. Cell viability of cells after VFL and COL treatment fits between these border values.
- MTDs effect on cell proliferation is significant after 72 hours of their exposure to drugs. For shorter exposure times, the effect of MTDs is negligible.

- Among investigated MTDs, VFL was a drug characterized by the lowest potential to reduce drug resistance in DU145 cells

Low and high drug concentrations chosen for the study were below (100 nM VFL, 1 nM DTX and 0.1 nM COL) and above IC_{50} (750 nM VFL, 5 nM DTX and 0.5 nM COL). From the clinical point of view, the most relevant are low doses. In the presented work, just at this step, it was possible to discriminate between drugs in their potential to kill cancer cells after 72h, where DTX is the strongest one, COL is intermediate, while VFL is a drug characterized by the lowest ability to kill cancer cell after 72 h. All drugs are capable of inhibiting the proliferation of DU145 cells not earlier than after 72 h. Here, decreased cell number for those treated with DTX might also result from its higher cytotoxicity than other drugs.

7. Time-dependent deformability of DU145 cells upon MTDs action

7. 1 Introduction

The impact of anticancer drugs on cellular mechanics has already been investigated for different types of drugs and times of drug treatment (see Table 2, Chapter 2.4). Multiple drugs lead to the stiffening of cancerous cells after treatment. However, some do not affect the stiffness of cells, and a minority of drugs cause softening of cells. One drawback of those research is that the total treatment time was relatively short in most cases, and the doses of drugs were relatively high. Such an approach is far from physiological conditions present during chemotherapy, where treatment time is long, and the drug dose/concentration is as low as possible. It has recently been shown that the mechanical properties of breast cancer cells change transiently during metastasis. Importantly, transient increases in elastic modulus of cells have been observed before straight-forward biological symptoms of metastasis occurrence (69). In the light of such findings, it could be postulated that dynamic changes of physical parameters describing cells rather than their absolute values might serve as a diagnostic marker.

The main objective of the research described in this chapter was to answer whether dynamic changes in mechanical properties of prostate DU145 cancer cells might be used to describe drug action. To realize it, AFM working in force spectroscopy mode was applied to measure the mechanical properties of cells. DU145 cells were treated with three MTDs (VFL, DTX and COL) in two concentrations: high (750 nM VFL, 5 nM DTX and 0.5 nM COL) and low (100 nM VFL, 1 nM DTX and 0.1 nM COL) for 24, 48 and 72 hours. Cells were measured for each of the conditions using ORC8 pyramidal probes. Recorded force curves were analyzed by applying Hertz-Sneddon contact mechanics, assuming that a cone can approximate the shape of the tip. Because dynamic changes of mechanical properties were under consideration here, all determined values were also normalized to mean values of control cells.

7.2 Time-dependent effect of large MTDs concentrations

High MTDs concentrations potentially damage cells due to their ability to inhibit cellular proliferation (high cytotoxicity level, **Figs. 6.1, 6.2**). In the presented study, DU145 cells were exposed for 24, 48 and 72 h for high MTDS concentrations (VFL: 750 nM; DTX: 5 nM; COL: 0.5 nM). After 24 hours of treatment, most affected cells detach from the surface, making the AFM measurements difficult (as AFM requires the cell to be attached to the surface). What is more, the number of cells that are still alive after treatment with high drug concentrations is not changing over time (24, 48 72 h) for all drugs investigated here (**Fig 6.3**). Therefore, one can postulate that cells that remained on the surface after exposure to large MTDs concentrations represent a subpopulation of cells capable of surviving for at least 72 hours of drug treatment.

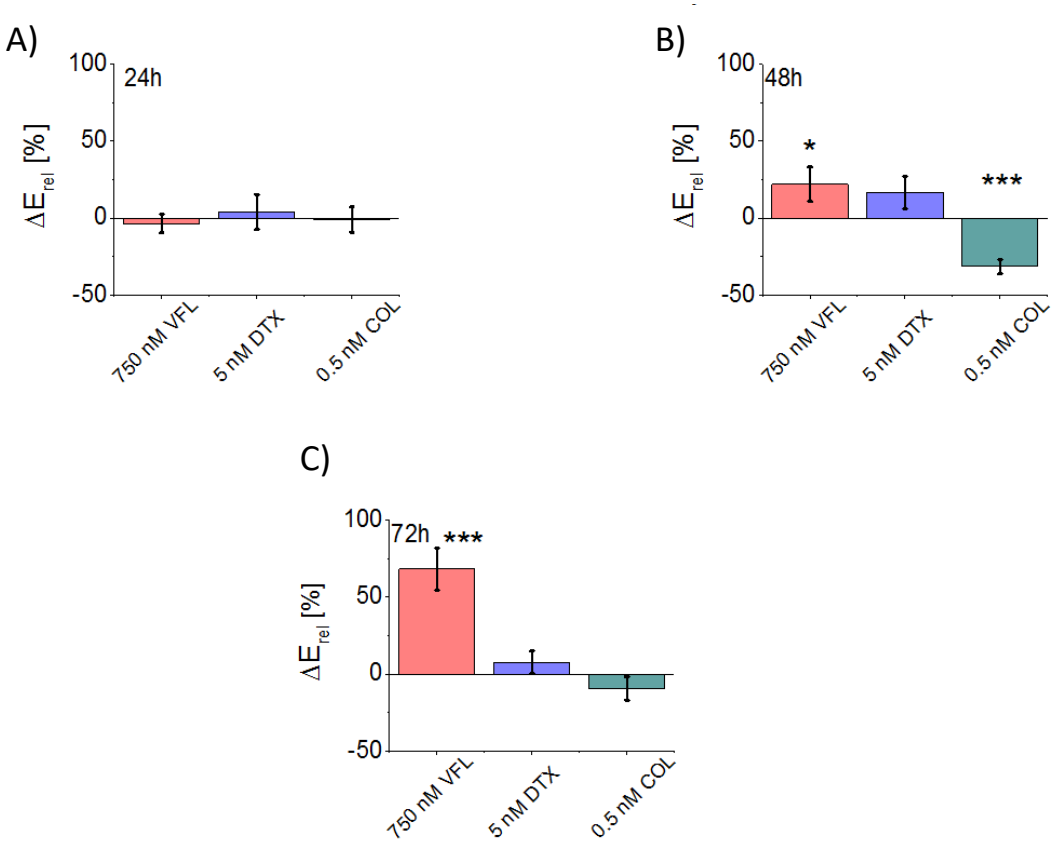

*Fig. 7.1. Changes in relative elastic modulus of DU145 cells treated with high drug concentrations (750 nM of VFL, 5 nM of DTX, and 0.5 nM of COL) after A) 24 hours, B) 48 hours, and C) 72 hours. Data are presented as mean values ± SD. Statistical significance in relation to NTC cells was determined using Student's t-test with p level: * p<0.05, *** p<0.001 (adapted from Kubiak et al. Nanoscale 13 (2021) 6212 with permission from The Royal Society of Chemistry).*

After 24 hours of drug treatment, elastic moduli of cells treated with all drugs were not affected while comparing them with control ones (**Fig. 7.1A**). After 48 hours of treatment with high doses of drugs, stiffening of cells treated with VFL and DTX was detected – but the significance of this change was achieved only for VFL (**Fig 7.1B**). In the case of this time point, cells treated with 0.5 nM of COL were reported to be robustly softer than control ones at this time point (**Fig. 7.1B**). Finally, after 72 hours of drug treatment, only VFL was shown to cause very robust stiffening of cells, while both DTX and COL did not affect elastic moduli of DU145 cells (**Fig 7.1C**). **Table 7.1.** summarizes the obtained results.

Table 7.1. *Mean apparent values ± standard deviation of elastic modulus of DU145 cells treated with MTDs for 24, 48, and 72 hours. The number of cells measured per condition is given in a round bracket, and p values are provided from Student's t-test comparing elastic modulus for a given condition and its corresponding control. Statistical significance vs control cells was calculated using Student's t-test, and p values lower than 0.05 are marked in red.*

time / ***MTDs treatment***	***24h*** *E ± s.e. (n) [kPa]*	***48h*** *E ± s.e. (n) [kPa]*	***72h*** *E ± s.e. (n) [kPa]*
	Vinflunine		
NTC	3.1 ± 0.2 (94)	2.2 ± 0.1 (93)	1.5 ± 0.1 (96)
750 nM VFL	3.0 ± 0.2 (76) *p = 0.7147*	2.7 ± 0.2 (88) *p = 0.0412*	2.5 ± 0.2 (91) *p = 0.0001*
	Docetaxel		
NTC	4.2 ± 0.3 (88)	2.9 ± 0.2 (88)	2.6 ± 0.1 (89)
5 nM DTX	4.4 ± 0.4 (83) *p = 0.7280*	3.4 ± 0.3 (86) *p = 0.1085*	2.8 ± 0.1 (87) *p = 0.2971*
	Colchicine		
NTC	3.3 ± 0.17 (90)	3.0 ± 0.15 (91)	2.2 ± 0.1 (90)
0.5 nM COL	3.3 ± 0.2 (87) *p = 0.9140*	2.0 ± 0.1 (88) *p = 0.0001*	2.0 ± 0.2 (88) *p = 0.2520*

7.3 The effect of MTs destabilizing agents (VFL, COL) on mechanics of DU145 cells

Low concentrations of MTDs applied to cells were not detrimental, although they affect the microtubular network (102). The effect of MT destabilizing agents (VFL and COL) on the mechanical properties of cells was quantified after 24h - 72h exposure to low concentrations of VFL (100 nM) and COL (0.1 nM). AFM measurements (pyramidal cantilevers, ORC8 were used) have been conducted on living cells at each time spot. All measurements were performed on living cells. The results are presented in **Fig. 7.2.**

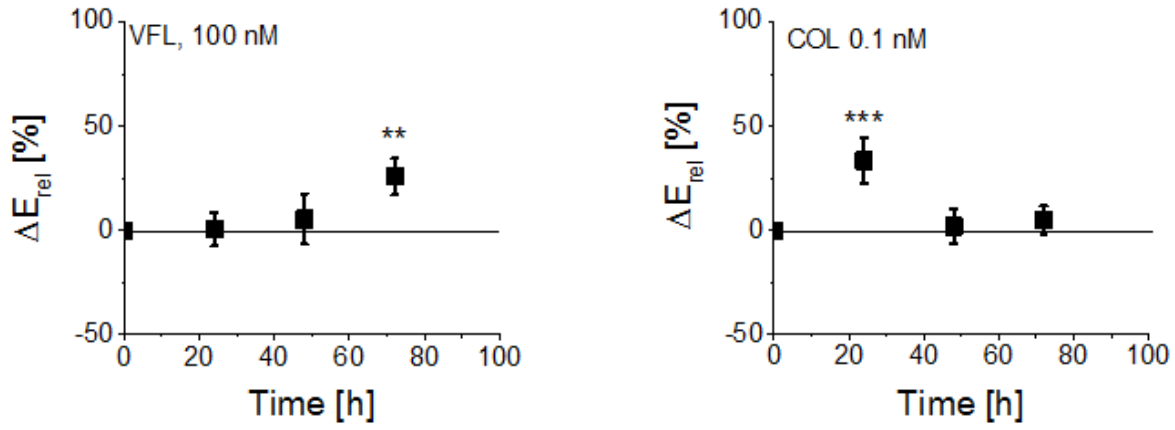

Fig. 7.2. *Time-dependent changes in elastic modulus of DU145 cells treated with a low dose of drugs destabilize microtubules: A) 100 nM vinflunine and B) 0.1 nM colchicine. The point represents the mean elastic modulus of DU145 cells, which is normalized to the corresponding elastic modulus of NTC cells. At least 85 cells were measured per condition. Whiskers present standard derivation. Statistical significances in relation to NTC cells was quantified using Student's t-test with p level: ** p<0.01, *** p<0.001; (adapted from Kubiak et al. Nanoscale 13 (2021) 6212 with permission from The Royal Society of Chemistry).*

VFL in low dose does not affect the mechanics of DU145 cell treated for 24 and 48 hours, while after 72 hours of drug treatment, significant stiffening of cells was reported (**Fig. 7.2A**). In the case of COL acting on cells in low concentration, a robust and significant stiffening of cells was observed just after 24 hours of treatment, while no significant changes in cells stiffness for 48 and 72 hours of treatment were noticed (**Fig. 7.2B**). A summary of the obtained Young's moduli is presented in Table 7.2.

Table 7.2. Mean apparent values ± standard deviation of elastic modulus of DU145 cells treated with VFL and COL for 24, 48, and 72 hours. The number of cells measured per condition is given in a round bracket, and p values are provided from Student's t-test comparing elastic modulus for a given condition and its corresponding control. Statistical significance in relation to control cells was calculated using Student's t-test, and p values lower than 0.05 are marked in red.

time / ***MTDs treatment***	***24h*** *E ± s.e. (n) [kPa]*	***48h*** *E ± s.e. (n) [kPa]*	***72h*** *E ± s.e. (n) [kPa]*
	Vinflunine		
NTC	3.1 ± 0.2 (94)	2.2 ± 0.1 (93)	1.5 ± 0.1 (96)
100 nM VFL	3.1 ± 0.3 (94) *p = 0.9512*	2.3 ± 0.3 (93) *p = 0.632*	1.9 ± 0.1 (93) *p = 0.0016*
	Colchicine		
NTC	3.3 ± 0.17 (90)	3.0 ± 0.15 (91)	2.2 ± 0.1 (90)
0.1 nM COL	4.4 ± 0.3 (88) *p = 0.0012*	2.9 ± 0.2 (86) *p = 0.7853*	2.3 ± 0.1 (87) *p = 0.4623*

Two MTDs applied in the study depolymerize microtubules by binding to different domains at tubulin dimers. They are vinflunine and colchicine. Although depolymerization of microtubules was primarily suspected in both drugs, stiffening of cells was observed in both cases with the reservation that the time scale of the stiffening was drug-dependent. In the case of vinflunine, which has been reported to possess the lowest potential to kill cancerous cells, this stiffening appeared after 72 hours, while for colchicine, stiffening of cells was observed just after 24 hours of drug treatment (**Fig. 7.2.**). This observation concludes that in the case of drugs known to exert a similar effect on the microtubular network, the stiffening appears earlier in the drug, which is more cytotoxic for cells (**Fig. 6.2, Fig. 6.3**). Interestingly, in colchicine, after an increase of cellular stiffness, which occurs after 24 h after treatment with drugs, cellular elasticity reach the level of the NTC cells and remains constant during measurements in the following time points: 48 h and 72 h. Such mechanical behaviour of cells suggests that stiffening might be the stress-induced response of cancer cells to drug treatment. In the case of colchicine, most of the cells were still living and proliferating seems to strongly support such a hypothesis (**Figs. 6.1., 6.2., 6.3.**).

7.4 The effect of MTs stabilizing agent (DTX) on mechanics of Du145

Stabilizing agents belonging to taxanes are believed to contribute to cell stiffening, although not always **(**see **Table 2.1** in Chapter 2**)**. Therefore, DU145 cells were treated with DTX for 24h, 48h, and 72h, followed by AFM measurements of mechanical properties. The results are presented in **Fig. 7.3.**

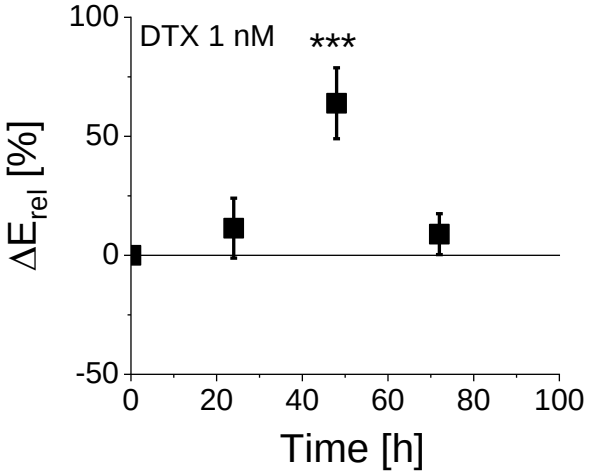

Fig. 7.3. Time-dependent changes in elastic modulus of DU145 cells treated with a low dose of docetaxel – a drug that stabilizes microtubules Point represents the mean elastic modulus of DU145 cells, which is normalized to the corresponding elastic modulus of NTC cells. Whiskers present standard derivation (adapted from Kubiak et al. Nanoscale 13 (2021) 6212 with permission from The Royal Society of Chemistry).

In the case of docetaxel, transient stiffening of DU145 cells was observed. Cells became significantly stiffer after 48 h of docetaxel treatment. After 24 h and 72 h, no significant changes were noted between drug-treated and non-treated cells (**Fig. 7.3**). Such observation seems to lead to interesting conclusions. Although the docetaxel action mechanism is opposite to colchicine, their mechanical response is similar in time. In the case of both drugs, after initial stiffening, a return to the elastic modulus of non-treated cells has been observed (**Figs. 7.2B, 7.3**). This is quite different behaviour than in the case of cells treated with vinflunine when stiffening was reported non earlier than after 72 hours (**Fig. 7.2A**). In the latter case, it could be that after a more extended period of observation, a return to elastic moduli characteristic for NTC would also be observed for cells treated with VFL. Obtained results are summarized in Table 7.3.

Table 7.3. *Mean apparent values ± standard deviation of elastic modulus of DU145 cells treated with DTX for 24, 48, and 72 hours. The number of cells measured per condition is given in a round bracket, and p values are provided from Student's t-test comparing elastic modulus for a given condition and its corresponding control. Statistical significance vs control cells was calculated using Student's t-test, and p values lower than 0.05 are marked in red.*

time / ***MTDs treatment***	***24h*** *E ± s.e. (n) [kPa]*	***48h*** *E ± s.e. (n) [kPa]*	***72h*** *E ± s.e. (n) [kPa]*
	Docetaxel		
NTC	4.2 ± 0.3 (88)	2.9 ± 0.2 (88)	2.6 ± 0.1 (89)
1 nM DTX	4.7 ± 0.4 (86) *p = 0.3610*	4.8 ± 0.4 (83) *p = 0.0001*	2.8 ± 0.2 (89) *p = 0.2977*

7.5. Discussion

Up to date, multiple drugs have been already shown to increase cellular stiffness (**Table 2.1,** (28,47)). Such observation was recently reported for prostate cancer cells treated with cisplatin and docetaxel. Although in those experiments, prostate cancer cells were treated with indicated drugs only for 24 hours and doses used for treatment were significantly higher than 1 nM for DTX in this study (28). On the contrary, paclitaxel, which is another member of the *taxanes* family of microtubules stabilizers, was shown to decrease cell stiffness for prostate cancer PC-3 cell treated for 24 hours with 2 and 10 μM (50), B16F10 melanoma cells treated for 30 hours with 287 nM (103) and Ishikawa endometrial cancer cells treated for 6-18 hours with 50 μM (104). On the other hand, B16F10 cells after 14 hours of treatment with 24 nM paclitaxel, do not exhibit significant changes in their elastic moduli (103). Such observation for taxanes indicates considerable variability in the cell mechanical response against those drugs. A proper interpretation of such changes concerning time-dependency offers a promising way of using biophysical data regarding the impact of taxanes on the mechanical properties of cells. Among MTDs, that tend to depolymerize MTs, colchicine was shown to induce stiffening of hepatocellular carcinoma SMCC-7721 cells after treatments with 100 nM for 4 and 6 hours (105). 10 μM nocodazole has been shown to increase the stiffness of HT 1080 fibrosarcoma and HUH-7 hepatocellular carcinoma cells after 30

minutes of drug treatment (105). Ultimately variety of non-tubulin interacting drugs (Disulfiram, Tomatine, BAY 11-7082 - an inhibitor of κB kinase, vaproic acid, 12-O-tetradecanoylphorbol-13-acetate, Celebrex, MK-2206 – an allosteric inhibitor of a serine/threonine-specific protein kinase B) have been shown to increase the stiffness of prostate cancer cells (50). It could be concluded that cellular response against chemotherapeutic agents seems to be associated with cell stiffening. Such a process occurs at different stages of cellular drug response and is associated with drug action. It should be underlined here that such conclusions might be somehow surprising – especially while thinking about drugs that are known to depolymerize microtubules if used in very high concentrations. Thus, at this point, it was essential to describe the cellular cytoskeleton after treatment with those drugs to answer the question of which particular cellular components are responsible for observed changes.

7.5 Summary

Vinflunine, docetaxel and colchicine are compounds belonging to microtubule-targeted drugs. They have been chosen to answer whether the mechanical properties of cells can serve as a non-labelled biomarker of MTDs effectiveness. The results obtained from the assessments of biological effects on DU145 prostate cancer cells shows that:

- high concentration of DTX (5 nM) does not affect the mechanical properties of DU145 cells, COL treatment (0.5 nM) leads to transient cell softening, while VFL treatment (750 nM) resulted in gradual stiffening over time
- low concentration of COL (0.1 nM) induces cell stiffening after 24 hours of cell exposure to the drug
- for low DTX concentration (1 nM), the maximum stiffening was observed after 48 hours of DU145 exposure.
- cell stiffening induced by low VFL concentration (100 nM) was observed after 72 hours of cell exposure to the drug

MTDs acting in low concentrations (100 nM VFL, 1 nM DTX, and 0.1 nM COL) display various biological response after 72 hours treatment. As determined by proliferation assay in the case of all MTDs, the significant inhibition of proliferation was observed not earlier than after 72 hours of treatment, independently of the drug type (**Figs. 5.1, 5.2**). Consequently, a more sensitive method, i.e., flow cytometry, could not distinguish drugs based on their ability

to kill cancer cells until 72 h treatment (**Fig 5.3A,B**). Only AFM measurements provided sufficient information to distinguish between drugs based on their dynamical changes (**Figs. 5.5, 5.6**). Those drugs, which caused earlier mechanical response, were more cytotoxic after 72h hours than VFL, characterized by the lowest cytotoxicity. Flow cytometry and MTS assay provide drug potency to kill prostate cancer cells after 72 hours: DTX > COL > VFL. Thus presented data allow for the conclusion that measurements of cells' mechanical properties serve as a method that allows detecting cellular response to antitumor action before the appearance of biological markers of such drug action.

8. MTDs induced alterations in cell morphology and cytoskeleton

8. 1 Introduction

It is already well known that the cytoskeleton and nucleus are key elements responsible for cellular mechanical properties (24,105). Since the use of various drugs affects the mechanical properties of cells, it is rational to ask questions about particular mechanisms responsible for such changes (47). It is well established that microtubules targeting drugs affect the organization of the cytoskeleton. Thus, in the field of observation described in the previous chapter, it is crucial to understand the physical phenomenon behind changes in the mechanical properties of cells. The possible ones are changes in how microtubules and actin filaments are organized – because those elements of the cytoskeleton are responsible for the maintenance of the mechanical properties of the cell. On the other hand cell nucleus – which is the biggest cellular organelle should be also considered here. Changes in its organization potentially induced by action of mitosis affecting drugs might also contribute to overall mechanical properties of cells. This chapter describes the research focused on morphological and cytoskeleton-related changes in DU145 cells treated with MTDs. To do it epifluorescent microscopy and confocal microscopy were applied. Actin filaments, microtubules and cell nuclei were stained by fluorescent dies and visualized by use of those two aforementioned techniques. Such observations are crucial for a better understanding of the mechanical changes which appear during drug treatment.

8.2 MTDs induced changes in cell nucleus morphology

The cell nucleus serves as a cellular organelle responsible for storing genetic information about the cell and its life program (106). Such information is stored in the form of DNA, which is then used by cells in transcription and translation to synthesise proteins. DNA strands have to be released from their native, densely packed form to allow particular genes encoded in DNA to be transcribed to mRNA. Such release requires changes in DNA condensation, which are somehow connected with cell nuclei architecture. Thus changes in nuclear morphology might be a marker of changes taking place in the cell. To probe it,

fluorescent images of cell nuclei were acquired for DU145 cells treated with VFL, COL, and DTX, both with low as well as high concentrations **(Fig. 8.1).**

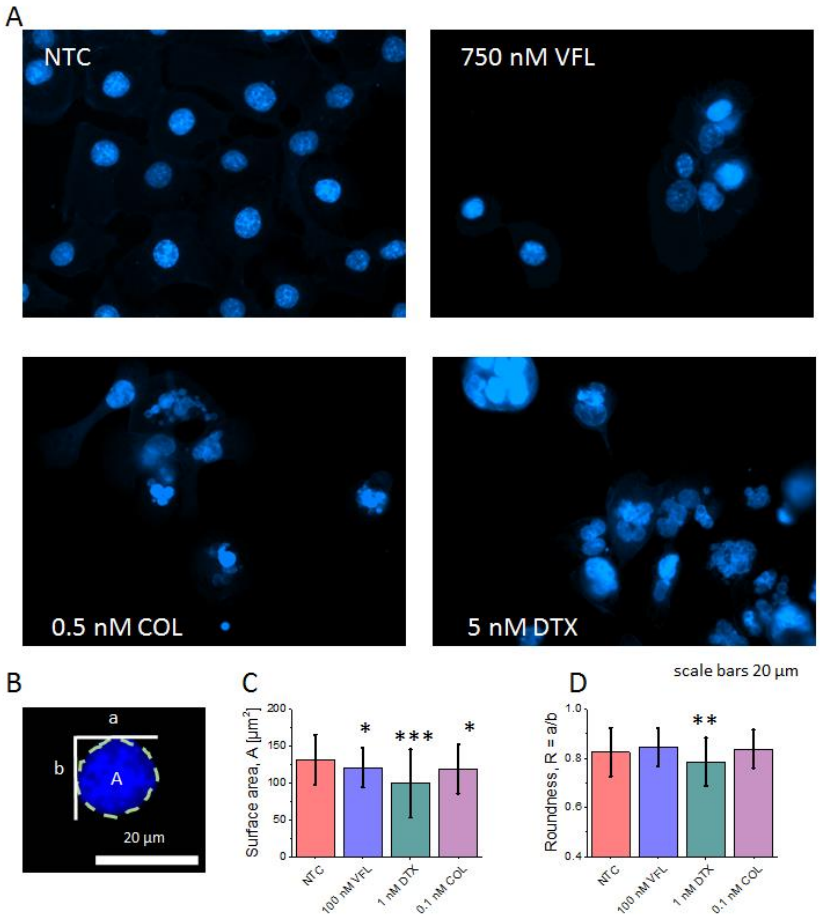

Fig. 8.1. Changes in nuclear morphology after treatment with microtubules-interacting agents. A) fluorescent images showing the morphology of NTC cells and cells treated with high concentrations of drugs. B) Calculation of nuclear morphological parameters: A denotes surface area, a, b are long and short axes (the nucleus is round when a equals B), C) Surface area of nuclei for NTC and cells treated with low MTDs concentrations (data are presented as a mean ± standard deviation from n = 79 - 105 cells), D) Nuclei roundness of NTC and cells treated with low MTDs concentrations (data are presented as a mean ± standard deviation from n = 79 - 105 cells); (reprinted with permission from Kubiak et al. Nanoscale 13 (2021) 6212 from The Royal Society of Chemistry).

Cell nuclei for non-treated DU145 cells (referred here as NTC cells) are round with evenly distributed DNA (**Fig. 8.1A**). Treatment of DU145 cells with a high concentration of drugs

led to very robust destruction of cell nuclei – especially in the case of COL and DTX (**Fig 8.1A**). Cell nuclei of DU145 cells treated with 750 nM of VFL were not destroyed as in the case of two other drugs what suggests that even if most of the cells were killed after 750 nM VFL action, the resistant ones were in better shape than 0.5 nM COL and 5 nM DTX survivors (**Fig. 6.1., Fig. 6.3, Fig. 6.4, Fig. 8.1a**). Similar nuclei morphology was observed in fluorescent images in the case of cells treated with low MTDs concentrations.

Thus, to answer whether drug treatment affects their morphology, quantification of the nuclei projection area and roundness was applied (**Fig. 8.1B-D**). In the case of area very significant decrease in it was observed for cells treated with DTX (99.5 ± 46.1 μm^2; n = 105) while comparing to (NTC 131.4 ± 34.2 μm^2; n = 80). In the case of cells treated with VFL (120.9 ± 26.9 μm^2; n = 79) and COL (119.0 ±33.5 μm^2; n = 96), a decrease in the area was observed, although its significance was lower than in DTX treated cells (**Fig. 8.1C**). Consequently, in the case of roundness determination, a significant decrease in this parameter was only observed in DTX treated cells (0.785 ± 0.097) compared to NTC (0.825 ± 0.098). Those data are in line with previously described, showing that DTX acting in low concentrations is the most potent of the drugs used in the present study when potency is understood as an ability to alter cancer cells' morphology and physiological functioning. Parallelly lower impact of VFL high concentrations on DU145 cell nuclei indicates that those cells tend to gain resistance against this compound (**Fig. 6.1 - 6.4, Fig. 8.1A**).

8.3 MTDs effect on the microtubule organization in DU145 cells

MTDs chosen for the study binds differently to α/β dimer forming microtubules ((31), also schematically presented in **Fig. 2.1**). The changes in protein structures caused by the binding of the drug to particular sites of tubulin dimer are resulting in corresponding changes in the behaviour of the whole microtubules leading to either destabilization (VFL and COL) or destabilization (DTX, (31). Therefore, microtubules were fluorescently labelled to visualise their organization in DU145 cells treated with MTDs for 72h. Epi-fluorescent images are presented in **Fig. 8.2**.

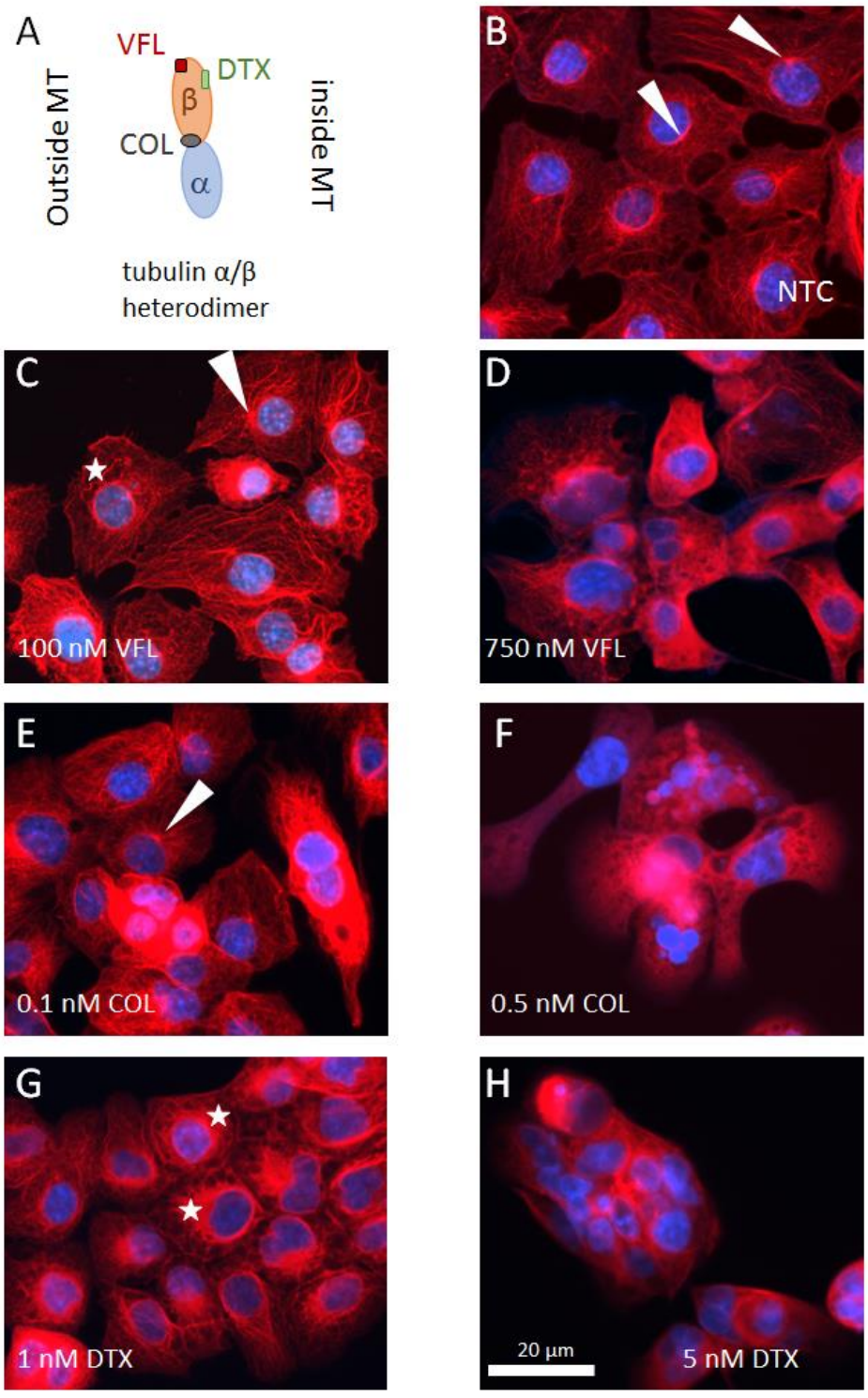

Fig. 8.2. Scheme of the idea of different microtubules-interacting agents binding to tubulin dimer – A). Changes in organization of microtubules in DU145 cells treated with: B) control – non-treated cells C) 100 nM VFL, D) 750 nM VFL, E) 0.1 nM COL, F) 0.5 nM COL. G) 1 nM DTX and H) 5 nM DTX for 72 hours (reprinted with permission from Kubiak et al. Nanoscale 13 (2021) 6212 from The Royal Society of Chemistry).

Non-treated DU145 cells are characterized by the presence of a well-organized microtubular network with pronounced and well visible microtubules-organizing centre (MTOC) (**white arrow; Fig.8.1B**). After treatment with 100 nM of VFL, the overall organization of microtubules cytoskeleton is weakly altered with clearly visible MTOC (**Fig. 8.2C**, white arrow)). Although after treatment with 100 nM VFL, single microtubular rings around cellular nuclei started to appear, leading to the conclusion that such treatment affects microtubular organization (**Fig. 8.2 C**, white star). In the case of 750 nM concentration of VFL microtubular cytoskeleton was ultimately destroyed. A lack of a microtubular network and clusters of depolymerized tubulin were observed (**Fig. 8.2D**). DU145 prostate cancer cells treated with 0.1 nM colchicine, similarly to those treated with 100 nM VFL, were characterized with a weakly affected microtubular cytoskeleton. Here, both establish the multi-branched microtubular network and MTOCs (white arrow) were presented (Fig. **8.2E**). Consequently, for DU145 cells treated with 0.5 nM of COL, microtubular network destruction is observed with aggregation of depolymerised tubulin clusters (**Fig.8.2F**). Among all drugs used in low concentrations, DTX in 1 nM concentration affects the microtubular network in the most visible way. In most cells treated with DTX presence of a microtubular ring around cell nuclei is observed (white arrow; **Fig. 8.2G**), with the remark that those rings were usually thicker than rings observed after treatment with VFL (**Fig. 8.2C**). Albeit microtubules were still organized in the network, it is less pronounced than in both NTC and cells treated with low concentrations of VFL and COL (**Fig. 8.2B,C,E)**. Such a phenomenon is connected with the already described concentration of tubulin in the nuclear ring. While they are recruited to those rings when docetaxel stabilizes them, a lack of tubulin dimers in the tubulin network branched around cellular lamellipodia is observed. Finally, in DU145 cells treated with 5 nM DTX, the microtubular network is disrupted, and tubulin aggregates are visible (**Fig. 8.2H**).

Taking those data together, one can divide the impact of MTDs depending on their concentration. A similar effect of drugs is associated with the drug action mechanism in low drug concentrations (100 nM VFL, 1 nM DTX and 0.1 nM COL). Here, drugs that depolymerize microtubules have no or weak effect on the microtubular organization of DU145 cells (**Fig. 8.2C,E**). In contrast, for a drug that leads to polymerization of microtubules, more significant microtubular cytoskeleton changes were observed, e.g. formation of microtubular ring around cell nuclei and weakening of microtubular network (**Fig. 8.2G**). On the contrary, for high MTDs concentrations (750 nM VFL, 5 nM DTX and 0.5 nM COL), the drug action negatively impacts the final microtubular organization. In fact,

in the case of all drugs used in high concentrations, the microtubular network was disrupted, tubulin aggregates were observed, and MTOC were no longer present (**Fig. 8.2D,F,H**).

Epi-fluorescent images were insufficient to explain which structural changes in cytoskeleton make DU145 cells treated with VFL for 72h stiffer. Therefore, confocal fluorescent microscopy was applied to obtain images of microtubule organization with higher resolution. Confocal fluorescent images of DU145 cells confirm previously observed cytoskeletal features recorded using a standard epifluorescent microscope. In the case of NTC, a well-developed, multi-branched microtubular network was present (**Fig. 8.3A**). Hardly any difference was observed when cells were treated with 100 nM VFL as well as 0.1 nM COL (**Fig. 8.B,C**). Tendency to forming thin microtubular rings was also observed in confocal fluorescent imaging (white star; **Fig. 8.3C**). While in the case of cells treated with 1 nM of DTX, the formation of the thick tubular ring (white arrow; **Fig. 8.3D**) and a local decrease in microtubular network density (thick white arrow; **Fig 8.3D**) have been reported.

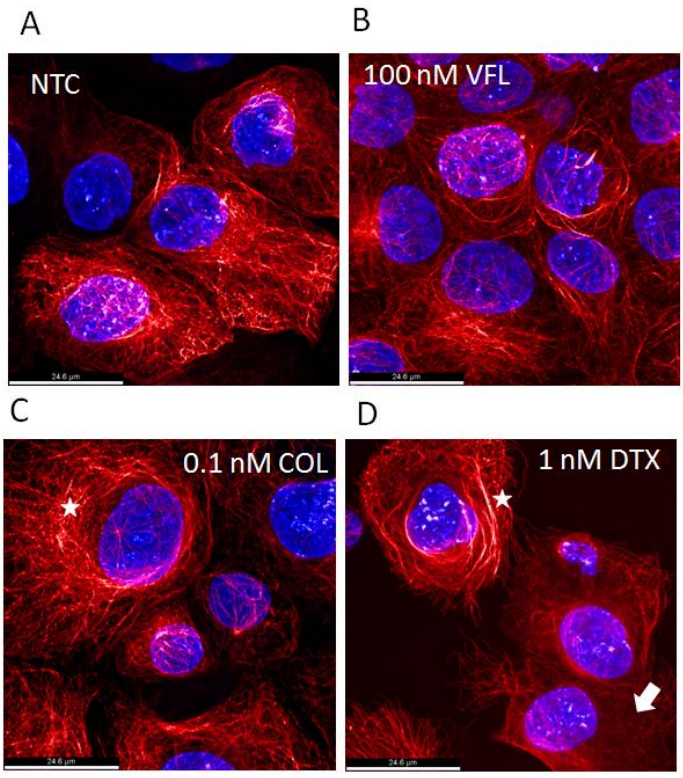

Fig. 8.3. Fluorescent confocal images of microtubules organization in DU145 cells treated with: A) non-treated cells, B) 100 nM VFL, C) 0.1 nM COL and D) 1 nM DTX for 72 hours. (scale bar = 24.6 µm; (reprinted with permission from Kubiak et al. Nanoscale 13 (2021) 6212 from The Royal Society of Chemistry).

Taking those imaging data together, changes observed in the microtubular network after 72 hours of treatment with low drug concentrations are insufficient to explain alterations in the mechanical properties of DU145 cells (see Chapter 7). Notably, the most significant changes were observed for cells treated with 1 nM DTX. Small changes in the microtubular network were visible for cells treated with 0.1 nM COL and 100 nM VFL. Nevertheless, those changes were more evident for cells treated with 0.1 nM COL than 100 nM VFL. The trend in mechanical changes has been ultimately opposite. After 72 hours of treatment with MTD, only cells treated with 100 nM VFL showed significant Young's modulus increase (Fig. 7.2a). In light of such observation, further investigation of the cellular cytoskeleton was required to explain the phenomenon of stiffening of cells induced by 72 hours incubation with 100 nM VFL.

8.4 MTDs affect the organization of actin filaments

Apart from microtubules, the cellular cytoskeleton consists of two other components: actin bundles and intermediate filaments. Actin filaments are a key element responsible for cellular morphology, motion, and mechanical stability (107). Therefore, in parallel to MTs organization, the arrangement of these filaments was acquired, too.

Single stress fibres were observed in NTC cells together with the relatively uniform actin organization characterized by rather weak fibrillation (**Fig. 8.4A**). In the case of cells treated with 100 nM VFL, stress fibres and other actin structures became more prominent (**Fig. 8.4B**). Importantly the weakest fibrillation of actin cytoskeleton was observed both after treatments with 0.1 nM COL as well as 1 nM DTX (**Fig. 8.4C,D**). Gathering these data together, one can say that actin fibres may play an important role in mechanical response to drug treatment in the case of prostate cancer DU145 cells. To investigate whether the actin cytoskeleton is responsible for the stiffening of DU145 prostate cells upon 100 nM VFL treatment for 72 hours, cells were treated with cytochalasin D. Cytochalasin D is a mycotoxin that has the potential to inhibit actin cytoskeleton polymerization by binding to F-actin in a way that prevents new actin monomers from binding to already created actin fibre. As a result, such activity of this compound has been widely used in various studies aiming to determine the role of the actin cytoskeleton in various cellular processes and ultimately in the establishment of cellular mechanical properties (66,105,108–110).

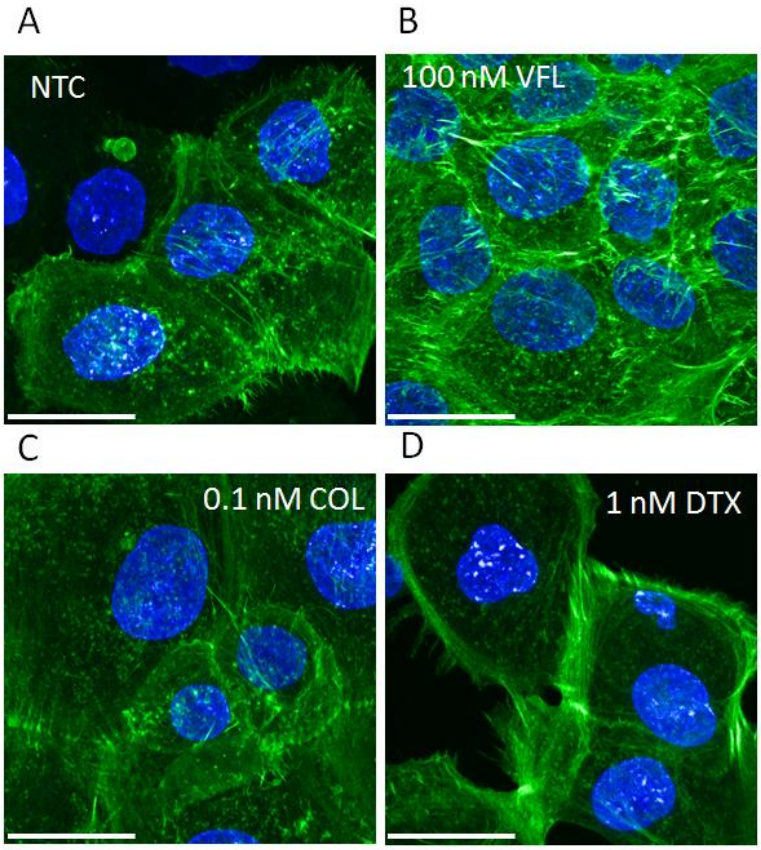

Fig. 8.4. Fluorescent confocal images of actin bundles organization in DU145 cells treated with: a) non-treated cells, b) 100 nM VFL, c) 0.1 nM COL and d) 1 nM DTX for 72 hours (scale bar = 25.0 μm; (reprinted with permission from Kubiak et al. Nanoscale 13 (2021) 6212 from The Royal Society of Chemistry).

Cells treated with 100 nM VFL very ultimately significantly stiffer than control ones (NTC). When control cells were treated with cytochalasin D, a lack of significant changes in both median and a mean of Young's modulus was observed (**Fig. 8.5**).

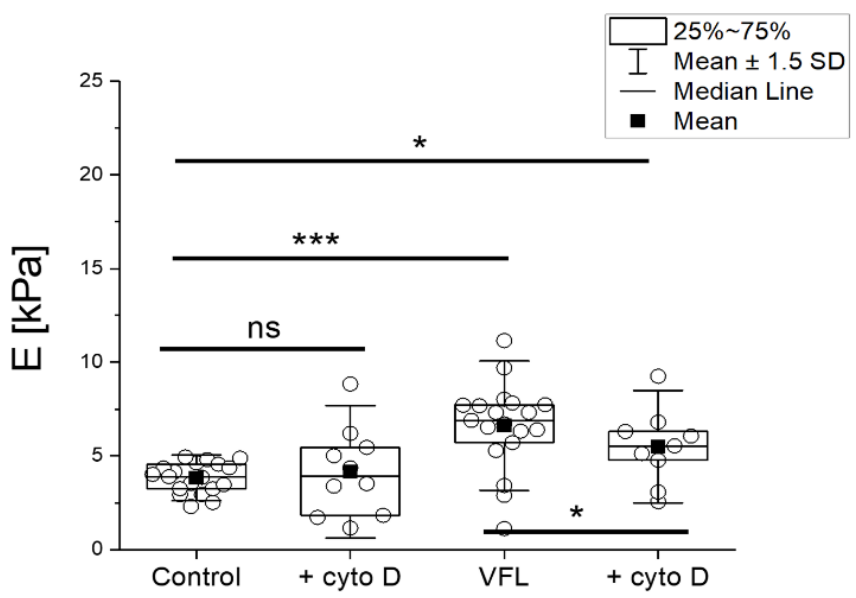

Fig. 8.5. *Impact of cytochalasin D on mechanical properties of DU145 cells treated with 100 nM VFL for 72 hours. Cells were treated with 20 µM cytochalasin D for 30 min and then added with 380 µM cytochalasin D for 15 min. Statistical significance was determined with the use of both t-Student (mean values) and Mann-Whitney U (median) tests at the level of 0.05 (* p< 0.05, ** p < 0.01, *** p < 0.001); (reprinted with permission from Kubiak et al. Nanoscale 13 (2021) 6212 from The Royal Society of Chemistry).*

Notably, in the case of cells treated with 100 nM VFL for 72 hours, additional treatment with cytochalasin D leads to a significant drop in Young's modulus. Those results confirm the previously coined statement that the actin cytoskeleton is a crucial one responsible for stiffening of DU145 prostate cancer cells in response to 72-hour treatment with 100 nM VFL (**Fig. 8.5**).

8.5 Discussion

Treatment of cancer cells with chemotherapeutic agents leads to multiple changes in their cytoskeleton and nucleus architecture organisation. For example, microtubules destabilizer, nocodazole in 250 nM concentration, have been shown to induce meaningful malformations of cell nuclei in MCF-7 breast cancer cells after 12 hours of treatment. Those malformations were maintained or even enlarged after 24 hours of treatment with this compound (111). Similarly, MCF-7 cell line 48 hours treatment with 10 nM docetaxel led to

micronuclei formation and ultimately mitotic catastrophes (112). Such observations align with data acquired in this work, where high concentrations of DTX and COL led to nuclei segmentation (**Fig. 8.1**). Interestingly, not only drugs have been reported to affect nuclear architecture. In a recent study, nuclei of neurons localized close to the tumour were showed to be malformed, and some neuronal cells even undergo apoptosis due to pathological physical factor from their surroundings (113). Consequently, an impact of numerous chemotherapeutic agents on the cytoskeleton organization in cancer cells has also been observed (36). Treatment of widely applied model of ovarian cancer, i.e. HeLa cells with nocodazole (which binds to a similar domain like colchicine), led to a significant disaggregation of the microtubular network in a well-organized control HeLa cells. In this case, changes in the actin organization were not so pronounced. However, this work focused on short action (~ 40 minutes) of a relatively high concentration of nocodazole (10 μM) (114). Vinflunine, which is used in the present study, has been shown to destroy the microtubular network while acting in 500 nM concentration on SK-N-SH neuroblastoma cells, nevertheless while acting in lower concentrations, its impact on the microtubular network was not significantly observed (90) – similarly to data obtained in the present work. Finally, aggregation of microtubules around the cell nucleus, even more, pronounced than in the present work, was observed for IGR-3 melanoma cells treated with 20 nM DTX for 3 hours (115).

8.5 Summary

Microtubules affect the mechanical properties of prostate cancer DU145 cells in a time-dependent manner. Drugs characterized by the weakest biological action – vinflunine increased the rigidity of DU145 cells not earlier than after 72 hours. Fluorescent images, together with the mechanical characterization of DU145 cells treated with cytochalasin D (an agent depolymerizing actin filaments), unravel which structural element was responsible for the observed mechanical changes. After 72 hours of drug treatment, images of the microtubular network indicated that the most significant changes in its organization are observed for DTX. Surprisingly DTX treatment does not introduce significant changes in cells mechanical properties after 72 hours. On the other hand, cells treated with 100 nM of VFL, which cause significant stiffening after 72 hours, does not exhibit any alteration in microtubular network organization. Thus confocal fluorescent imaging allowing for the acquisition of higher resolution of images of F-actin organization have been performed. Cells treated with 100 nM VFL for 72 hours were characterized by the visible increase of actin

fibres density. This indicated that the actin cytoskeleton plays an important role in the stiffening of DU145 cells in response to VFL treatment. Actin depolymerisation, caused by cytochalasin D, leads to softening of cells treated with 100 nM VFL but not NTC cells. Thus, stiffening of DU145 cells caused by VFL action results from changes in its actin cytoskeleton functionality and organization.

9. MTDs included changes in mechanical properties of cell nuclear and peripheral regions

9.1 Introduction

Gathered results on time- and dose-dependent changes of morphology, cytoskeleton, and mechanical properties of DU145 cells exposed to MTDs were driving force to answer whether there is any specificity and localization of drug action within a cell. Are nuclear or peripheral regions of cells equally affected by MTDs? To elaborate the posed questions, a specifically tailored data analysis protocol was employed (as described in Chapter 4). Briefly, four conditions of mechanical properties of cells were considered. A mean elastic modulus of all points of cell clusters seems to be burdened with large inaccuracy because it considers all points measured over cellular clusters with no regard to differences in mechanical response to drugs, which occurs between particular cellular compartments. The two following cases address the mechanical properties of cell nuclei. Two indentation regimes were studied: shallow indentation (~5-15% of force curve – 1st range) and deep indentation (~20-40% of force curve – 2nd range). This part of the analysis was chosen by applying the nuclear mask (described precisely in Chapter 4). Such an approach allows determining separately mechanical properties of the perinuclear cytoskeleton (1st range) and cellular nucleus *per se* (2nd range). Finally, mechanical properties of lamellipodia regions were assessed by application of the mask analogous to nuclear mask. While lamellipodia are fragile structures, even though finite-thickness correction was applied in the presented studies, only shallow indentation was considered to avoid artefacts.

9.1 Elasticity maps of DU145 cells upon VFL and COL treatments

A lack of significant changes in the mean elastic modulus of whole clusters was observed in VFL-treated cells regardless of the drug concentration (100 nM & 750 nM) (**Fig. 9.1A**).

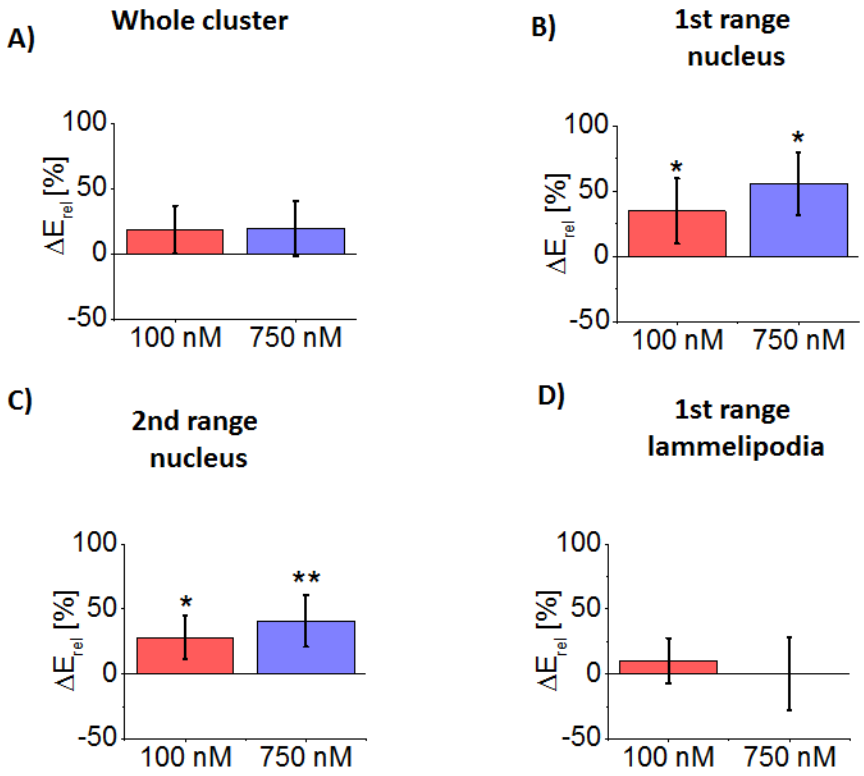

Fig.9.1. *Results of elasticity mapping of DU145 cells treated with various VFL concentrations. Mean elastic moduli (± SD) for particular cellular compartments are shown here for A) whole clusters, B) 1st range of nuclear region, C) 2nd range of nucleus, D) 1st range of lamellipodia. Statistical significance was calculated using Student's-test at the confidence level of 0.05. Notation: * p<0.05, ** p<0.01); (adapted from Kubiak et al. Nanoscale 13 (2021) 6212 with permission from The Royal Society of Chemistry).*

Significant changes were noted for both vinflunine concentrations (100 nM & 750 nM) and indentation regions when the nuclear region was considered. In this case, treatment with VFL led to a significant stiffening of DU145 cells (**Fig. 9.1B,C).** Importantly those stiffening was even more significant for data obtained from deeper indentation (**Fig. 9.1C**). Consequently, a lack of significant changes in the mean elastic modulus of lamellipodia was observed for cells treated with VFL (**Fig. 9.1D**). Thus, data obtained using elasticity maps and spherical probe are in line with the results observed with pyramidal cantilevers and smaller maps recorded above the nuclear region (**Fig. 7.1C, 7.2A**). These results underline that the stiffening of cells after drug treatment is concentrated around the nucleus. Such observation is ultimately important because all changes in the nuclear cytoskeleton might be responsible for affected gene expression and thus answer cells against drug treatment.

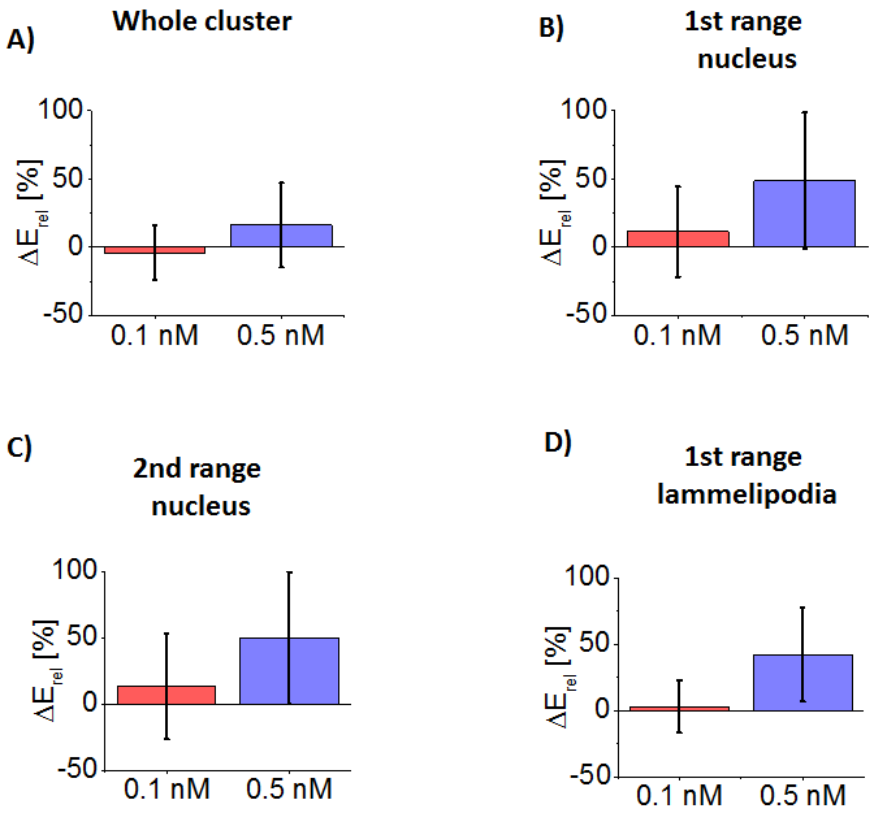

Fig.9.2. *Results of elasticity mapping of DU145 cells treated with various COL concentrations. Mean elastic moduli (± SD) for particular cellular compartments are shown here for A) whole clusters, B) 1st range of nuclear region, C) 2nd range of nucleus, D) 1st range of lamellipodia. Statistical significance was calculated using Student's-test at the confidence level of 0.05. Notation: * p<0.05, ** p<0.01); (adapted from Kubiak et al. Nanoscale 13 (2021) 6212 with permission from The Royal Society of Chemistry).*

For COL-treated cells, a lack of significant changes was observed for all conditions measured (**Fig. 9.2**). Some differences in mean elastic modulus might be visible for high concentration (0.5 nM) in the nuclear (**Fig. 9.2B,C**) and also lamellipodia (**Fig. 9.2D**) regions. However, variation was very high in those samples, as it is associated with severe damage of treated cells (**Fig. 8.2F**). To sum up, measurements undertaken for colchicine using spherical probes agree with those obtained with a pyramidal probe for smaller maps over the nuclear region (**Fig. 7.1C, Fig. 7.2B**). In the case of both microtubules destabilizers (VFL and COL), some alteration in nuclear stiffness of cells treated with high concentrations of drugs were observed – although such is rather resulting from overall damage to cells than the particular direction of cytoskeleton reorganization.

9.3 Elasticity maps of DU145 cells upon DTX treatment

Treatment of DU145 cells with a low concentration of docetaxel (1 nM) does not affect the cell mechanical properties with no regard to the cellular compartment analyzed (**Fig. 9.3A-D**).

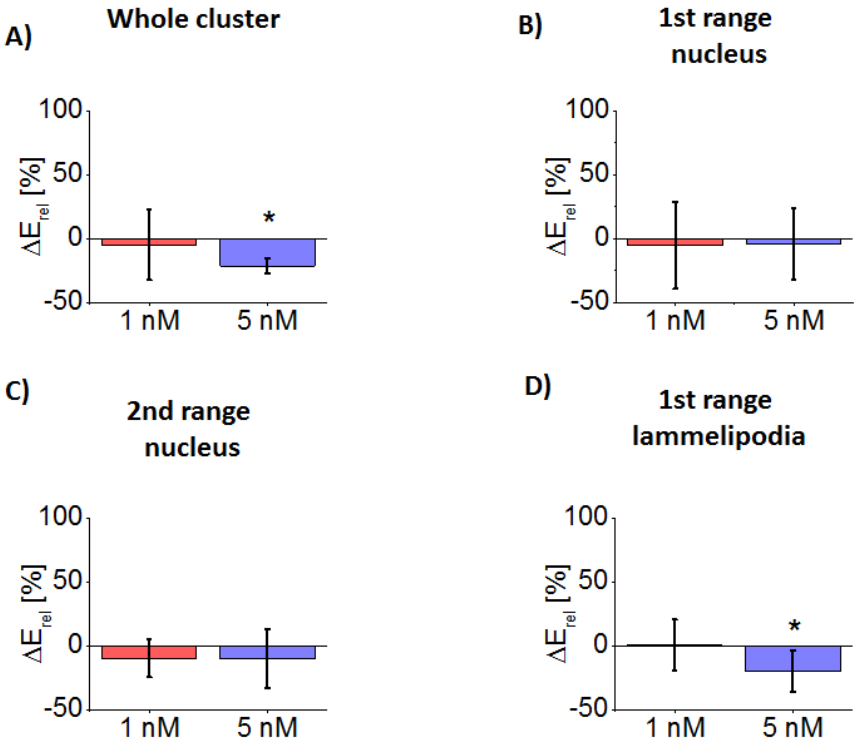

Fig. 7.7. *Results of elasticity mapping of DU145 cells treated with various docetaxel concentrations. Mean elastic moduli (±SD) for particular cellular compartments are shown here for A) whole clusters, B) 1st range of nuclear region, C) 2nd range of nucleus, D) 1st range of lamellipodia. Statistical significance was calculated using Student's-test at the confidence level of 0.05. Notation: * p<0.05, ** p<0.01; (adapted from Kubiak et al. Nanoscale 13 (2021) 6212 with permission from The Royal Society of Chemistry).*

Such observation – especially for the nuclear region – is strongly in line with results obtained during measurements with pyramidal tip, where a lack of changes in mechanical properties of DU145 cell was noted (**Fig. 7.3**). On the contrary, significant softening of lamellipodia of DU145 cells was visible in cells were treated with a high concentration of docetaxel (**Fig. 9.3D**). Consequently, a significant drop of elasticity was observed in the case of whole clusters of DU145 cells treated with 5 nM of DTX (**Fig. 9.3A**) – which results from the fact that the overall contribution of a lamellipodial region is larger than nuclear regions due to

extensive area occupation by those cellular compartments. In the case of high drug concentrations, similarly to results obtained for experiments performed on VFL and COL treated cells, changes in mechanical properties were observed, although the direction of those changes is opposite after DTX treatment. First of all, high drug concentrations lead to the robust destruction of cells with no drug specificity. The mechanism of their action, which is pronounced in high concentrations, might imply some functional explanation for such behaviour. Since docetaxel is the stabilizer of microtubules, in cells that can resist 5 nM treatment, microtubules are over stabilized in central but not peripheral regions (**Fig. 8.2H**). Thus lamellipodia lost one of their mechanical support, i.e. microtubules, leading to cells softening in lamellipodia – but not in the nuclear region.

9.5 Discussion and summary

Elasticity maps of cells have been proposed as an attractive method of investigating cellular mechanical properties (44,72). Notably, the multilayer approach proposed by Kaushik et al. is enhancing how such data are interpreted. Since the primary approach was designed to investigate tissues organized in multilayers, the same approach might be successfully applied for cells (70). In the present work, thanks to force curves segmentation (in principle, thanks to focusing on the deep indentation of the nuclear region), it was possible to determine more exact information about the mechanical properties of the nuclear region of cells. Such findings are essential in the field of recent developments in the field of biomechanics and mechanotransduction. It is vital because forces acting on cells might affect the nucleoskeleton of cells (116). One of the most important changes in how the cell nucleus interacting cytoskeleton is organized is changes in gene expression (117). Changing physical signal into biological ones is referred to as mechanotransduction and is directly connected with dynamic changes in cellular cytoskeleton dynamics and organization (117,118). Recently, numerous reports have shown that changes in the mechanical properties of cells microenvironment might affect how cells respond to chemotherapy (15,119). In breast cancer, treated with drugs like paclitaxel, changes of stiffness of the matrix on which those cells are cultured could increase their drug resistance even more than 1000 times. The authors of that work show that changes in physical interaction alter the expression of numerous genes involved in drug resistance - i.e. Cyp1a1, Ephx1, Tubb4b, Trp53, Bax (15). In the field of such developments, the results obtained here for VFL are interesting. This is a drug in the effect of which use significant stiffening of cells is observed only in its nuclear compartment. What is more, the

data presented regarding the potential action of this drug against DU145 cells show that they are the most sensitive against VFL but not COL and DTX. Thus, it indicates that those physical changes might be a factor involved in the process of inducing of resistance, or at last, a marker of cellular adaptation against drug action. Such statements might be somehow confirmed by previously published data showing that stiffening of cancer cells is associated with their higher invasiveness (68,69) and is a feature of cells that resisted drug action (28).

10. Mechanical properties of starved prostate cancer cells

10.1 Introduction

One of the largest problems to be solved while designing anticancer therapy is cancer cell resistance against therapeutics agents (120). For MTDs, such drug resistance might be achieved by a mutation in tubulin but also by the expression of transmembrane protein channels that pumps drugs away from the cell body (121). On the other hand, there is another source of resistance of cancer cells against antimitotic drugs (including MTDs) – their low proliferation rate or even senescence (122). Such cells possess stem cell-like characteristics with the potential capability to restore tumours, even if the ultimate majority of proliferating cancer cells are killed. The possible source of such cells (referred to as cancer stem cells) is the necrotic core of the tumour (123). Tumours are complicated, three-dimensional structures made of multiple cell types and consist of multiple layers of cells. As a result, the inner part of the tumour is poorly fed due to a low number of blood vessels supplying it with oxygen and major nutrients and metabolites like glucose or glutamine. Such a process results in creating a necrotic core of the tumour, in which only the most resistant cells are capable of surviving in such unfavourable conditions (122). As described in previous Chapters, dynamic changes of elastic modulus of prostate cancer cells might serve as descriptors of drug action. In the field of multiple mechanisms of drug resistance, there is a need to answer whether physical factors might be utilized directly to predict such resistance.

In terms of drug resistance experiments, cells originating from the necrotic core are interesting because they resist the unfavourable conditions of ultimate starvation. Spheroids can model a simple three-dimensional (3D) structure of tumours, in which it is possible to distinguish three distinct regions: rapidly proliferating region being the outermost layer of the spheroid, quiescent region located in the middle between the outer layer and the third region – necrotic core (Fig. 10.1).

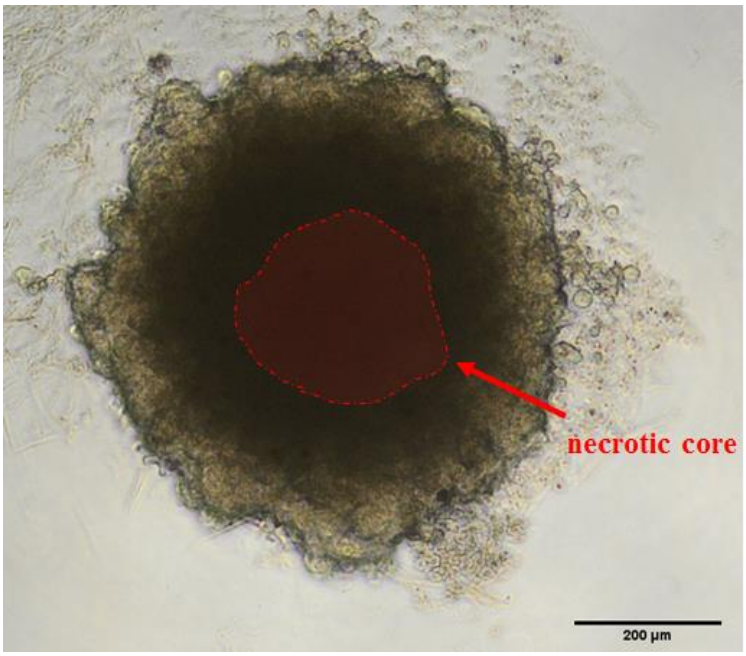

Fig. 10.1. *Brightfield image of the spheroid formed from DU145 cells. The red zone shows the necrotic core, in which cells suffer from a lack of nutrients. Scale bar – 200 µm.*

As the isolation of those cells from the 3D spheroid is a very challenging procedure, 2D models can be applied to assess the properties of cells in conditions of insufficient nutrients. Thus, to obtain a simpler system, prostate DU145 cancer cells were cultured in L-glutamine (L-GLN) starvation conditions. L-GLN starvation mimics the conditions inside the necrotic core of the tumour (124–127). The properties of starved cells (here, referred to as GLN- cells) were quantified by applying various methods, namely, MTS assay (proliferation), wound healing assay (migration), AFM (biomechanics of cells), fluorescent confocal imaging. The studies aimed to answer whether the mechanical properties of prostate cancer cells might be treated as an indicator of cellular resistance against antitumor therapy by docetaxel (DTX).

10.2 Viability of GLN- DU145 cells

The viability of DU145 cells cultured in conditions of L-GLN depletion was assessed by MTS assay (described in Chapter 3). Control cells (CTR cells) were cultured in the standard condition in Dulbecco's Modified Eagle's Medium (DMEM, Sigma-Aldrich) with low glucose supplemented with 2 mM L-glutamine and 10% of heat-inactivated Fetal Bovine Serum (FBS, Sigma-Aldrich). Starvation of cells was achieved by seeding cells in a medium

without L-glutamine. The MTS results show that after 24 hours, the number of GLN- cells decreased in relation to NTC cells (**Fig.10.2**).

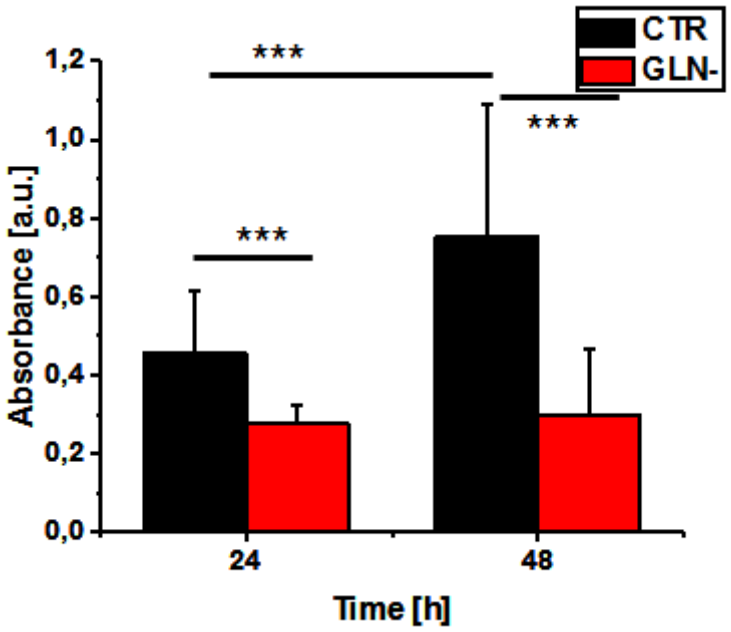

Fig. 10.2. *MTS assay showing lower absorbance for GLN- cells after 24h and 48h of culture in conditions of L-GLN depletion (CTR denotes control cells cultured in standard cell culture medium containing 2 nM glutamine). Absorbance is related to the number of cells. Data are presented as a mean ± standard deviation (SD) from n = 4 repetitions. Statistical significance was calculated using the Student's t-test at the confidence level of 0.05 (*** $p < 0.001$).*

Longer cell culturing in the absence of L-glutamine, i.e. up to 48h, shows the increase in the number of CTR cells in control conditions indicating that the number of cells increases with time. These are proliferating cells. In L-GLN depletion conditions, the number of GLN- cells remained at a similar level as in the case of 24h. This confirms that starvation of prostate cancer cells induced by the L-GLN depletion from the culture medium inhibits cell proliferation. The relative difference between CTR and GLN- cells is larger after a longer culture time (~31% decrease in absorbance after 24 hours and ~60% decrease after 48 hours).

10.3. Migratory properties of GLN- DU145 cells

Since the migration of cancer cells plays a crucial role in disease progression (128), in the next step, the migration of GLN- cells was evaluated based on a wound-healing assay

using culture – inserts 2 well in (ibidi, **Fig. 10.3 A**). They were used to form wound areas without jagged and lumpy borders at the initial point of the experiment.

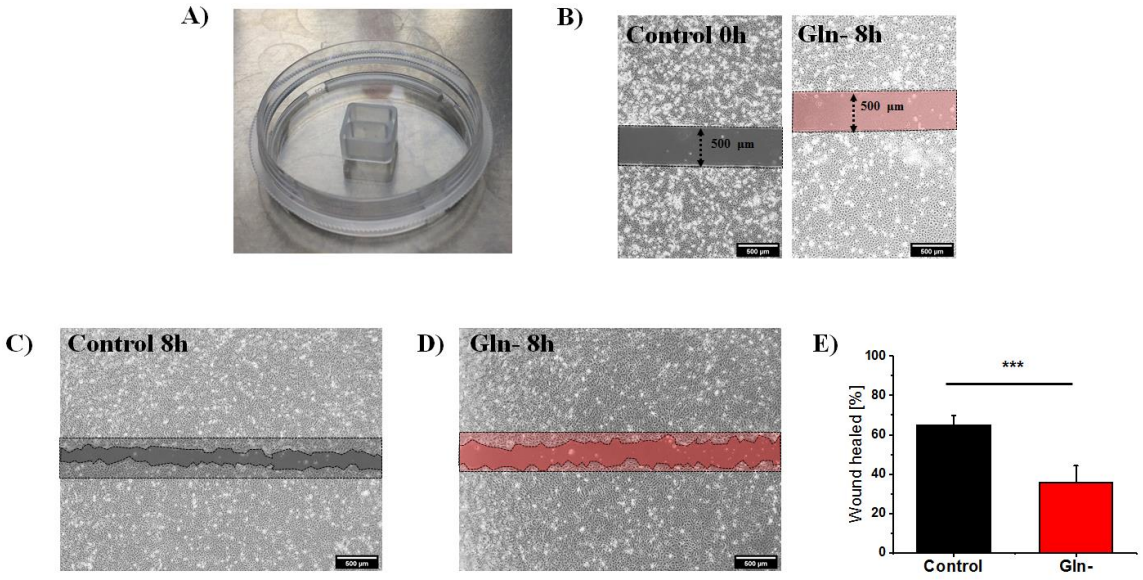

Fig. 10.3. *Comparison of migratory properties of CTR and GLN- prostate DU145 cancer cells assessed using a wound-healing assay. A) photography of cell culture insert allowing preparation of cells for wound healing experiment. B) Brightfield microscopy images of DU145 cells at the initial point of measurement. Representative brightfield images showing wound area covered by cells after 8 hours of experiments for C) control cells and D) GLN- cells. E) Bar plot illustrating the percentage of wound healing after 8 hours of measurement. Data are presented as mean values ± SD from n = 5-6. Statistical significance was calculated using the Student's t-test at the confidence level of 0.05 (*** p < 0.001).*

In the case of both CTR and GLN- cells initial wound area was the same (**Fig. 10.3B**). The wound healing outcome is expressed as a percentage of wound area covered by cells after 8 hours of observation. Its larger values indicate that the wound grows faster. Such value is related to the migratory properties of cells as they migrate towards the centre of the wound. The results show that CTR cells migrate faster than GLN- cells (after the same time of culture, the width of the wound is smaller for CTR cells, **Fig. 10.3C,D**). For the CTR cell, after a relatively short period of 8 hours, the wound healing outcome was characterized by a mean value of 66.90 ± 3.28% (an error is the standard deviation). For GLN- cells, the wound coverage was lower and equalled 33.61 ± 8.31% (**Fig. 10.3E**). In conclusion, eliminating L-glutamine from cell culture media leads to decreased mobile capabilities of DU145 cells.

10.4. Mechanical properties of GLN- DU145 cells

Mechanical properties of GLN- cells were measured with AFM working in force spectroscopy mode. Young's modulus was determined for two starvation times, i.e., after 24h and 48h of cell culture in conditions of L-glutamate depletion. Results are presented in **Fig. 10.4**.

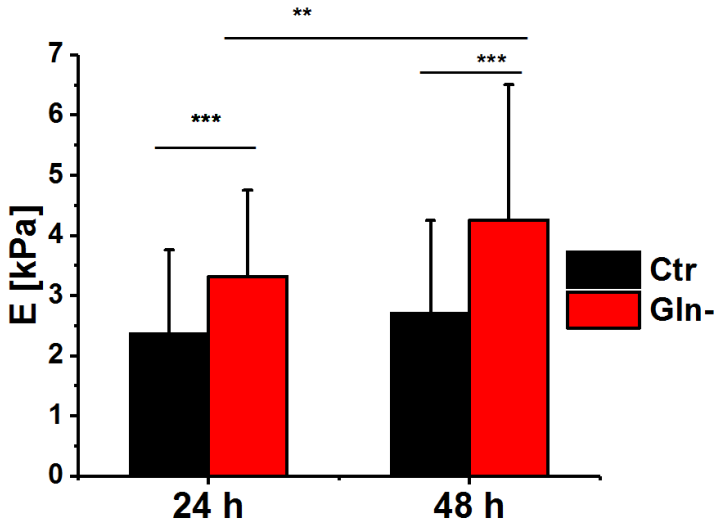

Fig. 10.4. *Changes in elastic modulus of CTR and GLN- cells cultured for 24 and 48 hours in the absence of L-GLN. Data are presented as mean values ± SD from n = 66 - 103 cells. Statistical significance was calculated using the Student's t-test at the confidence level of 0.05 (** p < 0.01, *** p < 0.01).*

After 24 hours of cell culture, the mechanical properties of DU145 cells are characterized by Young's modulus of 2.36 ± 1.38 kPa (expressed as mean ± SD, *n* = 92 cells). After the same culture time, Young's modulus of GLN- cells was larger (3.31 ± 1.43 kPa, *n* = 66 cells). After a longer culture time (48 hours), the mechanical properties of CTR cells remained at a similar level of 2.70 ± 1.53 kPa (*n* = 103 cells). After the same time of culture, Young's modulus for GLN- cells increased to 4.25 ± 2.24 kPa (n = 80 cells). This value was about 30% larger than that obtained after 24 hours of culture in conditions of GLN depletion. The results show that the prolonged absence of L-glutamine in cell culture media leads to stiffening of prostate DU145 cancer cells.

10.5 Spatial distribution of mechanical properties in GLN- cells

To better understand changes in mechanical properties of GLN- DU145 prostate cancer cells, elasticity maps were recorded for cell clusters. DU145 cells tend to grow in clusters. CTR cells tend to grow in larger clusters of 7-8 cells, particularly visible after 48 hours of cell culture. In conditions of L-GLN depletion, GN- cells proliferate slower or even are in a state of quiescence. As a consequence, GLN- cells grow in small clusters of 2-4 cells. Thus, to compare the distribution of mechanical properties, the clusters of 4 cells were chosen. For such clusters, both topography and mechanical properties were measured by mapping whole clusters by AFM. Exemplary images showing the surface topography and mechanical properties of CTR and GLN- cells are presented in **Fig. 10.5**. To correlate cell topography with elasticity, cells were fixed in 3,7 propionaldehyde for 30 minutes. Such an approach has been already proposed and proved that fixation of cells increases absolute values of determining elastic moduli (cells stiffen) but does not affect the relationship between different sample elastic moduli (129). During the analysis, the finite-thickness correction was applied to eliminate the influence of stiff underlying surface on the mechanical properties of living cells. Control cells are growing in cellular clusters organized in a way, which allow counting four cells per clusters easily. Each cell possesses a high nuclear region and shorter lamellipodial regions (**Fig. 10.5A**). Control cells are characterized by a relatively uniform distribution of elastic modulus value within clusters (**Fig. 10.5B**). In the case of GLN- cells, they are also forming clusters organized by four different cells. Nevertheless, a short lamellipodial region within clusters is less pronounced than in control clusters (**Fig. 10.5C**). Moreover, in the case of GLN- clusters distribution of elastic modulus value is more heterogenous within clusters, and its values are higher than in control cells (**Fig. 10.5D**).

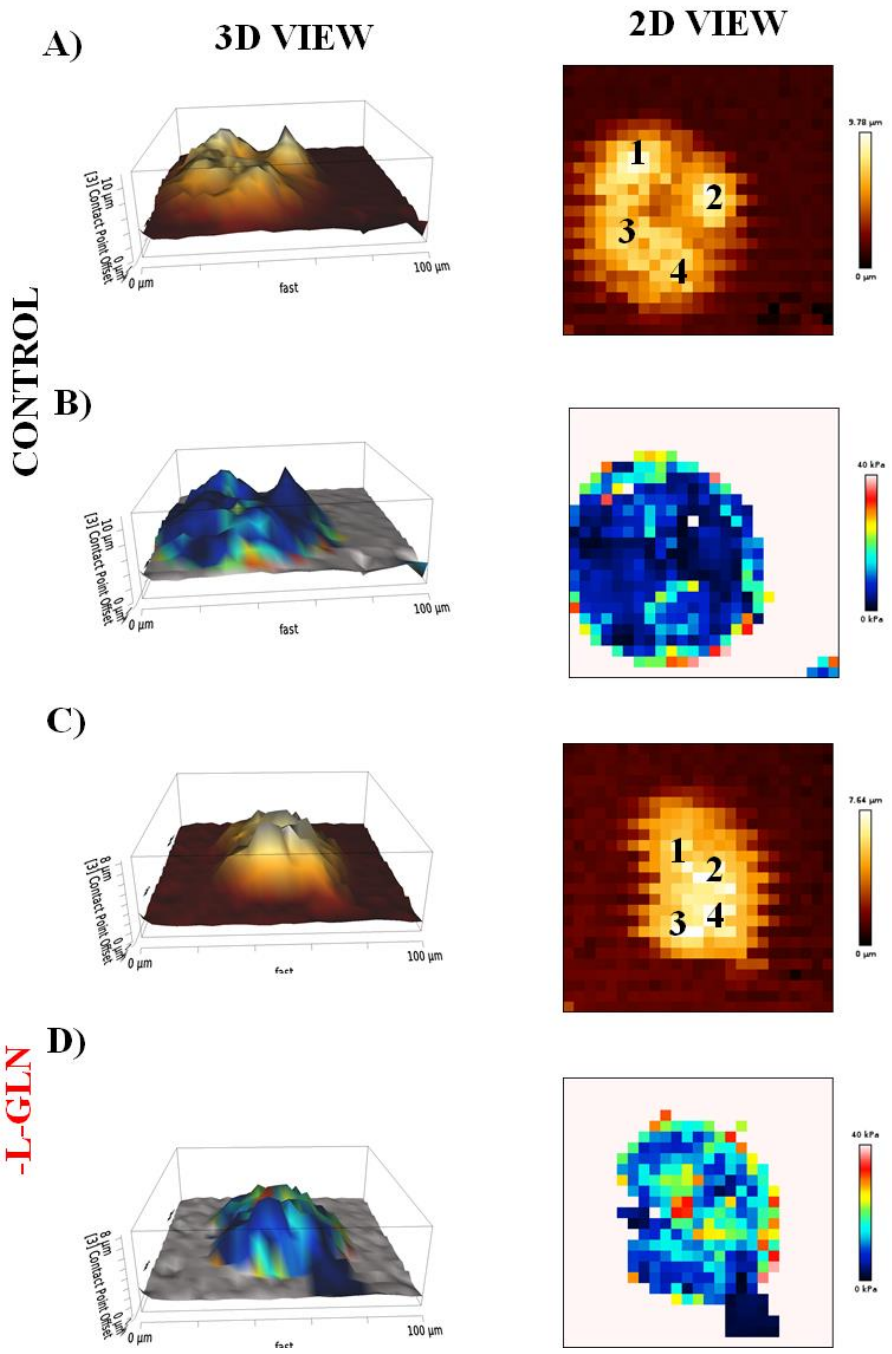

Fig. 10.5. *Surface topography and elasticity maps of fixed CTR and GLN- DU145 cell clusters. Cells were fixed in 3,7% paraformaldehyde, and elastic maps were acquired using Nanowizard 4.0 head. 3D views show three-dimensional images of clusters acquired with elasticity maps for A) control and C) GLN- DU145 cells. 2D views show the corresponding topography as well as elasticity maps for A),B) control and C),D) GLN- cells. The highest points indicating the nuclear region of every single cell forming a cluster are numbered from 1 to 4.*

The overall mean Young's modulus of the CTR and GLN- cell clusters was calculated from all analyzed force curves acquired for each of the analyzed clusters.

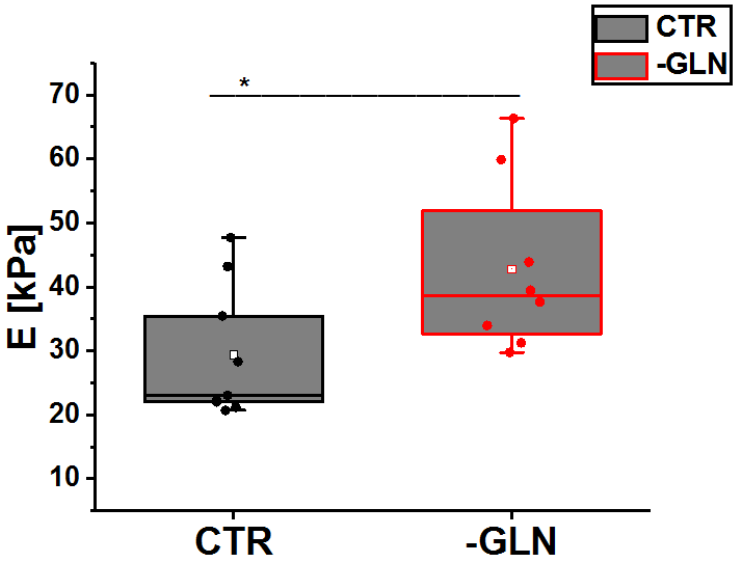

Fig. 10.6. *Young's modulus of CTR and GLN- cell clusters presented as boxplots. Dark dots represent the mean calculated for each cluster separately, straight-line represents the median, while open square – mean elastic modulus. Statistical significance was calculated using the Student's t-test at the confidence level of 0.05 (* $p < 0.05$).*

Due to the applied fixation, Young's modulus of cell clusters is higher than that of living cells (**Fig. 10.4**). However, the results show that GLN- cells are stiffer than CTR cells (**Fig. 10.6,** $p < 0.05$). The obtained moduli were 29.32 ± 10.31 kPa (n = 8 clusters) and 42.76 ± 13.45 kPa (n = 8 clusters) for CTR and GLN- cells, respectively. These findings reveal that the applied fixation of cells (3,7% of paraformaldehyde, 30 minutes) does not influence the relation between CTR and GLN- cells. Moreover, the stiffening of DU145 can be associated with intrinsic cellular properties that do not depend on the culture form.

10.6 Cell cytoskeleton organization of GLN- DU145 cells

Considering the relation between mechanical properties of cells and cytoskeleton, in the next step, confocal fluorescent microscopy was applied to visualize the organization of actin filaments and microtubules (**Fig. 10.7**).

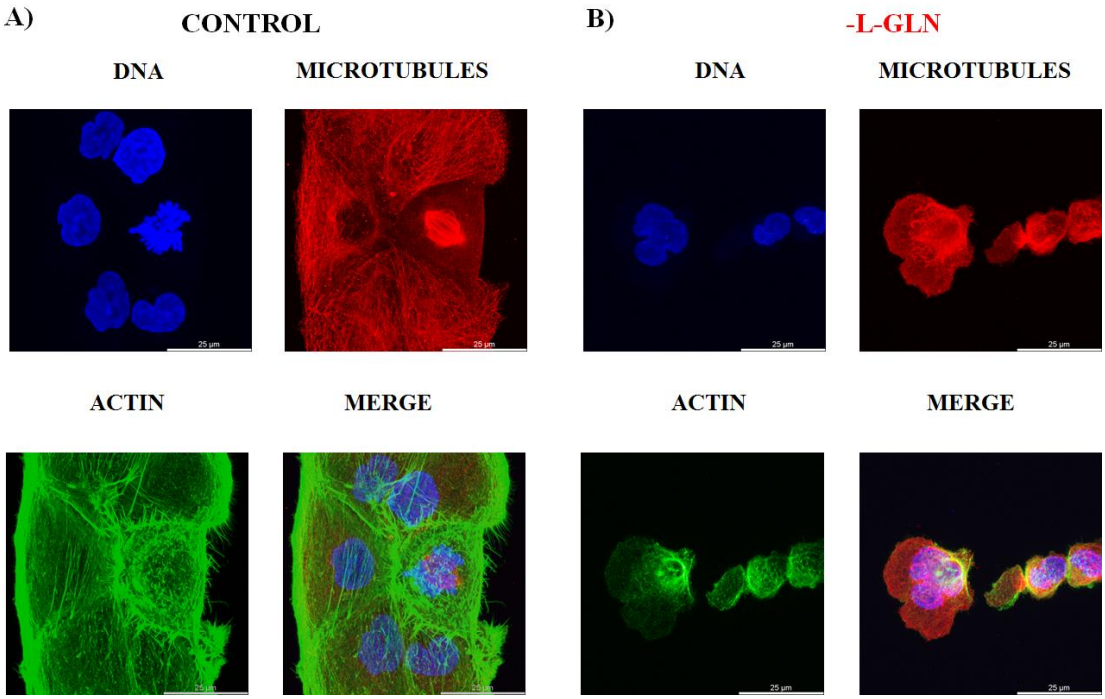

Fig. 10.7. *Maximal projection confocal images showing cytoskeleton of A) control and B) GLN- DU145 cells. Actin filaments are stained green, microtubules red, and nuclei blue. Scale bar = 25 μm.*

Control DU145 cells are characterized by prominent nuclei and well developed microtubular and actin cytoskeleton (**Fig. 10.7A**). Fluorescent images show that upon starvation, cells lost their well-shaped morphology. Both microtubular and actin cytoskeleton lost their ordered organization. Cells tend to cover smaller area (**Fig. 10.7B**). A similar trend of shrinking refers to nuclei of GLN- cells. What is more, nuclei of GLN- cells are more deformed than control ones. Control cells (0.78 ± 0.05) are characterized by significantly higher circularity than GLN- cells (0.70 ± 0.12) (**Fig. 10.8A**). Consequently, nuclear roundness is also significantly higher in control cells (0.83 ± 0.10) compared to GLN- cell nuclei (0.74 ± 0.12, **Fig. 10.8B**). In the case of nuclei shape descriptor, which is the roundness, the nuclei in control cells are characterized by ultimately lower variability in its values. The roundness of the nuclei in the GLN- cells is distributed more randomly, indicating that starvation strongly affects the nuclear morphology (**Fig. 10.8B**). The roundness of the nuclei in CTR cells (0.83 ± 0.10) was at the same level as for NTC (0.82 ± 0.09) derived from standard fluorescent images of cell nuclei (**Fig. 8.1D, Fig. 10.8A**).

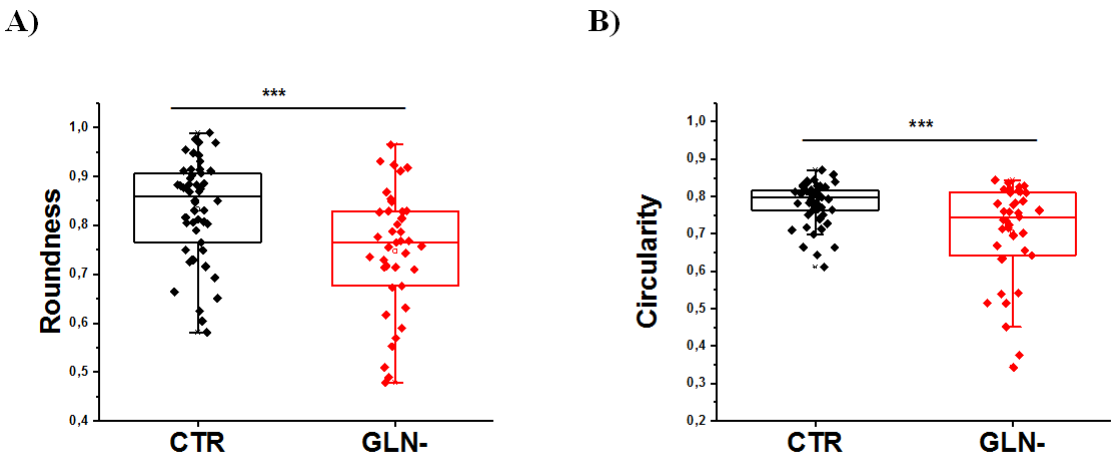

*Fig. 10.8. Distribution of shape descriptors describing changes in nuclei of DU145 cells: (A) roundness B) circularity) of DU145 cells, 50 CTR cells and 39 GLN- cells were considered. Data are presented in boxplots (25th~75th percentiles), with whiskers indicating a range within 1.5 IQR, horizontal line denotes the median, open square denotes mean, statistical significance was calculated using the Student's t-test at the confidence level of 0.05; *** - p<0.01.*

Confocal fluorescent imaging delivered a clue that changes in nuclear morphology might be one of the factors responsible for cell stiffening. Thus, the nucleus may contribute to the overall mechanical properties of cells and might also be responsible for cell stiffening after GLN starvation.

As depicted above, changes in the organization of intrinsic cellular morphology were characterized by aggregation instead of the uniform arrangement of cytoskeleton and alterations in the morphology of the nucleus. Among them, nuclear morphology seems to be responsible for the observed stiffening of DU145 cells after GLN starvation. The loss of well organized microtubular and the actin cytoskeleton makes the cell nucleus a part responsible for maintaining cell mechanical properties. Thus, in such an observation question arise whether loss of the cytoskeleton organisation makes the nucleus more important for mechanical properties of cells and whether the cell nucleus occupies a bigger part of the cell, thus even more robustly impacting its elastic properties. In the next step, images recorded using an epifluorescent microscope were acquired to quantify the nuclear to cell ratio (N/C ratio). This was realized by recording fluorescent images of the actin cytoskeleton used to calculate the surface area of a whole cell. Simultaneously, fluorescent images of the cell

nucleus were collected and used to determine its surface area. After 24 hours of cell culture, the surface area of GLN- cells significantly decreased as compared to CTR cells (**Fig. 10.9A**). The decrease remains similar also for cells cultured in control and GLN- conditions for 48 hours. These observations correlate with confocal images showing the smaller surface area of GLN- cells (**Fig. 10.7**). The nucleus surface projection area follows the relation observed for the cell surface projection area (**Fig. 10.9B**).

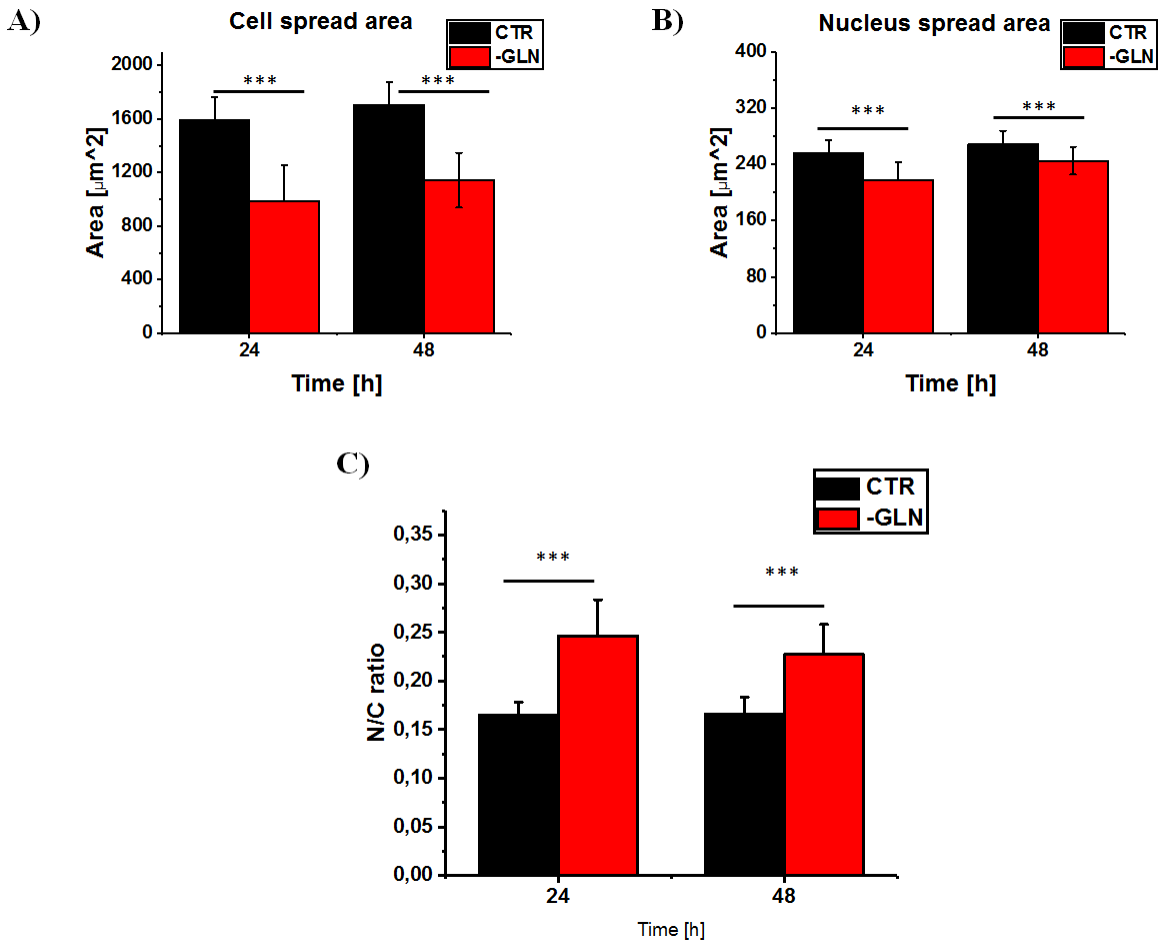

Fig 10.9. *Changes in the projection surface area of A) cells and B) nuclei observed in CTR and GLN- DU145 cells. C) Determined N/C ratio of DU145 cells. Statistical significance was calculated using the Student's t-test at the confidence level of 0.05; *** - p<0.01.*

The calculated N/C ratio shows that, regardless of the culture time (24 hours or 48 hours), the N/C ratio was larger for GLN- cells(**Fig. 10.9C**). This indicates that in starved cells nucleus occupies the largest part of the cell. In such a situation, for cells with the altered cytoskeleton uniform organization, the cell nucleus takes the leading role in maintaining the mechanical properties of cells. Here, such a phenomenon led to the increasing elastic moduli of cells

measured by AFM. Importantly such changes in the contribution of nuclei to the maintenance of mechanical properties of DU145 cells are also changing how the cell nucleus gains physical information from cell surroundings in the process of mechanotransduction (116–118,130,131).

10.7 DTX effect on GLN- DU145 cells

Changes in nuclear mechanics are known to affect mechanotransduction, one of the processes responsible for drug-resistance development (15,16,116,119,131,132). Therefore, the effect of docetaxel (DTX) on GLN- cells was studied. Prostate cancer DU145 cells were cultured under control (GLN+) and GLN- conditions for 48 hours. After this time, the cell culture medium was replaced with a control medium containing DTX for 72 hours of cell culture. DTX concentration of 2.9 nM, representing IC_{50} dose (calculated based on data shown in **Fig. 6.1b**), was applied in this experiment. After this time, MTS cytotoxicity assays were performed to assess the impact of DTX on cell viability **(Fig. 10.10)**.

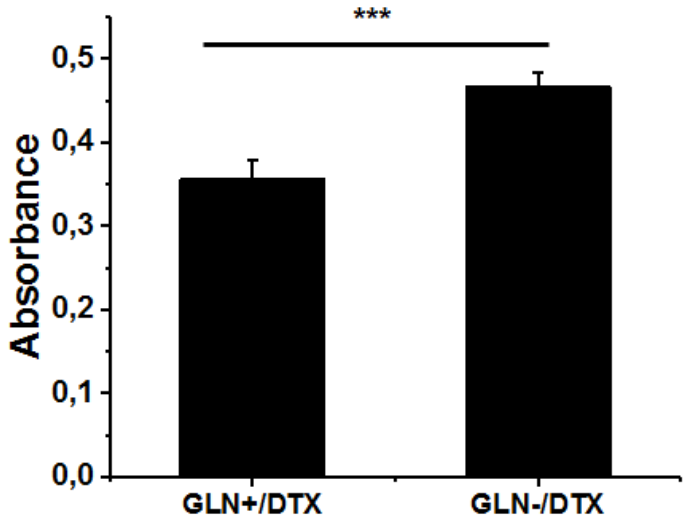

Fig. 10.10 *Relative change in the viability of DU145 cells treated by 2.9 nM DTX after 72 hours of culture. Data are expressed as a mean ± standard deviation (n = 5 samples). Relative absorbance is calculated by dividing the absorbance of DTX treated cells by the absorbance of the corresponding control. Statistical significance was calculated using the Student's t-test at the confidence level of 0.05; *** - p<0.01.*

After 72 hours of cell exposure to 2.9 nM DTX, the viability of DU145 cells shows condition-dependent relation. The number of DU145 cells cultured in conditions of GLN depletion before adding the DTX was more significant than the number of cells cultured in control conditions (with L-glutamate) before adding DTX. These results indicate that starved cells are significantly more resistant to the applied 2.9 nM (IC_{50}) concentration of DTX than CTR cells.

10.8 Effect of DTX and GLN- on mechanical properties of DU145 cells

Knowing that DTX affects the mechanical properties of cells, Young's modulus of CTR and GLN- cells was determined using AFM. Cells were cultured in control and GLN depleted conditions for 48 hours. For both control and L-GLN depleted cells, DTX in 1 nM dose was added for the time of their culture. The results of the analysis of AFM mechanical properties of cells are shown in **Fig. 10.11**.

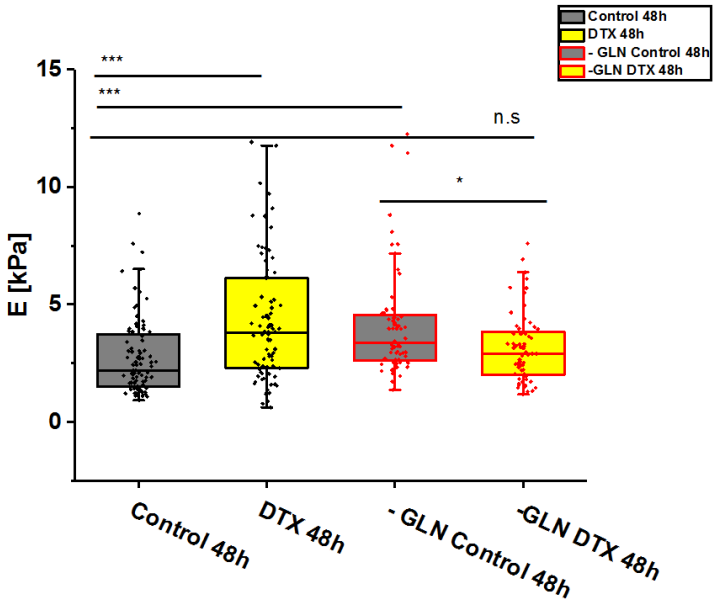

Fig. 10.11 *Youg's modulus calculated for CTR and GLN- cells treated with DTX (1 nM) for 48 hours. Data are presented in boxplots (25th~75th percentiles), with whiskers indicating a range within 1.5 IQR, horizontal line denotes the median, open square denotes mean. The number of measured cells: CTR cells - 88, CTR cells treated with DTX - 83, GLN- cells – 64, and GLN- cells treated with DTX – 64. Statistical significance was calculated using the Student's t-test at the confidence level of 0.05, *** - $p < 0.001$, * $p < 0.05$, ns – not statistically different.*

For cells cultured in control conditions (with L-glutamine), DTX treatment of prostate cancer DU145 cells caused cell stiffening. Young's moduli were 2.74 ± 1.63 kPa (n = 88 cells) and 4.50 ± 3.23 kPa (n = 83 cells) for CTR and CTR treated with DTX cells, respectively. In the case of the GLN- condition, the opposite effect was observed. Young's modulus for GLN- cells was 4.15 ± 2.33 kPa (n = 64 cells), and it decreased for cells treated with DTX to 3.16 ± 1.46 kPa (n = 64 cells). Knowing that mechanical properties are linked with cytoskeleton organization and that DTX interacts with microtubules, fluorescent images of the microtubular network were recorded (**Fig. 10.12)**.

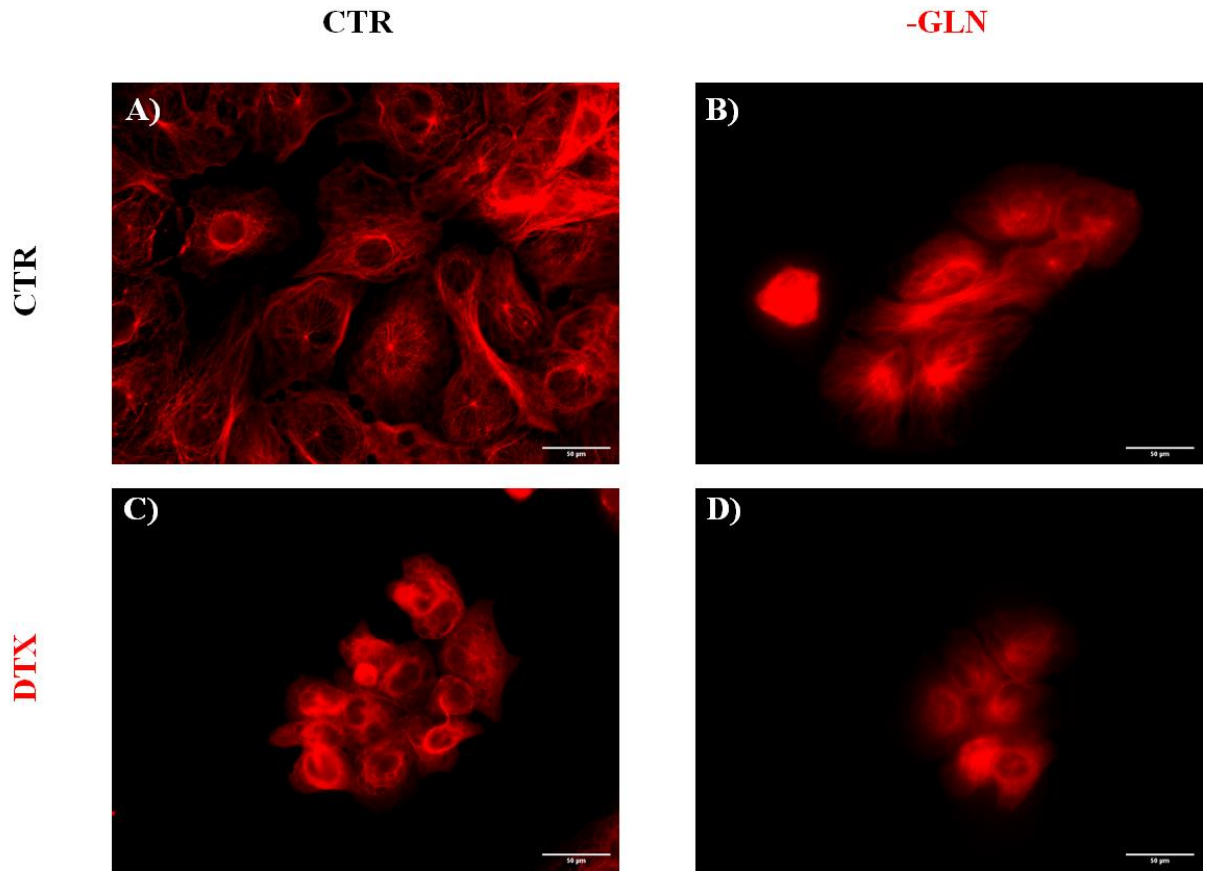

Fig. 10.12 *Fluorescent images of a microtubular network of DU145 cells: A) CTR, and B) GLN- cells, C) CTR cells treated with 1 nM DTX, D) GLN- cells treated with 1 nM DTX (scale bar = 50 μm).*

In CTR cells, the microtubular network is very well organized with multi-branched filaments (**Fig. 10.12A**). The DTX treatment leads to cell shrinking and pronounced aggregation of the microtubular network around the cell nucleus (ring-like structures are observed to form around the nucleus) with parallel loss of the microtubular network in the cell periphery (**Fig.**

10.12C). In contrast, in GLN- cells, the microtubular network is not well developed. These cells are characterized by a more compact shape with a weaker distribution of MTs in the cell periphery. (**Fig. 10.12B**). After DTX treatment, the microtubular network of the GLN- cells was similar to that observed for DTX treated CTR cells. However, the ring-like structures in these cells were weakly visible (**Fig. 10.12D**).

Such observation of changes in the microtubular cytoskeleton explains changes in mechanical properties of DU145 cells during simultaneous GLN depletion and DTX treatment. Two distinct mechanisms are responsible for the stiffening of cells (**Fig. 10.11**): random aggregation of tubulin in GLN depleted cells (**Fig. 10.12B**) and aggregation of tubulin around cell nuclei in the case of DTX treated control cells (**Fig. 10.12C**). Finally, in the case of cells that are both starved of GLN and treated with DTX, the balance between aggregation of tubulin in rings and random places inside cells is observed, leading to restoration of mean elastic moduli to a level similar to in control cells (**Fig. 10.11, Fig. 10.12C**).

10.9 Discussion

Cancerous cells are well known to be characterized by affected metabolism – including the Wartburg effect and deregulated demand on amino acids, including glutamine (133). In principle, glucose and glutamine are crucial metabolites required by cancerous cells to grow and proliferate. In detail, glutamine is catabolized in TCA to deliver energy for cancerous cells (134). Nevertheless, in prostate cancer cells, Wartburg effects are not so often observed like other cancers. In turn, prostate cancers were reported to rely on lipids metabolism. As such, glutamine is one essential metabolite since it is utilized for the *de novo* synthesis of lipids. Lipids are then the fuel of energy generation – ultimately at lower grades of prostate cancer (135). Prostate cancer cells originating from bone metastasis (PC3 cells) and their more invasive subline PC3M have been shown to rely on glutamine (136). It was suggested that glutamine deprivation might be a strategy for treating multiple cancers, including prostate cancer (137). Multiple inhibitors of GLN transporter have been suggested for therapeutic approaches (138). Despite promising results obtained from *in vitro* studies (124,125,137,139–142), such therapies are still not fully successful. It was reported that the cancer cell microenvironment is characterized by low glutamine concentration. Consequently, Gabra M. et al. showed that cancerous cells adapt to a glutamine starved environment and survive within it (143). Low glutamine concentration has been shown to induced de-

differentiation of cancerous cells. As a result, cancerous cells were more resistant against action inhibitors of the B-Raf enzyme, a targeted chemotherapeutic agent (known under market name Zelboraf, (144). Recently, Shih-Jung F. et al. has reported that glutamine depletion in cancer cells stimulates them to secrete exosomes. Those exosomes contain bioactive molecules which exert action promoting tumour development. This mechanism was considered as one of how cells adapt to stressing starvation conditions (145). On the other hand, tumour-derived exosomes have recently been shown to affect the mechanical properties of the lungs. In principle, they led to softening of the lung by changes in the expression of ECM proteins, promoting metastasis to this organ (146). Changes in the mechanical properties of cells resulting from changes in their metabolism may activate events promoting drug resistance. Such stiffness-mediated drug resistance awakeness has been already shown for different types of cancers (15,119,132).

10.9 Summary

The presented chapter showed that depletion of GLN in cell culture medium results from the inhibition of prostate cancer cell proliferation and metabolic activity (**Fig. 10.2**). Migratory properties of DU145 cells were also significantly decreased after depletion of GLN in cell culture medium (**Fig. 10.3**). Parallelly, the DU145 cells became significantly stiffer just after 24 hours of GLN depletion, and this stiffening was even pronounced after 48h of GLN starvation (**Fig. 10.4**). To understand whether this stiffening results from culture form (starved cells growth in small clusters while control cells might form larger cellular colonies) or intrinsic properties of the cell, elasticity maps of whole clusters of cells were acquired. Such a method allowed to precisely trace the morphology of analyzed clusters and compare only those clusters made of four cells for both investigated conditions (**Fig. 10.6**). The same trend was preserved after utilising such an approach – GLN starved cells were significantly stiffer than control ones (**Fig. 10.7**). This observation allowed us to conclude that stiffening results from changes in the biological sample's intrinsic properties after GLN starvation. In the next step, the cellular cytoskeleton was analyzed by confocal fluorescent microscopy, which allowed to observe that the GLN's cytoskeleton tends to be more agitated (**Fig. 10.7**). The analysis of shape descriptors of cell nuclei showed that after GLN depletion, its roundness and circularity are significantly lower than in CTR cells (**Fig. 10.8**). Therefore, a hypothesis was proposed that nuclear malformation and aggregation of the cytoskeleton lead to cell stiffening. To verify the hypothesis, fluorescent images of actin and cell nuclei were analyzed to

compare CTR and GLN- cell and nuclei projection areas. As a result, it was showed that the nucleus to cell ratio is higher in GLN depleted cells (**Fig. 10.9**). Thus it was justified to state that increased contribution of the cell nucleus leads to increased stiffness of DU145 cells after its GLN starvation. The contribution of the nucleus to overall cellular stiffness has already been shown for breast cancer cells (24). Finally, it was shown that GLN- cells were more resistant to DTX treatment (**Fig. 10.10**), explained by changes in the mechanical properties of cells. While both starvation alone and DTX treatment alone led to an increase of DU145 cells stiffness, simultaneous DTX treatment and GLN starvation do not affect DU145 elastic moduli in a significant way (**Fig. 10.11**). Consequently, those relationships were confirmed in the pattern of changes in the microtubular network – where simultaneous DTX treatment and GLN starvation affected the microtubular network in the lower way while comparing to DTX treatment and GLN depletion alone (**Fig. 10.12**).

To sum up, the obtained results show that conditions of GLN depletion led to a stiffening of cells. The effect of DTX on GLN- cells was weaker, indicating that docetaxel was less harmful to these cells than CTR cells, most probably due to a lower degree of damages caused in the microtubular network of GLN- cells (**Fig. 10.10, Fig.10.12**).

11. Summary and conclusions

Atomic force microscopy (AFM) has been already used in studying the mechanical properties of cells. To obtain more precise information about the nature of mechanical changes in cells – especially with consideration that cytoskeleton fibres are expanded into the different cellular area, AFM mapping of whole cells and cellular clusters have been exploited to answer the question of whether changes in mechanical properties of cells due to drug action are unique for particular cellular compartments. Such an approach was validated in the first step for very well characterized T24 and HCV29 bladder cell lines. Here elasticity maps allow correlating better the mechanical properties of cells with their cytoskeleton organization. Elasticity maps of DU145 cellular clusters were recorded using AFM, followed by a tailored analysis of the obtained data. Multilayer models were applied to determine the elastic modulus of mechanically distinct layers (characterized by homogenous elastic modulus within a layer). Not only distinct mechanical layers were taken under consideration at this point but also different cellular compartments (i.e. nuclear region and lamellipodia). Such discrimination was possible thanks to the topographical characterization of cellular clusters. Finally, due to the large radius of probes and relatively low sample height in the case of lamellipodia, finite thickness correction was applied during data analysis to avoid the impact of the rigid substrate. The application of finite thickness correction was crucial to observe changes in cellular stiffness induced by the action of VFL.

The next two chapters showed that AFM working in force spectroscopy mode allows obtaining information about drug action *a priori* to biological assays. In case of drugs which were shown to exerts more damage to DU145 cells (DTX and COL) transient mechanical stiffening was observed earlier after drug addition (24h or 48 h) while in case of drug with the lowest potential to kill DU145 cancerous cells (VFL) this stiffening was noted after 72 hours of drug treatment. Cells treated with VFL parallelly to increased rigidity exhibited the larger activity of transporters responsible for pumping drugs away from the cellular body. The latter observation allows supporting hypothesis about the relation between stiffening of cells and their drug resistance. It was essential to understand what phenomenon is responsible for the stiffening of DU145 prostate cancer cells after their treatment with VFL. To answer this question, the cellular cytoskeleton was visualized using standard epifluorescent microscopy and confocal fluorescent microscopy. Surprisingly, even though VFL is acting on microtubules, a lack of changes after its action in the organization of microtubules was observed. On the other hand, the actin cytoskeleton is strengthened after treatment with VFL

but not COL and DTX. Finally, to confirm that the actin cytoskeleton is responsible for the stiffening of DU145 cells in response to VFL action, it was disrupted using cytochalasin D, and cellular elastic moduli were determined using AFM. As a result, disruption of the actin cytoskeleton was shown to lower elastic modulus of VFL – treated cells to the level of NTC cells, ultimately confirming that actin cytoskeleton rearrangements are responsible for changes in cellular elasticity due to drug treatment.

Finally, a multilayer approach was applied to characterize DU145 cells to gather information about changes in mechanical properties of particular compartments of cells. As such, mechanical maps were acquired using self-manufactured colloidal probes. The protocol relies on differences in the physical properties of surfaces at which colloidal probes were placed. It enabled to attach probes to AFM cantilevers only thanks to capillary forces. Then such a system was placed into the oven to obtain permanent binding between the sphere and AFM cantilever. After 72 hours of drug treatment, major changes in mechanical properties were observed in cells treated with VFL. Similarly to results obtained using pyramidal probes, DU145 cells treated with VFL were stiffening after 72 hours in drug-dose dependent matter. Application of multilayer approach together with elasticity maps collected for whole cellular clusters allowed to observe that stiffening of cells was localized only in the nuclear regime but not in lamellipodia. Such observation implies that since the nucleus is responsible for storing genetic information, any alteration in its mechanical properties might affect gene expression and lead even to drug resistance (15,117).

Last but not least, a model of tumour core proposed by culturing prostate cancer cells under GLN starvation conditions. Such cells from the tumour core are usually considered to be the most resistant against anticancer therapy. It was shown that GLN depletion led to a significantly depleted proliferation of cells and decreased metabolic activity. AFM measurements of whole clusters of cells showed that starved prostate cancer cells are significantly stiffer than control ones at the mechanical level. Stiffening of those cells was explained by increased nucleus contribution to the maintenance of cell mechanical properties in starved cells. Those stiffer cells are more resistant to docetaxel therapy than control ones.

Taking those data together, the gathered results shows that by assessing changes in physical parameters of cells (here elastic modulus measured with the use of AFM), one can predict whether particular cells will be more or less resistant against chemotherapeutic agents. Thus, those findings provide a new biomechanical marker to assess drug activity in various tumour models, which might serve as a promising tool in expanded therapy.

12. Bibliography

1. Hanahan D, Weinberg RA. The hallmarks of cancer. Cell [Internet]. 2000;100(1):57–70. Available from: http://www.ncbi.nlm.nih.gov/pubmed/10647931
2. Eurostat [Internet]. Available from: https://ec.europa.eu/eurostat/statistics-explained/index.php/Causes_of_death_statistics
3. Pickup MW, Mouw JK, Weaver VM. The extracellular matrix modulates the hallmarks of cancer.
4. Lekka M, Laidler P, Gil D, Lekki J, Stachura Z, Hrynkiewicz AZ. Elasticity of normal and cancerous human bladder cells studied by scanning force microscopy. Eur Biophys J. 1999;28(4).
5. Alibert C, Goud B, Manneville J-BB. Are cancer cells really softer than normal cells? Biol cell. 2017;1–36.
6. Bauer J, Emon MAB, Staudacher JJ, Thomas AL, Zessner-Spitzenberg J, Mancinelli G, et al. Increased stiffness of the tumor microenvironment in colon cancer stimulates cancer associated fibroblast-mediated prometastatic activin A signaling. Sci Rep [Internet]. 2020 Dec 9;10(1):50. Available from: http://www.nature.com/articles/s41598-019-55687-6
7. Krouskop TA, Wheeler TM, Kallel F, Garra BS, Hall T. Elastic moduli of breast and prostate tissues under compression. Ultrason Imaging. 1998;20(4):260–74.
8. Lekka M. Discrimination Between Normal and Cancerous Cells Using AFM. Bionanoscience [Internet]. 2016 Mar 30;6(1):65–80. Available from: http://link.springer.com/10.1007/s12668-016-0191-3
9. Stylianou A, Lekka M, Stylianopoulos T. AFM assessing of nanomechanical fingerprints for cancer early diagnosis and classification: From single cell to tissue level. Nanoscale. 2018;10(45):20930–45.
10. Yamauchi M, Barker TH, Gibbons DL, Kurie JM. The fibrotic tumor stroma. J Clin Invest. 2018;128(1):16–25.
11. Karagiannis GS, Poutahidis T, Erdman SE, Kirsch R, Riddell RH, Diamandis EP. Cancer-associated fibroblasts drive the progression of metastasis through both paracrine and mechanical pressure on cancer tissue. Mol Cancer Res. 2012;10(11):1403–18.
12. Leight JL, Drain AP, Weaver VM. Extracellular matrix remodeling and stiffening

modulate tumor phenotype and treatment response. Annu Rev Cancer Biol. 2017;1:313–34.

13. Reid SE, Kay EJ, Neilson LJ, Henze A, Serneels J, McGhee EJ, et al. Tumor matrix stiffness promotes metastatic cancer cell interaction with the endothelium. EMBO J. 2017;36(16):2373–89.
14. Joyce MH, Lu C, James ER, Hegab R, Allen SC, Suggs LJ, et al. Phenotypic Basis for Matrix Stiffness-Dependent Chemoresistance of Breast Cancer Cells to Doxorubicin. Front Oncol [Internet]. 2018 Sep 5;8:337. Available from: https://www.frontiersin.org/article/10.3389/fonc.2018.00337/full
15. Medina SH, Bush B, Cam M, Sevcik E, Delrio FW, Nandy K, et al. Identification of a mechanogenetic link between substrate stiffness and chemotherapeutic response in breast cancer. Biomaterials. 2019;
16. Edmondson R, Adcock AF, Yang L. Influence of matrices on 3D-cultured prostate cancer cells' drug response and expression of drug-action associated proteins. PLoS One. 2016;11(6):1–23.
17. Schrader J, Gordon-Walker TT, Aucott RL, van Deemter M, Quaas A, Walsh S, et al. Matrix stiffness modulates proliferation, chemotherapeutic response, and dormancy in hepatocellular carcinoma cells. Hepatology. 2011;53(4):1192–205.
18. Liu C, Liu Y, Xie H, Zhao S, Xu X, Fan L, et al. Role of three-dimensional matrix stiffness in regulating the chemoresistance of hepatocellular carcinoma cells. Biotechnol Appl Biochem [Internet]. 2015 Jul;62(4):556–62. Available from: http://doi.wiley.com/10.1002/bab.1302
19. Shea MP, O'Leary KA, Wegner KA, Vezina CM, Schuler LA. High collagen density augments mTOR-dependent cancer stem cells in ERα+ mammary carcinomas, and increases mTOR-independent lung metastases. Cancer Lett [Internet]. 2018 Oct;433(1):1–9. Available from: https://linkinghub.elsevier.com/retrieve/pii/S0304383518304233
20. Long JE, Wongchenko MJ, Nickles D, Chung WJ, Wang B er, Riegler J, et al. Therapeutic resistance and susceptibility is shaped by cooperative multi-compartment tumor adaptation. Cell Death Differ. 2019;26(11):2416–29.
21. Rice AJ, Cortes E, Lachowski D, Cheung BCH, Karim SA, Morton JP, et al. Matrix stiffness induces epithelial-mesenchymal transition and promotes chemoresistance in pancreatic cancer cells. Oncogenesis. 2017;6(7):1–9.
22. Erickson AE, Lan Levengood SK, Sun J, Chang F-C, Zhang M. Fabrication and

Characterization of Chitosan-Hyaluronic Acid Scaffolds with Varying Stiffness for Glioblastoma Cell Culture. Adv Healthc Mater [Internet]. 2018 Aug;7(15):1800295. Available from: http://doi.wiley.com/10.1002/adhm.201800295

23. Shin JW, Mooney DJ. Extracellular matrix stiffness causes systematic variations in proliferation and chemosensitivity in myeloid leukemias. Proc Natl Acad Sci U S A. 2016;113(43):12126–31.
24. Fischer T, Hayn A, Mierke CT. Effect of Nuclear Stiffness on Cell Mechanics and Migration of Human Breast Cancer Cells. Front Cell Dev Biol. 2020;8(May):1–18.
25. Gill NK, Ly C, Nyberg KD, Lee L, Qi D, Tofig B, et al. A scalable filtration method for high throughput screening based on cell deformability. Lab Chip. 2019;19(2):343–57.
26. Sharma S, Santiskulvong C, Rao J, Gimzewski JK, Dorigo O. The role of Rho GTPase in cell stiffness and cisplatin resistance in ovarian cancer cells. Integr Biol (United Kingdom). 2014;6(6):611–7.
27. Kim JJ, Yin B, Christudass CS, Terada N, Rajagopalan K, Fabry B, et al. Acquisition of paclitaxel resistance is associated with a more aggressive and invasive phenotype in prostate cancer. J Cell Biochem. 2013;114(6):1286–93.
28. Raudenska M, Kratochvilova M, Vicar T, Gumulec J, Balvan J, Polanska H, et al. Cisplatin enhances cell stiffness and decreases invasiveness rate in prostate cancer cells by actin accumulation. Sci Rep [Internet]. 2019 Dec 7;9(1):1660. Available from: http://www.nature.com/articles/s41598-018-38199-7
29. Hanahan D, Weinberg RA. Hallmarks of cancer: The next generation. Cell [Internet]. 2011;144(5):646–74. Available from: http://dx.doi.org/10.1016/j.cell.2011.02.013
30. Pan ST, Li ZL, He ZX, Qiu JX, Zhou SF. Molecular mechanisms for tumour resistance to chemotherapy. Clin Exp Pharmacol Physiol. 2016;43(8):723–37.
31. Jordan MA, Wilson L. Microtubules as a target for anticancer drugs. Nat Rev Cancer. 2004;4(4):253–65.
32. Brouhard GJ, Rice LM. Microtubule Dynamics: an interplay of biochemistry and mechanics.
33. Barbier P, Tsvetkov PO, Breuzard G, Devred F. Deciphering the molecular mechanisms of anti-tubulin plant derived drugs. Phytochem Rev. 2014;13(1):157–69.
34. Beswick RW, Ambrose HE, Wagner SD. Nocodazole, a microtubule depolymerising agent, induces apoptosis of chronic lymphocytic leukaemia cells associated with changes in Bcl-2 phosphorylation and expression. Leuk Res. 2006;30(4):427–36.

35. Attia SM. Molecular cytogenetic evaluation of the mechanism of genotoxic potential of amsacrine and nocodazole in mouse bone marrow cells. J Appl Toxicol. 2013;33(6):426–33.
36. Wang X, Tanaka M, Krstin S, Peixoto H, Wink M. The Interference of Selected Cytotoxic Alkaloids with the Cytoskeleton: An Insight into Their Modes of Action. Molecules [Internet]. 2016 Jul 12;21(7):906. Available from: http://www.mdpi.com/1420-3049/21/7/906
37. Rotsch C, Radmacher M. Drug-induced changes of cytoskeletal structure and mechanics in fibroblasts: An atomic force microscopy study. Biophys J [Internet]. 2000;78(1):520–35. Available from: http://dx.doi.org/10.1016/S0006-3495(00)76614-8
38. González-Cruz RD, Fonseca VC, Darling EM. Cellular mechanical properties reflect the differentiation potential of adipose-derived mesenchymal stem cells. Proc Natl Acad Sci U S A. 2012;109(24).
39. Szydlak R, Majka M, Lekka M, Kot M, Laidler P. AFM-based analysis of Wharton's jelly mesenchymal stem cells. Int J Mol Sci. 2019;20(18).
40. Raczkowska J, Orzechowska B, Patryas S, Awsiuk K, Kubiak A, Kinoshita M, et al. Effect of Substrate Stiff ness on Physicochemical Properties of Normal and Fibrotic Lung Fibroblasts. Materials (Basel). 2020;13(20):1–17.
41. Orzechowska B, Pabijan J, Wiltowska-Zuber J, Zemła J, Lekka M. Fibroblasts change spreading capability and mechanical properties in a direct interaction with keratinocytes in conditions mimicking wound healing. J Biomech. 2018;74:134–42.
42. Mathur AB, Collinsworth AM, Reichert WM, Kraus WE, Truskey GA. Endothelial, cardiac muscle and skeletal muscle exhibit different viscous and elastic properties as determined by atomic force microscopy. J Biomech. 2001;34(12):1545–53.
43. Spedden E, White JD, Naumova EN, Kaplan DL, Staii C. Elasticity maps of living neurons measured by combined fluorescence and atomic force microscopy. Biophys J. 2012;103(5):868–77.
44. Zemła J, Bobrowska J, Kubiak A, Zieliński T, Pabijan J, Pogoda K, et al. Indenting soft samples (hydrogels and cells) with cantilevers possessing various shapes of probing tip. Eur Biophys J [Internet]. 2020 Sep 17;49(6):485–95. Available from: https://doi.org/10.1007/s00249-020-01456-7
45. Zemła J, Danilkiewicz J, Orzechowska B, Pabijan J, Seweryn S, Lekka M. Atomic force microscopy as a tool for assessing the cellular elasticity and adhesiveness to identify cancer cells and tissues. Semin Cell Dev Biol [Internet]. 2017; Available from:

http://linkinghub.elsevier.com/retrieve/pii/S1084952117301805

46. Lekka M. Cellular Analysis by Atomic Force Microscopy. Pan Stanford Publishing Pte Ltd; 2016.
47. Kubiak A, Zieliński T, Pabijan J, Lekka M. Nanomechanics in Monitoring the Effectiveness of Drugs Targeting the Cancer Cell Cytoskeleton. Int J Mol Sci [Internet]. 2020 Nov 20;21(22):8786. Available from: https://www.mdpi.com/1422-0067/21/22/8786
48. Lekka M, Laidler P, Ignacak JJ, Labd M, Lekki J, Struszczyk H, et al. The effect of chitosan on stiffness and glycolytic activity of human bladder cells. Biochim Biophys Acta - Mol Cell Res. 2001;1540(2):127–36.
49. Gaspar D, Freire JM, Pacheco TR, Barata JT, Castanho MARB. Apoptotic human neutrophil peptide-1 anti-tumor activity revealed by cellular biomechanics. Biochim Biophys Acta - Mol Cell Res [Internet]. 2015 Feb;1853(2):308–16. Available from: https://linkinghub.elsevier.com/retrieve/pii/S0167488914003954
50. Ren J, Huang H, Liu Y, Zheng X, Zou Q. An atomic force microscope study revealed two mechanisms in the effect of anticancer drugs on rate-dependent Young's modulus of human prostate cancer cells. PLoS One. 2015;10(5).
51. Fang Y, Iu CYY, Lui CNP, Zou Y, Fung CKM, Li HW, et al. Investigating dynamic structural and mechanical changes of neuroblastoma cells associated with glutamate-mediated neurodegeneration. Sci Rep. 2014;4:1–10.
52. Zhang Q, Shi Y, Xu H, Zhou L, Gao J, Jiang J, et al. Evaluating the efficacy of the anticancer drug cetuximab by atomic force microscopy. RSC Adv. 2018;8(39):21793–7.
53. Iturri J, Weber A, Moreno-Cencerrado A, Vivanco MD, Benítez R, Leporatti S, et al. Resveratrol-induced temporal variation in the mechanical properties of MCF-7 breast cancer cells investigated by atomic force microscopy. Int J Mol Sci. 2019;20(13).
54. Yang Y, Li M, Sun X, Zhou C, Wang Y, Wang L, et al. The selective cytotoxicity of DSF-Cu attributes to the biomechanical properties and cytoskeleton rearrangements in the normal and cancerous nasopharyngeal epithelial cells. Int J Biochem Cell Biol. 2017;84:96–108.
55. Olugbami JO, Damoiseaux R, France B, Gbadegesin MA, Stieg AZ, Sharma S, et al. Atomic force microscopy correlates antimetastatic potentials of HepG2 cell line with its redox/energy status: effects of curcumin and Khaya senegalensis. J Integr Med. 2017;15(3):214–30.

56. Lam WA. Chemotherapy exposure increases leukemia cell stiffness. 2007;
57. Pyka-Fościak G, Zemła J, Lis GJ, Litwin JA, Lekka M. Changes in spinal cord stiffness in the course of experimental autoimmune encephalomyelitis, a mouse model of multiple sclerosis. Arch Biochem Biophys. 2020;680.
58. Nebuloni M, Albarello L, Andolfo A, Magagnotti C, Genovese L, Locatelli I, et al. Insight On Colorectal Carcinoma Infiltration by Studying Perilesional Extracellular Matrix. Nat Publ Gr. 2016;
59. Lekka M. A tip for diagnosing cancer. Nat Nanotechnol [Internet]. 2012 Nov 6;7(11):691–2. Available from: http://www.nature.com/articles/nnano.2012.196
60. Hill BT, Riddle PR, Franks LM, Highman WJ, Trejdosiewicz LK. Tissue Culture Model of Transitional Cell Carcinoma: Characterization of Twenty-two Human Urothelial Cell Lines. Cancer Res. 1986;46(7):3630–6.
61. Binnig G, Quate C, Gerber C. Atomic Force Microscope [Internet]. Vol. 56, Physical Review Letters. 1986. p. 930–3. Available from: http://link.aps.org/doi/10.1103/PhysRevLett.56.930%5Cnpapers2://publication/uuid/551F6513-EAC6-4BC0-A144-AB381B706D40
62. Indrieri M, Podestà A, Bongiorno G, Marchesi D, Milani P. Adhesive-free colloidal probes for nanoscale force measurements: Production and characterization.
63. Search H, Journals C, Contact A, Iopscience M, Address IP, Herminghaus S, et al. Roughness-induced non-wetting. Europhys Lett [Internet]. 2000;52(2):165–70. Available from: http://iopscience.iop.org/0295-5075/52/2/165%0Ahttp://links.isiglobalnet2.com/gateway/Gateway.cgi?GWVersion=2&SrcAuth=mekentosj&SrcApp=Papers&DestLinkType=FullRecord&DestApp=WOS&KeyUT=000089938400007
64. Matei GA, Thoreson EJ, Pratt JR, Newell DB, Burnham NA. Precision and accuracy of thermal calibration of atomic force microscopy cantilevers. Rev Sci Instrum. 2006;77(8):083703.
65. Sneddon IN. The relation between load and penetration in the axisymmetric boussinesq problem for a punch of arbitrary profile. Int J Eng Sci. 1965;3(1):47–57.
66. Ramos JR, Pabijan J, Garcia R, Lekka M. The softening of human bladder cancer cells happens at an early stage of the malignancy process. Beilstein J Nanotechnol. 2014;5(1).
67. Lekka M. Atomic force microscopy: A tip for diagnosing cancer. Nat Nanotechnol [Internet]. 2012;7(11):691–2. Available from:

http://dx.doi.org/10.1038/nnano.2012.196

68. Nguyen A V., Nyberg KD, Scott MB, Welsh AM, Nguyen AH, Wu N, et al. Stiffness of pancreatic cancer cells is associated with increased invasive potential. Integr Biol (United Kingdom) [Internet]. 2016;8(12):1232–45. Available from: http://dx.doi.org/10.1039/C6IB00135A
69. Tavares S, Vieira AF, Taubenberger AV, Araújo M, Martins NP, Brás-Pereira C, et al. Actin stress fiber organization promotes cell stiffening and proliferation of pre-invasive breast cancer cells. Nat Commun [Internet]. 2017 Aug 16;8(1):15237. Available from: http://www.nature.com/articles/ncomms15237
70. Kaushik G, Fuhrmann A, Cammarato A, Engler AJ. In Situ Mechanical Analysis of Myofibrillar Perturbation and Aging on Soft, Bilayered Drosophila Myocardium. Biophys J [Internet]. 2011 Dec;101(11):2629–37. Available from: https://linkinghub.elsevier.com/retrieve/pii/S0006349511012744
71. Dimitriadis EK, Horkay F, Maresca J, Kachar B, Chadwick RS. Determination of elastic moduli of thin layers of soft material using the atomic force microscope. Biophys J [Internet]. 2002;82(5):2798–810. Available from: http://www.ncbi.nlm.nih.gov/pubmed/11964265
72. Puricelli L, Galluzzi M, Schulte C, Podestà A, Milani P. Nanomechanical and topographical imaging of living cells by atomic force microscopy with colloidal probes. Rev Sci Instrum [Internet]. 2015 Mar;86(3):033705. Available from: http://aip.scitation.org/doi/10.1063/1.4915896
73. Lekka M, Gil D, Pogoda K, Dulińska-Litewka J, Jach R, Gostek J, et al. Cancer cell detection in tissue sections using AFM. Arch Biochem Biophys. 2012;518(2):151–6.
74. Bobrowska J, Awsiuk K, Pabijan J, Bobrowski P, Lekki J, Sowa KM, et al. Biophysical and biochemical characteristics as complementary indicators of melanoma progression. Anal Chem. 2019;91(15):9885–92.
75. Zemła J, Danilkiewicz J, Orzechowska B, Pabijan J, Seweryn S, Lekka M. Atomic force microscopy as a tool for assessing the cellular elasticity and adhesiveness to identify cancer cells and tissues. Semin Cell Dev Biol [Internet]. 2018;73:115–24. Available from: https://doi.org/10.1016/j.semcdb.2017.06.029
76. Handorf AM, Zhou Y, Halanski MA, Li WJ. Tissue stiffness dictates development, homeostasis, and disease progression. Organogenesis. 2015;11(1):1–15.
77. Wirtz D, Konstantopoulos K, Searson PC. The physics of cancer: the role of physical interactions and mechanical forces in metastasis. Nat Rev Cancer [Internet]. 2011 Jul

1;11(7):512–22. Available from: http://www.nature.com/articles/nrc3080

78. Syed Asif SA, Wahl KJ, Colton RJ, Warren OL. Quantitative imaging of nanoscale mechanical properties using hybrid nanoindentation and force modulation. J Appl Phys. 2001;90(3):1192–200.

79. Chopinet L, Formosa C, Rols MP, Duval RE, Dague E. Imaging living cells surface and quantifying its properties at high resolution using AFM in QI^{TM} mode. Micron. 2013;48:26–33.

80. Gavara N, Chadwick RS. Determination of the elastic moduli of thin samples and adherent cells using conical atomic force microscope tips. Nat Nanotechnol [Internet]. 2012 Nov 30;7(11):733–6. Available from: http://www.nature.com/articles/nnano.2012.163

81. Garcia PD, Garcia R. Determination of the Elastic Moduli of a Single Cell Cultured on a Rigid Support by Force Microscopy. Biophys J [Internet]. 2018;114(12):2923–32. Available from: https://doi.org/10.1016/j.bpj.2018.05.012

82. Gavara N, Chadwick RS. Determination of the elastic moduli of thin samples and adherent cells using conical atomic force microscope tips. Nat Nanotechnol. 2012;7(11):733–6.

83. Kubiak A, Chighizola M, Schulte C, Bryniarska N, Wesołowska J, Pudełek M, et al. Stiffening of DU145 prostate cancer cells driven by actin filaments – microtubule crosstalk conferring resistance to microtubule-targeting drugs. Nanoscale. 2021;6212–26.

84. Rheinlaender J, Dimitracopoulos A, Wallmeyer B, Kronenberg NM, Chalut KJ, Gather MC, et al. Cortical cell stiffness is independent of substrate mechanics. Nat Mater [Internet]. 2020 May 25; Available from: http://www.nature.com/articles/s41563-020-0684-x

85. Bennouna J, Delord JP, Campone M, Nguyen L. Vinflunine: A new microtubule inhibitor agent. Clin Cancer Res. 2008;14(6):1625–32.

86. Kruczynski A, Hill BT. Vinflunine, the latest Vinca alkaloid in clinical development: A review of its preclinical anticancer properties. Crit Rev Oncol Hematol. 2001;40(2):159–73.

87. Gerullis H, Wawroschek F, Köhne C-H, Ecke TH. Vinflunine in the treatment of advanced urothelial cancer: clinical evidence and experience. Ther Adv Urol [Internet]. 2017;9(1):28–35. Available from: http://journals.sagepub.com/doi/10.1177/1756287216677903

88. Honoré S, Pagano A, Gauthier G, Bourgarel-Rey V, Verdier-Pinard P, Civiletti K, et al. Antiangiogenic vinflunine affects EB1 localization and microtubule targeting to adhesion sites. Mol Cancer Ther [Internet]. 2008;7(7):2080–9. Available from: http://mct.aacrjournals.org/content/7/7/2080%5Cnhttp://mct.aacrjournals.org.gate2.inist.fr/content/7/7/2080.full.pdf%5Cnhttp://mct.aacrjournals.org.gate2.inist.fr/content/7/7/2080.long%5Cnhttp://www.ncbi.nlm.nih.gov/pubmed/18645018
89. Rovini A, Gauthier G, Bergès R, Kruczynski A, Braguer D, Honoré S. Anti-Migratory Effect of Vinflunine in Endothelial and Glioblastoma Cells Is Associated with Changes in EB1 C-Terminal Detyrosinated/Tyrosinated Status. PLoS One. 2013;8(6):1–12.
90. Pourroy B, Carré M, Honoré S, Bourgarel-Rey V, Kruczynski A, Briand C, et al. Low concentrations of vinflunine induce apoptosis in human SK-N-SH neuroblastoma cells through a postmitotic G1 arrest and a mitochondrial pathway. Mol Pharmacol. 2004;66(3):580–91.
91. Kruczynski A, Barret JM, Etiévant C, Colpaert F, Fahy J, Hill BT. Antimitotic and tubulin-interacting properties of vinflunine, a novel fluorinated Vinca alkaloid. Biochem Pharmacol. 1998;55(5):635–48.
92. Aggarwal A, Kruczynski A, Frankfurter A, Correia JJ, Lobert S. Murine leukemia P388 vinorelbine-resistant cell lines are sensitive to vinflunine. Invest New Drugs. 2008;26(4):319–30.
93. Aparicio LA, Castosa R, Haz-Conde M, Rodríguez M, Blanco M, Valladares M, et al. Role of the microtubule-targeting drug vinflunine on cell-cell adhesions in bladder epithelial tumour cells. BMC Cancer [Internet]. 2014;14(1):507. Available from: http://bmccancer.biomedcentral.com/articles/10.1186/1471-2407-14-507
94. Ippolito L, Marini A, Cavallini L, Morandi A, Pietrovito L, Pintus G, et al. Metabolic shift toward oxidative phosphorylation in docetaxel resistant prostate cancer cells. Oncotarget. 2016;7(38):61890–904.
95. Lee BY, Hochgrafe F, Lin H-M, Castillo L, Wu J, Raftery MJ, et al. Phosphoproteomic Profiling Identifies Focal Adhesion Kinase as a Mediator of Docetaxel Resistance in Castrate-Resistant Prostate Cancer. Mol Cancer Ther [Internet]. 2014;13(1):190–201. Available from: http://mct.aacrjournals.org/cgi/doi/10.1158/1535-7163.MCT-13-0225-T
96. Lin KC, Torga G, Sun Y, Axelrod R, Pienta KJ, Sturm JC, et al. The role of heterogeneous environment and docetaxel gradient in the emergence of polyploid, mesenchymal and resistant prostate cancer cells. Clin Exp Metastasis [Internet].

2019;36(2):97–108. Available from: http://dx.doi.org/10.1007/s10585-019-09958-1

97. Luty M, Piwowarczyk K, Łabędź-Masłowska A, Wróbel T, Szczygieł M, Catapano J, et al. Fenofibrate augments the sensitivity of drug-resistant prostate cancer cells to docetaxel. Cancers (Basel). 2019;11(1).
98. Dalbeth N, Lauterio TJ, Wolfe HR. Mechanism of Action of Colchicine in the Treatment of Gout. Clin Ther. 2014;36(10):1465–79.
99. Wang Y, Zhang H, Gigant B, Yu Y, Wu Y, Chen X, et al. Structures of a diverse set of colchicine binding site inhibitors in complex with tubulin provide a rationale for drug discovery. FEBS J. 2016;283(1):102–11.
100. Kuo MC, Chang SJ, Hsieh MC. Colchicine significantly reduces incident cancer in gout male patients: A 12-year cohort study. Med (United States). 2015;94(50):1–6.
101. McLoughlin EC, O'boyle NM. Colchicine-binding site inhibitors from chemistry to clinic: A review. Pharmaceuticals. 2020;13(1):1–43.
102. Weber A, Iturri J, Benitez R, Zemljic-Jokhadar S, Toca-Herrera JL. Microtubule disruption changes endothelial cell mechanics and adhesion. Sci Rep. 2019;9(1):1–12.
103. Lin CCK, Yang CH, Ju MS. Cytotoxic and biomechanical effects of clinical dosing schemes of paclitaxel on neurons and cancer cells. Cancer Chemother Pharmacol. 2020;86(2):245–55.
104. Kim KS, Cho CH, Park EK, Jung MH, Yoon KS, Park HK. AFM-Detected apoptotic changes in morphology and biophysical property caused by paclitaxel in Ishikawa and HeLa cells. PLoS One. 2012;7(1).
105. Grady ME, Composto RJ, Eckmann DM. Cell elasticity with altered cytoskeletal architectures across multiple cell types. J Mech Behav Biomed Mater [Internet]. 2016 Aug;61:197–207. Available from: https://linkinghub.elsevier.com/retrieve/pii/S1751616116000254
106. Guo T, Fang Y. Functional organization and dynamics of the cell nucleus. 2014;5(August):1–12.
107. Svitkina T. The actin cytoskeleton and actin-based motility. Cold Spring Harb Perspect Biol. 2018;10(1):1–21.
108. Schliwa M. Action of cytochalasin D on cytoskeletal networks. J Cell Biol. 1982;92(1):79–91.
109. Wakatsuki T, Schwab B, Thompson NC, Elson EL. Effects of cytochalasin D and latrunculin B on mechanical properties of cells. J Cell Sci. 2001;114(Pt 5):1025–36.
110. Rotsch C, Radmacher M. Drug-Induced Changes of Cytoskeletal Structure and

Mechanics in Fibroblasts: An Atomic Force Microscopy Study. Biophys J [Internet]. 2000;78(1):520–35. Available from: http://linkinghub.elsevier.com/retrieve/pii/S0006349500766148

111. Choi HJ, Fukui M, Zhu BT. Role of cyclin B1/Cdc2 up-regulation in the development of mitotic prometaphase arrest in human breast cancer cells treated with nocodazole. PLoS One. 2011;6(8).
112. Morse DL, Gray H, Payne CM, Gillies RJ. Docetaxel induces cell death through mitotic catastrophe in human breast cancer cells. 2005;4(October):1495–505.
113. Seano G, Nia HT, Emblem KE, Datta M, Ren J, Krishnan S, et al. Solid stress in brain tumours causes neuronal loss and neurological dysfunction and can be reversed by lithium. Nat Biomed Eng. 2019;3(3):230–45.
114. Chang Y-C, Nalbant P, Birkenfeld J, Chang Z-F, Bokoch GM. GEF-H1 Couples Nocodazole-induced Microtubule Disassembly to Cell Contractility via RhoA. Mol Biol Cell [Internet]. 2008 May 1;19(5):2147–53. Available from: http://www.molbiolcell.org/cgi/doi/10.1091/mbc.E07-12-1269
115. Mhaidat NM, Thorne RF, Edo C, Bock D, Dong X, Hersey P. Melanoma cell sensitivity to Docetaxel-induced apoptosis is determined by class III b -tubulin levels. 2008;582:267–72.
116. Guilluy C, Burridge K. Nuclear mechanotransduction: Forcing the nucleus to respond. Nucleus. 2015;6(1):19–22.
117. Wang N, Tytell JD, Ingber DE. Mechanotransduction at a distance: Mechanically coupling the extracellular matrix with the nucleus. Nat Rev Mol Cell Biol. 2009;10(1):75–82.
118. Hughes-Fulford M, Boonstra J. Cell mechanotransduction: cytoskeleton and related signaling pathways.
119. Marturano-Kruik A, Villasante A, Yaeger K, Ambati SR, Chramiec A, Raimondi MT, et al. Biomechanical regulation of drug sensitivity in an engineered model of human tumor. Biomaterials [Internet]. 2018;150:150–61. Available from: https://doi.org/10.1016/j.biomaterials.2017.10.020
120. Rebucci M, Michiels C. Molecular aspects of cancer cell resistance to chemotherapy. Biochem Pharmacol [Internet]. 2013 May;85(9):1219–26. Available from: https://linkinghub.elsevier.com/retrieve/pii/S0006295213001214
121. Luqmani YA. Mechanisms of drug resistance in cancer chemotherapy. Med Princ Pract. 2005;14(SUPPL. 1):35–48.

122. Triana-Martínez F, Loza MI, Domínguez E. Beyond Tumor Suppression: Senescence in Cancer Stemness and Tumor Dormancy. Cells. 2020;9(2).
123. Vinogradov S, Wei X. Cancer stem cells and drug resistance: The potential of nanomedicine. Nanomedicine. 2012;7(4):597–615.
124. Wise DR, Thompson CB. Glutamine Addiction: A New Therapeutic Target in Cancer. Trends Biochem Sci [Internet]. 2011;35(8):427–33. Available from: http://www.sciencedirect.com/science/article/pii/S0968000410000915
125. Jiang J, Srivastava S, Zhang J. Starve cancer cells of glutamine: Break the spell or make a hungry monster? Cancers (Basel). 2019;11(6).
126. Jang M, Kim SS, Lee J. Cancer cell metabolism: Implications for therapeutic targets. Exp Mol Med. 2013;45(10):1–8.
127. Choi YK, Park KG. Targeting glutamine metabolism for cancer treatment. Biomol Ther. 2018;26(1):19–28.
128. Krakhmal N V., Zavyalova M V., Denisov E V., Vtorushin S V., Perelmuter VM. Cancer invasion: Patterns and mechanisms. Acta Naturae. 2015;7(2):17–28.
129. Targosz-Korecka M, Daniel Brzezinka G, Danilkiewicz J, Rajfur Z, Szymonski M. Glutaraldehyde fixation preserves the trend of elasticity alterations for endothelial cells exposed to TNF-α. Cytoskeleton. 2015 Mar 1;72(3):124–30.
130. Martino F, Perestrelo AR, Vinarský V, Pagliari S, Forte G. Cellular mechanotransduction: From tension to function. Front Physiol. 2018;9(JUL):1–21.
131. Dupont S, Morsut L, Aragona M, Enzo E, Giulitti S, Cordenonsi M, et al. Role of YAP/TAZ in mechanotransduction. Nature [Internet]. 2011;474(7350):179–84. Available from: http://dx.doi.org/10.1038/nature10137
132. Aw Yong KM, Sun Y, Merajver SD, Fu J. Mechanotransduction-Induced Reversible Phenotypic Switching in Prostate Cancer Cells. Biophys J [Internet]. 2017;112(6):1236–45. Available from: http://dx.doi.org/10.1016/j.bpj.2017.02.012
133. Pavlova NN, Thompson CB. The Emerging Hallmarks of Cancer Metabolism. Cell Metab [Internet]. 2016;23(1):27–47. Available from: http://dx.doi.org/10.1016/j.cmet.2015.12.006
134. Intlekofer AM, Finley LWS. Metabolic signatures of cancer cells and stem cells. Nat Metab [Internet]. 2019;1(2):177–88. Available from: http://dx.doi.org/10.1038/s42255-019-0032-0
135. Eidelman E, Twum-Ampofo J, Ansari J, Siddiqui MM. The metabolic phenotype of prostate cancer. Front Oncol. 2017;7(JUN):1–6.

136. Zacharias NM, McCullough C, Shanmugavelandy S, Lee J, Lee Y, Dutta P, et al. Metabolic Differences in Glutamine Utilization Lead to Metabolic Vulnerabilities in Prostate Cancer. Sci Rep. 2017;7(1):1–11.
137. Fung MKL, Chan GCF. Drug-induced amino acid deprivation as strategy for cancer therapy. J Hematol Oncol. 2017;10(1):1–18.
138. Yoo HC, Yu YC, Sung Y, Han JM. Glutamine reliance in cell metabolism. Exp Mol Med [Internet]. 2020;52(9):1496–516. Available from: http://dx.doi.org/10.1038/s12276-020-00504-8
139. White MA, Lin C, Rajapakshe K, Dong J, Shi Y, Tsouko E, et al. Glutamine transporters are targets of multiple oncogenic signaling pathways in prostate cancer. Mol Cancer Res. 2017;15(8):1017–28.
140. Altman BJ, Stine ZE, Dang C V. From Krebs to clinic: glutamine metabolism to cancer therapy. Nat Rev Cancer [Internet]. 2016 Oct 29;16(10):619–34. Available from: http://www.nature.com/articles/nrc.2016.71
141. Dorai T, Dorai B, Pinto JT, Grasso M, Cooper AJL. High levels of glutaminase ii pathway enzymes in normal and cancerous prostate suggest a role in 'glutamine addiction.' Biomolecules. 2020;10(1):1–16.
142. Zhang J, Mao S, Guo Y, Wu Y, Yao X, Huang Y. Inhibition of GLS suppresses proliferation and promotes apoptosis in prostate cancer. Biosci Rep. 2019;39(6).
143. Ishak Gabra MB, Yang Y, Lowman XH, Reid MA, Tran TQ, Kong M. IKKβ activates p53 to promote cancer cell adaptation to glutamine deprivation. Oncogenesis [Internet]. 2018;7(11). Available from: http://dx.doi.org/10.1038/s41389-018-0104-0
144. Pan M, Reid MA, Lowman XH, Kulkarni RP, Tran TQ, Liu X, et al. Regional glutamine deficiency in tumours promotes dedifferentiation through inhibition of histone demethylation. Nat Cell Biol [Internet]. 2016 Oct 12;18(10):1090–101. Available from: http://www.nature.com/articles/ncb3410
145. Fan S, Kroeger B, Marie PP, Bridges EM, Mason JD, McCormick K, et al. Glutamine deprivation alters the origin and function of cancer cell exosomes. EMBO J. 2020;39(16):1–27.
146. Barenholz-Cohen T, Merkher Y, Haj J, Shechter D, Kirchmeier D, Shaked Y, et al. Lung mechanics modifications facilitating metastasis are mediated in part by breast cancer-derived extracellular vesicles. Int J Cancer. 2020;147(10):2924–33.

List of figures

List of tables